

Dissertation  
submitted to the  
Combined Faculty of Natural Sciences and Mathematics  
of the Ruperto Carola University Heidelberg, Germany  
for the degree of  
Doctor of Natural Sciences

Presented by  
M.Sc. Sophie Alessa Herbst née Rabe  
born in Hamburg

Oral examination: 22.10.2020



Systematic analysis of cell-intrinsic and extrinsic  
factors in chronic lymphocytic leukemia to  
understand functional consequences for  
drug response and clinical outcome

Referees: Prof. Dr. Benedikt Brors  
PD. Dr. Sascha Dietrich



# Abstract

Chronic lymphocytic leukemia (CLL) is an indolent B-cell malignancy with a very heterogeneous clinical course. Even though many aspects of the biology of CLL have been thoroughly described, the underlying molecular cause for this heterogeneity has still not been completely understood. To fill this gap, this thesis presents a comprehensive analysis of cancer cell-intrinsic and extrinsic factors which modify drug response phenotypes and patient outcome in a cohort of 81 primary CLL patient samples.

Some cancer cell-intrinsic factors, like the genome or transcriptome of CLL, have been comprehensively explored. However, proteomic profiling of a large CLL patient cohort and its integration with other molecular layers is currently lacking. Therefore, this study performed a thorough characterisation of multiple CLL cell-intrinsic factors, including the proteome, the transcriptome and the genome. These were additionally linked to *ex-vivo* drug response profiles (43 drugs). This revealed associations between the different layers and functional consequences for drug response and clinical outcome. Unsupervised clustering of protein levels uncovered a previously unappreciated poor prognosis CLL subgroup, which was independent of established risk factors and characterised by a distinct protein and drug response profile. The existence of this subgroup could be validated in an external cohort. This comprehensive multi-omics analysis represents the first proteogenomic study of a large CLL patient cohort.

CLL cells additionally depend on cell-extrinsic signals provided by the microenvironment, such as the bone marrow niche. Such signals can modify and reduce the activity of selected drugs. However, a systematic analysis of how the bone marrow microenvironment influences drug response and resistance is lacking, because appropriate bone marrow model systems for high-throughput drug screening do currently not exist. To this end, a high-throughput co-culture drug-sensitivity testing platform was established. During the careful evaluation of different stroma cells as CLL cell support for the system, an unexpected phenomenon was discovered. Some bone marrow stroma cells had the ability to phagocytose apoptotic cells in large amounts. Phagocytosis decreased the total amount of cells and, thus, artificially increased the percentage of alive cells. This has implications for co-culture studies in general, as phagocytosis can cause a systematic bias and the misinterpretation of results if left unconsidered. Consequently, non-phagocytic stroma cells were chosen for the final screening platform.

Using this optimised system, responses to 43 different drugs were measured. A linear model was employed to distinguish between the effect of stroma cells on spontaneous and on drug-induced apoptosis of CLL cells. In accordance with the literature, stroma cells protected CLL cells from spontaneous apoptosis *ex-vivo*. Interestingly, effect sizes varied between patients and

especially samples with unmutated immunoglobulin heavy chain variable region and high degrees of spontaneous apoptosis profited from co-culturing. Moreover, the influence of stroma cells on drug responses was systematically assessed. While some drugs, like chemotherapeutics, were less active in co-cultures, other drugs had unchanged activity or were even more efficient in the context of stroma cells. Especially Janus kinase inhibitors could overcome the protective effect by stroma cells and kill CLL cells despite the presence of stroma. The systematic analysis of the impact of the bone marrow niche on drug response can help to understand and overcome microenvironment-induced resistances.

In conclusions, this thesis provides a systematic overview of how leukemia cell-intrinsic layers of CLL and the microenvironment determine drug response and patient outcome.

# Zusammenfassung

Die chronische lymphatische Leukämie (CLL) ist eine indolente B-Zell-Erkrankung mit einem sehr heterogenen klinischen Verlauf. Obwohl viele Aspekte der Biologie der CLL gründlich beschrieben wurden, ist die zugrunde liegende molekulare Ursache dieser Heterogenität noch immer nicht vollständig geklärt. Um diese Lücke zu schliessen, wurde in dieser Doktorarbeit eine umfassende Analyse von 81 primären CLL-Patientenproben durchgeführt. Hierbei wurden die krebszellintrinsicen und extrinsicen Faktoren charakterisiert, die den molekularen Phänotyp, das Ansprechen auf Medikamente und den klinischen Verlauf beeinflussen.

Einige krebszellintrinsiche Faktoren der CLL, wie das Genom oder das Transkriptom, sind umfassend erforscht worden. Allerdings existiert bisher keine Analyse des Proteoms einer großen CLL-Patientenkohorte, sowie deren Integration mit anderen molekularen Ebenen. Daher wurde in dieser Studie eine gründliche Charakterisierung mehrerer CLL zellintrinsiche Faktoren durchgeführt, darunter das Proteom, das Transkriptom und das Genom. Diese wurden zusätzlich mit dem *ex-vivo* Anprechen auf 43 unterschiedliche Medikamente verknüpft. Dadurch konnten Assoziationen zwischen den verschiedenen molekularen Ebenen und funktionelle Konsequenzen für Medikamentensensitivitäten und den klinischen Verlauf beschrieben werden. Ein unüberwachtes Clustern aller Proteinhäufigkeiten deckte eine bisher unbekannte Untergruppe der CLL mit schlechter Prognose auf. Diese war unabhängig von etablierten Risikofaktoren und zeichnete sich durch eine einzigartige Signatur der Proteine und Medikamentensensitivitäten aus. Die Existenz dieser Untergruppe konnte in einer externen Kohorte validiert werden. Diese umfassende Multiomik-Analyse stellt die erste proteogenomische Studie an einer großen CLL-Patientenkohorte dar.

CLL-Zellen sind zusätzlich auf zellextrinsiche Signale angewiesen, die von der Mikroumgebung, wie z.B. der Knochenmarksnische, bereitgestellt werden. Solche Signale können die Aktivität einzelner Medikamente modifizieren und reduzieren. Eine systematische Analyse, wie die Mikroumgebung des Knochenmarks das Ansprechen und Resistenzen auf Medikamente beeinflusst, fehlt jedoch, da es derzeit keine geeigneten Modellsysteme des Knochenmarks gibt, die für ein Wirkstoffscreening im Hochdurchsatz genutzt werden könnten. Daher wurde ein Co-Kultur Modell entwickelt, welches sich für Wirkstoffscreens im Hochdurchsatz eignet. Bei der sorgfältigen Evaluierung verschiedener Stromazellen als zelluläre Mikroumgebung für das System wurde ein unerwartetes Phänomen entdeckt. Einige Knochenmark-Stromazellen hatten die Fähigkeit apoptotische Zellen in großen Mengen zu phagozytieren. Phagozytose reduzierte die Gesamtanzahl der Zellen und erhöhte somit künstlich den Prozentsatz der lebenden Zellen. Dies hat Auswirkungen auf Co-Kultur-Studien im Allgemeinen, da Phagozytose, wenn sie nicht berücksichtigt wird, zu einem systematischen Fehler und daher Fehlinterpretation der Ergebnis-

se führen kann. Folglich wurden nicht-phagozytäre Stromazellen für die endgültige Screening-Plattform ausgewählt.

Mit diesem optimierten System wurde das Ansprechen der CLL Zellen auf 43 verschiedene Medikamente gemessen. Ein lineares Modell wurde verwendet, um zwischen dem Effekt von Stromazellen auf spontane und auf medikamenteninduzierte Apoptose der CLL-Zellen unterscheiden zu können. In Übereinstimmung mit der Literatur schützten Stromazellen CLL-Zellen vor spontaner Apoptose *ex-vivo*. Interessanterweise variierten die Effektstärken zwischen den Patienten. Insbesondere Proben mit unmutierter variabler Region der Immunglobulin-Schwerkette und hohen Graden spontaner Apoptose profitierten von der Co-Kultivierung. Darüber hinaus wurde der Einfluss von Stromazellen auf das Ansprechen auf Medikamente systematisch untersucht. Während einige Medikamente, wie z.B. Chemotherapeutika, in Co-Kulturen weniger aktiv waren, hatten andere Medikamente keine veränderte Aktivität oder waren bei Anwesenheit von Stromazellen sogar effizienter. Insbesondere Januskinase Inhibitoren konnten die protektive Wirkung von Stromazellen überwinden und CLL-Zellen trotz der Anwesenheit von Stromazellen abtöten. Die systematische Analyse des Einflusses der Knochenmarksnische auf das Ansprechen von Medikamenten kann helfen von der Mikroumgebung induzierte Resistenzen zu verstehen und zu behandeln.

Zusammenfassend bietet diese Arbeit einen systematischen Überblick darüber, wie die molekularen Charakteristika der CLL und der Einfluss der Mikroumgebung das Ansprechen auf Medikamente und den klinischen Verlauf bestimmen.

# Contents

Abstract . . . . .	V
Zusammenfassung . . . . .	VII
Table of contents . . . . .	IX
List of figures . . . . .	XIII
List of tables . . . . .	XV
Abbreviations . . . . .	XVII
Publications related to thesis . . . . .	XIX
Presentation of results of thesis at conferences . . . . .	XXI
Acknowledgements . . . . .	XXIII
Contributions . . . . .	XXV
<b>1 Introduction</b>	<b>1</b>
1.1 General disease characteristics and clinical course of CLL . . . . .	1
1.2 Cell of origin of CLL and IGHV status . . . . .	1
1.3 B-cell receptor signalling in CLL . . . . .	2
1.4 Genetics of CLL . . . . .	4
1.4.1 Recurrent mutations . . . . .	4
1.4.2 Recurrent structural aberrations . . . . .	5
1.5 The transcriptome of CLL . . . . .	6
1.6 Proteogenomic profiling . . . . .	7
1.6.1 The proteome of CLL . . . . .	7
1.6.2 Proteogenomic profiling in other cancer entities . . . . .	7
1.7 Targeted therapies for the treatment of CLL . . . . .	8
1.8 <i>Ex-vivo</i> drug sensitivity screening . . . . .	9
1.9 Importance of the microenvironment in CLL . . . . .	9
1.9.1 Models for mimicking the microenvironment in CLL . . . . .	10
1.9.2 Influence of the bone marrow niche on drug responses in CLL . . . . .	11
1.10 Aims of the thesis . . . . .	12
1.10.1 Aim 1: Establishment of a system for co-culture drug sensitivity screening in CLL . . . . .	12
1.10.2 Aim 2: Analysis of cell-intrinsic factors by proteogenomic characterisation of primary CLL patient samples . . . . .	13
1.10.3 Aim 3: Analysis of cell-extrinsic factors by systematic description of the influence of bone marrow stroma cells on drug response in CLL . . . . .	14
<b>2 Materials and methods</b>	<b>15</b>
2.1 Cell culture . . . . .	15

2.2	Patient samples . . . . .	15
2.3	Assays for the analysis of phagocytosis by stroma cells . . . . .	16
2.3.1	Comparing numbers and percentages of alive and dead cells in mono- and co-cultures using microscopy and flow cytometry . . . . .	16
2.3.2	Visualisation of disappearance of leukemia cells and presence of phagosomes by CellTracker and lysosomal staining . . . . .	16
2.3.3	Quantification of the amount of phagosomes . . . . .	17
2.3.4	Co-cultures of NKTert and apoptotic cells of different origins . . . . .	17
2.3.5	Flow cytometry of CD45 stained cells . . . . .	18
2.3.6	Experiment assessing phagocytosis by primary MSCs . . . . .	18
2.3.7	Proteomics of HS-5 and NKTert . . . . .	18
2.4	Proteogenomic profiling of CLL cells . . . . .	18
2.4.1	Preparation of samples for proteomics, RNA and panel sequencing . . . . .	18
2.4.2	Proteomics profiling of CLL samples . . . . .	19
2.4.3	IGHV status analysis . . . . .	20
2.4.4	DNA panel sequencing . . . . .	21
2.4.5	DNA copy number variants . . . . .	21
2.4.6	RNA Sequencing . . . . .	22
2.5	Co-culture drug screen . . . . .	22
2.5.1	Optimisation of seeding conditions for co-culture screen . . . . .	22
2.5.2	Preparation of screening plates . . . . .	22
2.5.3	Screen readout by spinning disk confocal microscopy . . . . .	24
2.5.4	Processing of images . . . . .	24
2.5.5	Validation of screening results in primary MSC co-cultures . . . . .	24
2.5.6	Western blots STAT3 . . . . .	25
2.6	Statistical analyses . . . . .	26
2.6.1	Analysis of differential proteins and mRNA . . . . .	26
2.6.2	Protein-mRNA correlation . . . . .	26
2.6.3	Analysis of time to next treatment . . . . .	26
2.6.4	Dimensionality reduction and consensus clustering . . . . .	27
2.6.5	Association of proteomics groups with genetic alterations . . . . .	27
2.6.6	<i>In-vivo</i> lymphocyte growth rate . . . . .	27
2.6.7	Analysis of differential splicing . . . . .	27
2.6.8	Gene ontology and KEGG gene set enrichment analyses . . . . .	28
2.6.9	Analysis of association between PG5 and drug response . . . . .	28
2.6.10	Validation of PG5 in published cohort . . . . .	28
2.6.11	Analysis of spontaneous apoptosis . . . . .	29
2.6.12	Calculation of drug-drug correlations . . . . .	29
2.6.13	Assessment of association between genetic alterations and co-culture drug response . . . . .	29
2.6.14	Linear model to describe the interaction of stroma cells with drug response . . . . .	29

<b>3</b>	<b>Results</b>	<b>31</b>
3.1	Establishment of a system for co-culture drug sensitivity screening in CLL . . . . .	31
3.1.1	General design considerations for the high-throughput drug sensitivity screen	31
3.1.2	Characterisation of bone marrow stroma cell model . . . . .	31
3.1.3	Optimisation of seeding conditions for co-culture screen . . . . .	37
3.1.4	Readout for co-culture drug screen . . . . .	39
3.1.5	Selection of the drug panel for the co-culture screen . . . . .	40
3.1.6	Co-culture drug sensitivity screen . . . . .	41
3.2	Proteogenomic characterisation of CLL patient samples . . . . .	46
3.2.1	Acquisition of multi-omics dataset of CLL . . . . .	46
3.2.2	Interplay between proteomics, transcriptomics and genetic alterations and functional consequences . . . . .	48
3.2.3	High abundance of BCR signalling proteins was associated with better outcome . . . . .	51
3.2.4	Proteomics based stratification of CLL identified six distinct subgroups .	53
3.2.5	Deregulated pathways and drug vulnerabilities of newly discovered poor outcome proteomics group 5 (PG5) . . . . .	55
3.2.6	Validation of the proteomics group 5 (PG5) in an independent cohort . .	60
3.3	Influence of the bone marrow microenvironment on drug response . . . . .	62
3.3.1	Spontaneous apoptosis of CLL cells in mono-cultures . . . . .	62
3.3.2	Protection of CLL cells from spontaneous apoptosis by bone marrow stroma cells . . . . .	63
3.3.3	Influence of bone marrow stroma cells on drug response by CLL cells . . .	64
3.3.4	Mechanistic insight into the increased sensitivity of stroma cell co-cultures to JAK inhibitors . . . . .	72
<b>4</b>	<b>Discussion</b>	<b>75</b>
4.1	Proteogenomic characterisation of CLL . . . . .	75
4.1.1	Effect of mutations on other molecular layers in CLL . . . . .	75
4.1.2	Interaction between IGHV status and trisomy 12 . . . . .	77
4.1.3	Identification of a new poor outcome subgroup . . . . .	77
4.1.4	Technical challenges and limitations of the experimental setup of the proteogenomic study . . . . .	78
4.2	Phagocytosis by bone marrow stroma cells . . . . .	79
4.2.1	Potential <i>in-vivo</i> function of phagocytosis by stroma cells . . . . .	79
4.2.2	Further directions for the investigation of phagocytosis by stroma cells . .	80
4.2.3	Implication of phagocytosis by stroma cells for co-culture studies . . . . .	80
4.3	High-throughput co-culture drug sensitivity screen . . . . .	81
4.3.1	Protection of CLL cells from spontaneous apoptosis by stroma . . . . .	81
4.3.2	Effect of stroma cells on drug-induced apoptosis by stroma . . . . .	82
4.3.3	Mono- versus co-culture high-throughput drug screens . . . . .	83
<b>5</b>	<b>Conclusion</b>	<b>85</b>

<b>Bibliography</b>	<b>87</b>
<b>Supplementary Figures</b>	<b>105</b>

## List of Figures

1.1	B-cell receptor signalling. . . . .	3
1.2	The CLL microenvironment. . . . .	10
1.3	Factors influencing outcome and drug response. . . . .	13
3.1	Dead CLL disappeared from NKTert co-cultures, artificially increasing the percentage of alive cells. . . . .	33
3.2	Microscopy images showing disappearance of dead CLL cells from drug treated co-cultures with NKTert. . . . .	34
3.3	Phagosomes observed in CLL-NKTert co-cultures. . . . .	35
3.4	NKTert cells also phagocytose dead cells of other origins. . . . .	36
3.5	Some MSCs also phagocytose apoptotic CLL. . . . .	37
3.6	Optimisation of HS-5 cell counts. . . . .	38
3.7	Evaluating nuclear area as readout to detect alive CLL cells. . . . .	41
3.8	Overview of the co-culture drug sensitivity screen. . . . .	42
3.9	Example image of a co-culture well in the high-throughput drug screen. . . . .	43
3.10	Correlation between replicates in co-culture drug sensitivity screen. . . . .	44
3.11	Edge effect in mono- and co-cultures in high-throughput drug screen. . . . .	45
3.12	Overview proteogenomics to characterise cell-intrinsic factors influencing CLL drug response and outcome. . . . .	46
3.13	Differential protein and transcript abundances in respect to genetic alterations. . . . .	49
3.14	Correlation of RNA and proteins. . . . .	50
3.15	Consequences of <i>TP53</i> mutations. . . . .	51
3.16	Relation of protein abundance and time to next treatment. . . . .	52
3.17	Genetics and outcome of proteomics groups identified by consensus clustering. . . . .	54
3.18	Comparison consensus cluster groups from protein and RNA. . . . .	55
3.19	Response of proteomics groups to B-cell receptor inhibitors and chemotherapeutics. . . . .	56
3.20	Heatmaps of protein abundances for enriched pathways in proteomics group 5. . . . .	57
3.21	Volcano plot of differential <i>ex-vivo</i> drug responses of proteomics group 5 in comparison to all other proteomics groups. . . . .	58
3.22	Relationship between splicing and proteomics group 5. . . . .	59
3.23	Validation of proteomics group 5 in an independent cohort. . . . .	61
3.24	Spontaneous apoptosis correlated with protein expression of DDB1 and DDB2. . . . .	62
3.25	Stroma cells protected CLL from spontaneous apoptosis <i>ex-vivo</i> . . . . .	64
3.26	Influence of the degree of spontaneous apoptosis and IGHV status on the protective effect by stroma cells. . . . .	65
3.27	Drug-drug correlations in mono- and co-cultures. . . . .	66

---

3.28	Relationship between <i>ex-vivo</i> drug response and genetic factors in mono- and co-cultures. . . . .	67
3.29	Influence of stroma cells on drug response of CLL. . . . .	68
3.30	Examples of drugs with decreased effect in co-cultures. . . . .	69
3.31	Example of drug with the same effect in co-cultures and mono-cultures. . . . .	70
3.32	Examples of drugs with increased effect in co-cultures. . . . .	71
3.33	STAT3 was activated by soluble factors secreted by stroma cells. . . . .	72
5.1	Overview of the work in this thesis. . . . .	85
S1	Enlargement of two phagosomes. . . . .	105
S2	CD45 flow cytometry of NKTert, HS-5 and control cells. . . . .	106
S3	Phagocytosis by different MSCs. . . . .	106
S4	Comparison of protein and gene expression patterns between NKTert and HS-5. . . . .	107
S5	Alive and dead CLL cells stained with Hoechst. . . . .	107
S6	Differential protein abundances in respect to chromosomal location. . . . .	108
S7	Differential transcript abundances in respect to chromosomal location. . . . .	109
S8	Consequences of <i>ATM</i> and <i>XPO1</i> mutations. . . . .	110
S9	Consensus cluster heatmap of proteomics data. . . . .	111
S10	T-distributed stochastic neighbour embedding and principal component analysis supported the partition into six subgroups. . . . .	112
S11	Response of proteomics groups to ibrutinib, BAY61-3606 and fludarabine. . . . .	112
S12	Mean protein abundances of B-cell receptor signalling proteins in the proteomics groups. . . . .	113

## List of Tables

2.1	Drugs and concentrations used in high-throughput drug screen. . . . .	23
2.2	Antibodies used for Western Blots. . . . .	26



## Abbreviations

<b>AKT</b>	Protein kinase B
<b>BCR</b>	B-cell receptor
<b>BLNK</b>	B-cell linker protein
<b>BMSC</b>	Bone marrow stroma cell
<b>BTK</b>	Bruton's tyrosine kinase
<b>CD38</b>	ADP-ribosyl cyclase/cyclic ADP-ribose hydrolase 1
<b>CLL</b>	Chronic lymphocytic leukemia
<b>CNV</b>	Copy number variation
<b>DDB1</b>	DNA damage-binding protein 1
<b>DDB2</b>	DNA damage-binding protein 2
<b>ERK/MAPK signalling</b>	Mitogen-activated protein kinase signalling
<b>FBS</b>	Fetal bovine serum
<b>FDR</b>	False discovery rate
<b>Gy</b>	Gray
<b>Ig</b>	Immunoglobulin
<b>IGHV</b>	Immunoglobulin heavy chain variable region
<b>IL</b>	Interleukin
<b>JAK</b>	Janus kinase
<b>M-CLL</b>	CLL with somatic hypermutations in IGHV loci
<b>MSC</b>	Mesenchymal stem cell
<b>NF<math>\kappa</math>B</b>	Nuclear factor kappa-light-chain-enhancer of activated B cells
<b>NOTCH</b>	Neurogenic locus notch
<b>OS</b>	Overall survival
<b>PBMC</b>	Peripheral blood mononuclear cells
<b>PCA</b>	Principal component analysis
<b>PG</b>	Proteomics group
<b>PI</b>	Propidium iodide
<b>PI3K</b>	Phosphoinositide 3-kinase
<b>PLC<math>\gamma</math>2</b>	1-Phosphatidylinositol-4,5-bisphosphate phosphodiesterase gamma-2
<b>t-SNE</b>	T-distributed stochastic neighbour embedding
<b>U-CLL</b>	CLL without somatic hypermutations in IGHV loci
<b>TOST procedure</b>	Two-one-sided t-tests procedure
<b>TTT</b>	Time to next treatment
<b>SF3B1</b>	Splicing factor 3B subunit 1
<b>STAT</b>	Signal transducer and activator of transcription
<b>SYK</b>	Spleen tyrosine kinase
<b>ZAP70</b>	Tyrosine-protein kinase ZAP-70



# Publications

## Publications directly related to thesis

**2020, Bone marrow stroma cells massively phagocytose apoptotic cells leading to misinterpretation of co-culture experiments**

**Herbst\***, Stolarczyk\*, Becirovic, Liu, Kolb, Herling, Müller-Tidow, Dietrich

*Manuscript submitted for publication*

**2020, Proteogenomic subtyping of chronic lymphocytic leukemia identifies a poor outcome population with a distinct drug response profile**

**Herbst\***, Vesterlund\*, Jafari, Siavelis, Stahl, Schitter, Iskar, Liebers, Roider, Bruch, Lu, Richter, Knoll, Kolb, Lenze, Cao, Scheinost, Ganzinger, Kriegsmann, Kriegsmann, Müller-Tidow, Dreger, Anders, Zapatka, Stilgenbauer, Zenz, Huber, Tausch, Lehtiö<sup>+</sup>, Dietrich<sup>+</sup>

*Manuscript submitted for publication*

**2020, The Influence of the Bone Marrow Niche on Drug Response Phenotypes of Blood Cancers**

**Herbst**, Kim, Schitter, Roider, Bruch, Kolb, Knoll, Lu, Hüllelein, von Kalle, Lutz, Dreger, Müller-Tidow, Huber, Zenz, Dietrich

*Manuscript in preparation*

**2020, Image Analysis Techniques for Compound Screening in Patient-derived Blood Cancer Co-culture**

Kim, **Herbst**, Roider, Dietrich, Huber

*Manuscript in preparation*

## Publications related to blood cancers and drug screening

**2020, Dissecting intratumor heterogeneity of nodal B cell lymphomas at transcriptional, genetic, and drug response levels**

Roider, Seufert, Uvarovskii, Frauhammer, Bordas, Abedpour, Stolarczyk, Mallm, **Herbst**, Bruch, Balke-Want, Hundemer, Rippe, Goeppert, Seiffert, Brors, Mechttersheimer, Zenz, Peifer, Chapuy, Schlesner, Müller-Tidow, Fröhling, Huber, Anders<sup>+</sup>, Dietrich<sup>+</sup>

*Nature Cell Biology. <https://doi.org/10.1038/s41556-020-0532-x>*

**2018, Drug-perturbation-based stratification of blood cancer.**

Dietrich\*, Oleś\*, Lu\*, Sellner, Anders, Velten, Wu, Hüllelein, da Silva Liberio, Walther, Wagner, **Rabe**, Ghidelli-Disse, Bantscheff, Oleś, Ślabicki, Mock, Oakes, Wang, Oppermann, Lukas, Kim, Sill, Benner, Jauch, Sutton, Young, Rosenquist, Liu, Jethwa, Lee, Lewis, Putzker, Lutz, Rossi,

Mokhir, Oellerich, Zirlik, Herling, Nguyen-Khac, Plass, Andersson, Mustjoki, von Kalle, Ho, Hensel, Dürig, Ringshausen, Zapatka, Huber<sup>+</sup>, Zenz<sup>+</sup>

*The Journal of Clinical Investigation*, 128(1), 427–445. <https://doi.org/10.1172/JCI93801>

**2018, TRRAP is essential for regulating the accumulation of mutant and wild-type p53 in lymphoma.**

Jethwa, Slabicki, Hüllelein, Jentzsch, Dalal, **Rabe**, Wagner, Walther, Klapper, Bohnenberger, Rettel, Lu, Smits, Stein, Savitski, Huber, Aylon, Oren, Zenz

*Blood*, 131(25), blood-2017-09-806679. <https://doi.org/10.1182/blood-2017-09-806679>

## Conference talks and poster

**2019, The Influence of the Bone Marrow Niche on Drug Response Phenotypes of Blood Cancers**

**Rabe**

*Invited speaker at Cytodata 2019 in Heidelberg, Germany*

**2019, The Influence of the Bone Marrow Niche on Drug Response Phenotypes of Blood Cancers**

**Rabe, Schitter, Roider, Kolb, Knoll, Lu, Bruch, Hüllelein, Stolarczyk, von Kalle, Lutz, Dreger, Müller-Tidow, Zenz, Huber, Dietrich**

*Talk at German Conference on Bioinformatics (GCB) in Heidelberg, Germany*

**2018, The Influence of the Bone Marrow Niche on Drug Response Phenotypes of Blood Cancers**

**Rabe, Schitter, Roider, Bruch, Kolb, Stolarczyk, Hüllelein, Lu, von Kalle, Lutz, Dreger, Müller-Tidow, Zenz, Huber, Dietrich**

*Talk at 60th ASH (American Society of Hematology) Annual Meeting in San Diego, US*

**2018, The Influence of the Bone Marrow Niche on Drug Response Phenotypes of Blood Cancers**

**Rabe, Schitter, Roider, Bruch, Kolb, Stolarczyk, Hüllelein, Lu, von Kalle, Lutz, Dreger, Müller-Tidow, Zenz, Huber, Dietrich**

*Poster at 1st German Cancer Research Congress (GCRC) in Heidelberg, Germany*

**2018, The Influence of the Bone Marrow Niche on Drug Response Phenotypes of Blood Cancers**

**Rabe, Schitter, Roider, Bruch, Kolb, Stolarczyk, von Kalle, Zenz, Huber, Dietrich**

*Talk at e:Med Meeting 2018 in Berlin, Germany*

**2017, Image based drug profiling in co-cultures with EBImage**

**Rabe**

*Invited Speaker at European Bioconductor Meeting in Cambridge, UK*



# Acknowledgements

First of all, I would like to thank all patients who contribute to this work by giving blood.

Most of all I thank Sascha Dietrich for being my mentor, for challenging, supporting and encouraging me and for giving me the opportunity to constantly broaden my skill set and improve as a scientist. I really enjoyed all of our scientific discussions and am very thankful that you always valued my opinion. Your research on the intersection of the clinic, biology and bioinformatics really inspired me and allowed me to look beyond my field of research and to interact with many interesting people.

I would like to thank Benedikt Brors for supervising this thesis, his time and his valuable input during the thesis advisory committee meetings. Additionally, I would like to thank Martina Seiffert, Christof von Kalle and Simon Anders for the helpful discussions during lab and thesis advisory committee meetings. Moreover, I am very grateful to Thorsten Zenz for supporting us during the founding phase of the lab and giving the group a first home. Special thanks goes to Wolfgang Huber for sparking my interest in bioinformatics and supporting me during these last years.

I had the pleasure to work in a very collaborative environment and would like to thank all of the people involved. I especially thank my colleagues from the Karolinska Institute for making long-distance collaborations so easy and such a pleasure. Janne Lehtiö, Mattias Vesterlund, Matthias Stahl, Rozbeh Jafari and Ioannis Severin - it was very productive and a lot of fun working with you. Moreover, I thank Vlad Kim for making un-analysable images analysable. Thank you also to the Huber group, the AG Seiffert, AG Müller-Tidow and AG Zenz for the fruitful discussions and support. I would like to mention especially Alexander Jethwa, Lena Wagner, Tatjana Walther, Junyan Lu, Maike Janssen, Yi Liu and Murat Iskar and thank them for the good collaborations.

A special thanks goes to Haja Dominike Radic, Eva Schitter and Tina Becirovic. You were great students and I was very lucky to be your supervisor. It was a pleasure working with you.

I would like to especially thank the AG Dietrich. I had so much fun during my time with you, regardless of whether in the lab or during the many activities outside of it. Thank you Tobias Roider, Berit Brinkmann and Peter-Martin Bruch for the helpful scientific discussions and for sharing the joy and frustration of the everyday life of a scientist. I could not have wished for better office colleagues. Thank you Carolin Kolb, Mareike Knoll and Angela Lenze for keeping the lab running and for the great experimental support. Without you the past years would have

been much less productive. Thank you Nora Liebers, Sarah Richter, Leandra Caille, Xi Wang, Felix Czernilofsky, Antonia Angeli, Holly Giles, Donnacha Fitzgerald and Johannes Mammen for all of the nice lunch breaks, corona-coffee breaks, help, discussions and for making the AG Dietrich a great place to work.

I thank all of my friends for supporting me during the PhD, either by listening to the ups and downs of my project or by helping me to get my mind off science. A special thanks goes to my DKFZ girls and the 'lab meeting of bad results'. Thank you for taking the journey of the PhD with me together. Especially, I would like to thank my close friends Hanna Meichsner and Nils Kurzawa for everything. I cannot list all of the things you have done for me during the past years.

I am very grateful for all of the support from my family. My grandfather would have loved to see me graduate. I thank my parents for getting me to where I am today and for giving me the confidence to follow my passion without doubts. Moreover, I have two amazing brothers, who have on the one hand taught me that taking risks can be very rewarding and on the other hand provide a safe harbour for me to come back to.

Most of all I would like to thank Konrad Herbst, my partner in life, but also in science. You have contributed so much to my research by critically discussing results, providing ideas, broadening my scientific knowledge and most of all by always having my back, helping me to deal with stress and catching me when I have had a frustrating day. I am very lucky to have you by my side.

## Contributions

Fig. 1.1 and 1.2 were originally published in Kipps et al. (2017) and reused with permission.

The results described in sections 3.1.2 and 2.3 have been submitted for publication (Herbst et al., 2020b). The text was originally written by me and has been modified for this thesis. The text in section 2.3.1 was in parts written by Marta Stolarczyk but was included in this thesis for the sake of completeness. The experiments described in sections 3.1.2 and 2.3 were performed with assistance from Marta Stolarczyk and Carolin Kolb. Proteomics of stroma cells and detection of differential proteins, described in sections 2.3.7 and 3.1.2.6 was performed by the Proteomics Core Facility at EMBL.

The experiment presented in Fig. 3.7 was conducted in a joined effort with Tobias Roeder. The analysis and figure were produced by Tobias Roeder and used with permission.

The results described in section 3.2 have been submitted for publication (Herbst et al., 2020c). The text in the manuscript was originally written by me and has been modified for this thesis. The sample preparation steps described in sections 3.2.1 and 2.4.1 were performed with technical assistance from Carolin Kolb, Mareike Knoll and Angela Lenze. The proteomic data acquisition described in section 2.4.2 was performed by our collaborators from Janne Lehtiö's group, Karolinska Institute, Stockholm. The corresponding methods section was written by them but included in this thesis for the sake of completeness. IGHV status analysis described in section 2.4.3 was performed by Bettina Maier from the University Hospital Heidelberg. DNA panel sequencing of CLL samples, described in section 2.4.4, was performed and variants were called by our collaborator Eugen Tausch from the Uniklinikum Ulm. DNA copy number assessment, described in section 2.4.5, was performed as routine analysis by the University Hospital Heidelberg. Stranded mRNA sequencing, described in section 2.4.6 was performed with assistance from the EMBL Genomic Core Facility. Alignment and counting of reads was performed by our collaborator Junyan Lu from the Huber group, EMBL. The analysis of time to next treatment, described in section 2.6.3 was performed in a joined effort with Tobias Roeder. Formatting of the multi-omics data was in parts done by Eva Schitter. Clinical data was gathered by Nora Liebers.

The results described in section 3.3 are currently in preparation for publication (Herbst et al., 2020a). The text was written by me for this thesis and will be modified for the publication. The MSC experiment described in section 2.5.5 was conducted with technical assistance from Carolin Kolb. The Western Blots described in section 2.5.6 were conducted with technical assistance from Carolin Kolb and Mareike Knoll.

# 1 Introduction

## 1.1 General disease characteristics and clinical course of CLL

Chronic lymphocytic leukemia (CLL) is the most common leukemia in adults in the Western world, with an incidence of  $\sim 6$  cases per 100 000 people in Europe (Kipps et al., 2017). Disease onset occurs at a median age of 70 years (Bosch and Dalla-Favera, 2019). The chronic neoplasm is characterised by an accumulation of malignant B-cells in the blood, secondary lymphoid tissues and the bone marrow (Bosch and Dalla-Favera, 2019). Advances in the past decade have highlighted the importance of B-cell receptor signalling for this chronic disease and dramatically changed the therapy of CLL. As new targeted agents, like the Bruton's tyrosine kinase (BTK) inhibitor ibrutinib, have shown great success in the clinic, treatment strategies are moving further away from standard chemotherapy (Scheffold and Stilgenbauer, 2020). Despite this promising development, CLL is still considered an incurable malignancy (Bosch and Dalla-Favera, 2019). Moreover, the disease is characterised by a very heterogeneous clinical course, with some patients dying within months, while others live with the disease for several decades (Boelens et al., 2009). Patients which are asymptomatic can be followed for years with a watch-and-wait approach, while others need frequent treatment (Hallek, 2017). Even though especially genetic aspects of this malignancy have been thoroughly characterised (Fabbri and Dalla-Favera, 2016), the underlying biology of the clinical heterogeneity has still not been completely understood.

## 1.2 Cell of origin of CLL and IGHV status

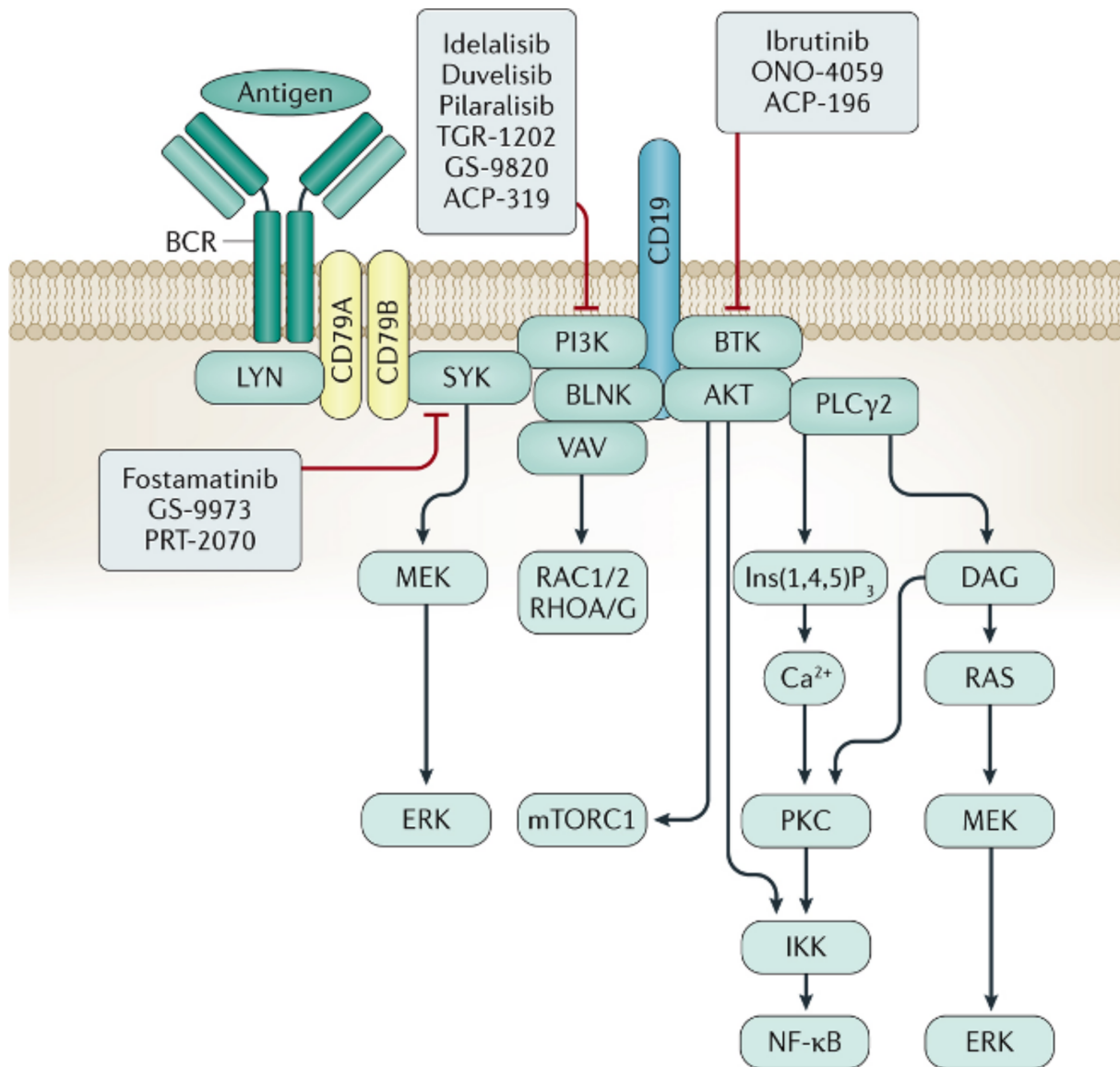
CLL originates from mature  $CD5^+CD23^+$  B-cells (Bosch and Dalla-Favera, 2019). B-cells are immune cells derived from the lymphoid lineage of hematopoiesis. During their development in the bone marrow from pro-B-cells to pre-B-cells and finally immature B-cells, the immunoglobulin (Ig) heavy- and light-chain genes are step-wise rearranged to form a functional B-cell receptor (BCR). The rearrangement contributes to the development of a diverse BCR repertoire. The process is tightly controlled to ensure good binding affinity and prevent reactivity of the BCR against autoantigens. During their development, B-cells are in close contact with bone marrow stroma cells (BMSCs), which provide signals required for B-cell survival and selection. Immature B-cells passing the quality criteria migrate to secondary lymphoid organs, like the lymph nodes, where they can encounter antigens. Mature B-cells which have not been exposed to their antigen are termed "naive" (Murphy, 2012). Upon binding of the right antigen, B-cells start to proliferate in germinal centres. Concurrently, somatic hypermutations introduce base pair changes into the genes of the immunoglobulin variable regions to further expand the B-cell repertoire (De Silva and Klein, 2015).

Two major subtypes of CLL exist, characterised by whether the cells have undergone this germinal centre reaction. This can be determined by the degree of somatic hypermutations in the immunoglobulin heavy-chain variable region (IGHV) genes. CLL cells with mutated IGHV (M-CLL) are believed to originate from antigen-experienced B-cells, having undergone the germinal centre reaction in secondary lymphoid organs. IGHV unmutated CLL (U-CLL) cells, on the other hand, did not go through the germinal centre reaction, however, it remains unclear whether they are derived from naive B-cells or a different line of precursor B-cells (Bosch and Dalla-Favera, 2019; Klein et al., 2001). In the past, protein levels of ZAP-70 and CD38 have been used as surrogate markers for IGHV status, as they closely correlate with the presence of somatic hypermutations in the IGHV locus (Crespo et al., 2003). The two subtypes are characterised by distinct molecular and clinical phenotypes. M-CLL is usually associated with a higher load of mutations outside the Ig loci than U-CLL, however, U-CLL show an enrichment for mutations in known drivers of CLL (Burns et al., 2018). This is in accordance with the more aggressive phenotype, shorter time to next treatment (TTT) and shorter overall survival (OS) of U-CLL. In contrast, many M-CLL patients can be followed by a watch-and-wait approach for years (Damle et al., 1999; Hamblin et al., 1999). Thus, IGHV mutational status is one of the most informative prognostic biomarkers in CLL.

### 1.3 B-cell receptor signalling in CLL

One of the most important pathways in CLL is the BCR signalling pathway (Fig. 1.1; Kipps et al. (2017)). This is illustrated by the clinical success of BCR signalling inhibitors, which have revolutionised CLL therapy in recent years (Byrd et al., 2013). Two BCR signalling modes have been described for normal and CLL B-cells: active and tonic BCR signalling (Kraus et al., 2004; Lam et al., 1997; Srinivasan et al., 2009). Active BCR signalling is triggered by the binding of an antigen to the BCR, leading to phosphorylation of SYK and subsequent signal transmission through the molecules BTK, BLNK and PLC $\gamma$ 2. The downstream pathways activated by these proteins include PI3K, AKT, ERK/MAPK and NF $\kappa$ B signalling (Fig. 1.1; Burger and Wiestner (2018); Kipps et al. (2017)). In CLL the mode of this active BCR signalling is dependent on the IGHV mutational status. U-CLL cells, which have not been subjected to the germinal centre reaction, express BCRs able to recognise various auto- or foreign antigens, making them more responsive to stimulation of the BCR (Burger and Wiestner, 2018; Lanham et al., 2003). M-CLL cells, on the other hand, have encountered their antigen and the BCRs have undergone further selection processes to increase affinity of antigen binding. Thus, BCRs from M-CLL patients only recognise very specific antigens and are, therefore, much harder to activate with a general stimulus (Burger and Wiestner, 2018).

Tonic BCR signalling, on the other hand, is believed to be especially required for the survival of B-cells (Kraus et al., 2004). It is probably independent of an antigen stimulus, as BCRs with a truncated antigen binding domain are still able to provide survival signals to B-cells (Kraus et al., 2004; Shaffer and Schlissel, 1997). In contrast to active BCR signalling, tonic BCR signalling does not activate all of the pathways shown in Fig. 1.1. The NF $\kappa$ B pathway, for example, is specific for active BCR signalling (Puła et al., 2019). PI3K, on the other hand, seems to be



Nature Reviews | Disease Primers

Figure 1.1: **B-cell receptor signalling.** Upon antigen binding the B-cell receptor (BCR) and its co-receptor CD19 get activated. Phosphorylation of CD79A and CD79B allows the binding and signal transmission by SYK. With the help of BTK, BLNK and PLCγ2 downstream pathways, like PI3K, AKT, ERK/MAPK and NFκB signalling can be induced. Some inhibitors blocking the activity of kinases within BCR signalling are shown. This figure was originally published in Kipps et al. (2017) and reused with permission.

one of the major players in tonic BCR signalling. This is supported by the observation that the lethality of mouse B-cell, induced by deletion of the BCR (Kraus et al., 2004; Lam et al., 1997), can be rescued by constitutive activation of PI3K (Srinivasan et al., 2009).

## 1.4 Genetics of CLL

### 1.4.1 Recurrent mutations

CLL has a mutational rate of  $\sim 0.9$  mutations per megabase, which is lower than in most adult solid tumours, but comparable to acute myeloid leukemia. Despite this low rate, the genetic landscape of CLL is very heterogeneous and only few mutations occur at a frequency of more than 5% (Bosch and Dalla-Favera, 2019). A common genetic driver across CLL patients is lacking, however, some genetic lesions in specific pathways have been shown to drive tumour progression in subsets of patients (Fabbri and Dalla-Favera, 2016).

As in most cancers, the DNA damage response pathway plays a major role in CLL development. Accordingly, the mutation with the strongest clinical impact occurs in *TP53*, a tumour suppressor gene protecting genome integrity. These alterations are present with a frequency of  $\sim 9\%$  (Bosch and Dalla-Favera, 2019; Zenz et al., 2010) and are associated with a very poor prognosis. This is partly because they convey resistance to chemotherapeutic agents (Zenz et al., 2010). Of note, *TP53* mutated CLL cells also do not respond to nutlin 3a, which is a drug not clinically approved, but often used in anti-cancer studies. Nutlin 3a inhibits MDM2, an E3-ubiquitin ligase responsible for the degradation of p53 (Jethwa et al., 2018). As tumour suppressor, the loss of native p53 function is implicated in instabilities of the genome and resistance to apoptosis (Fabbri and Dalla-Favera, 2016). However, not only loss-of-function but also gain-of-function phenotypes have been described for *TP53*. In these cases the mutant form of p53 acquires new functions promoting tumour formation and progression. This is usually accompanied by an accumulation of the mutant form of p53 within the cell (Dittmer et al., 1993; Oren and Rotter, 2010).

Upon DNA damage, activation of p53 occurs through the tumour suppressor ATM. ATM is a protein kinase which recognises DNA double strand breaks and initiates DNA damage response signalling through phosphorylation of its target proteins (Alberts et al., 2008; Austen et al., 2005). The *ATM* gene has been found to be recurrently mutated in CLL with a frequency of  $\sim 10\%$  (Bosch and Dalla-Favera, 2019). Mutations in *ATM* have been associated with shorter TTT and OS (Austen et al., 2005). In contrast to *TP53* mutations, *ATM* mutations have only been associated with a loss-of-function phenotype in CLL (Navrkalova et al., 2013).

Other genes directly or indirectly involved in DNA damage response and occasionally mutated in CLL are *POT1* and *XPO1*. *POT1* is responsible for protecting the ends of chromosomes from damage (Loayza and De Lange, 2003). *XPO1* is a protein involved in nuclear export. Among its many target proteins is also the tumour suppressor p53 (Camus et al., 2017). Thus, *XPO1*

indirectly contributed to DNA damage control. However, mutations in *POT1* and *XPO1* are rare in CLL and occur at frequencies below  $\sim 5\%$  (Fabbri and Dalla-Favera, 2016).

Apart from changes in DNA damage response pathways, the spliceosome is frequently affected by mutations in CLL. This involves mainly the gene for the splicing factor 3B subunit 1 (*SF3B1*), which is a crucial component of the spliceosome (Bosch and Dalla-Favera, 2019). Recently, missplicing of BRD9, a protein involved in chromatin-remodelling, has been suggested as potential oncogenic driver in *SF3B1* mutated cancers. Thus, altered splicing leads to the inclusion of a poison exon in BRD9 and, consequently, its degradation (Inoue et al., 2019). The frequency of *SF3B1* mutations increases from  $\sim 10\%$  at diagnosis to  $\sim 17\%$  in chemotherapy refractory patients, highlighting its importance in the progression of CLL (Bosch and Dalla-Favera, 2019).

With a frequency of  $\sim 12\%$  *NOTCH1* is the most commonly mutated gene in CLL at diagnosis (Bosch and Dalla-Favera, 2019). The NOTCH signalling pathway is one of the crucial players in development and the determination of cell fate. Signals are transmitted through the proteolytic cleavage of the intracellular domain of NOTCH1 (Alberts et al., 2008), leading to the expression of genes involved in metabolism, survival and proliferation (Bosch and Dalla-Favera, 2019; Fabbri and Dalla-Favera, 2016). In CLL the consequence of *NOTCH1* mutations is the removal of the PEST domain from the protein, conveying increased stability to the intracellular domain upon proteolytic cleavage and causing decreased OS of patients (Bosch and Dalla-Favera, 2019).

Other mutated pathways in CLL include the regulation of cell cycle control and apoptosis (e.g. *KRAS* mutations) and BCR–NF $\kappa$ B–TLR signalling (e.g. *BIRC3* and *EGR2* mutations), however, these mutations occur at frequencies below 5% (Fabbri and Dalla-Favera, 2016).

#### 1.4.2 Recurrent structural aberrations

In addition to mutations, recurrent structural aberrations are commonly found in CLL. In accordance with the strong phenotype of *TP53* mutations, deletion of the p13 arm of chromosome 17 (del17p13), on which *TP53* is located, has a strong clinical impact (Döhner et al., 1995, 2000). Del17p13 is present at frequencies of  $\sim 7\%$  (Kipps et al., 2017) and often co-occurs with *TP53* mutations ( $\sim 80\%$  of cases). The co-occurrence of these two alterations causes the loss of the native function of both copies of *TP53* (Bosch and Dalla-Favera, 2019). Similarly to *TP53* mutations, the presence of del17p13 reduces sensitivity of patients to chemotherapy (Döhner et al., 1995). *TP53* mutations as well as del17p13 are routinely assessed in the clinic and treatment decisions are based on their presence (Gaidano and Rossi, 2017).

The region deleted in the frequent chromosomal aberration del11q contains the tumour suppressor gene *ATM*, which has been suggested to be the main target of this variation (Fegan et al., 1995). Taken together, *ATM* mutations and del11q occur in  $\sim 20\%$  of patients (Bosch and Dalla-Favera, 2019). Like del17p13, del11q is understood as high-risk genetic lesion in CLL (Döhner et al., 2000).

With a prevalence of  $\sim 55\%$  del13q14 is the chromosomal aberration most commonly observed in CLL. Presence of del13q14 results in a better prognosis for patients (Döhner et al., 2000). The underlying pathological mechanism of del13q14 has been well described. The region affected in del13q14 contains the two micro-RNAs miR-15a and miR-16-1, which are responsible for the suppression of the G0-G1-transition and, thus, proliferation. In mouse models it has been shown that deletion of the miR-15a/16-1 locus is enough to lead to the development of clonal lymphoproliferation (Klein et al., 2010).

About 15-20% of CLL patients harbour a trisomy of chromosome 12 (Abruzzo et al., 2018; Bosch and Dalla-Favera, 2019). While for del17p13, del11q and del13q14 the underlying mechanisms have been thoroughly explored, the molecular cause of the biological changes induced by trisomy 12 still remain largely unknown (Bosch and Dalla-Favera, 2019). Trisomy 12 is found more often in M-CLL than U-CLL patients (Hamblin et al., 1999) and is associated with an abnormal cellular morphology (Bosch and Dalla-Favera, 2019) and an intermediate prognosis (Döhner et al., 2000). We recently described that the presence of trisomy 12 sensitises CLL samples to *ex-vivo* treatment with BCR inhibitors (Dietrich et al., 2018). However, a functional explanation for this sensitivity has to date not been found and requires further mechanistic investigations.

## 1.5 The transcriptome of CLL

In addition to the genetic landscape, the CLL transcriptome has been thoroughly described. Comparison of RNA sequencing results from normal and CLL B-cells has identified many deregulated pathways in CLL. CLL cells showed downregulation of genes involved in splicing, proteasomal and ribosomal genes, while genes involved in BCR, JAK and metabolic signalling were among the most upregulated in comparison to normal B-cells. Not only expression of coding, but also non-coding genes was changed in CLL. Additionally, differences in RNA splicing were identified between CLL and normal B-cells, among others involving the BCL-2 transcript (Ferreira et al., 2014).

As mentioned above, mutations in *SF3B1* are known to be important for CLL progression. As the involved gene encodes a splicing factor, this could have functional consequences for the CLL transcriptome. Indeed, the studies of Wang et al. (2016) and Ferreira et al. (2014) observed a characteristic splicing pattern for *SF3B1* mutated CLL, with differential splicing of especially 3' splice sites.

In addition, transcriptomics has been used to define signatures identifying patient groups with poor prognosis. Thus, Orgueira et al. (2019) have found a transcriptional pattern which, in addition to the IGHV status, subdivided CLL into four groups with different TTT. A similar division of patients, based on consensus clustering, had already been observed by Ferreira et al. (2014). The transcriptomic patterns, which were in addition to the IGHV status driving this grouping, were termed C1 and C2 in both studies. However, in Ferreira et al. (2014) the C1/M-CLL group had the most favourable outcome, while in Orgueira et al. (2019) this was the

case for the C2/M-CLL group. Similarly, C2/U-CLL had the worst prognosis in Ferreira et al. (2014), while in Orgueira et al. (2019) C1/U-CLL was the group with the worst outcome. Both studies did not provide a comprehensive characterisation of the underlying genetic backgrounds of the samples, thus, precluding the analysis of the groups in relation to any genetic alterations.

Other studies have focused on the understanding of how the different niches influence the gene expression of CLL cells. Herishanu et al. (2011), for example, have identified that the BCR and NF $\kappa$ B signalling pathways are upregulated in CLL cells residing in the compartment of the lymph node, in comparison to CLL cells from peripheral blood.

In a very recent study, we have shown for other B-cell cancer entities that single cell transcriptomic sequencing can track the evolution of resistant clones and uncover drug vulnerabilities (Roeder et al., 2020). Approaches to unravel the intra-tumour heterogeneity using such novel methodologies have also been used in CLL (Gohil and Wu, 2019). Thereby, novel drivers of CLL malignancy were suggested (Wang et al., 2017) and the clonal evolution of CLL cells of a single patient could be tracked over decades (Zhao et al., 2016). Further studies moving into the direction of single cell analysis will most likely provide exiting new insights into the evolution and clonal heterogeneity of the disease.

## 1.6 Proteogenomic profiling

### 1.6.1 The proteome of CLL

The proteome of CLL has been much less understood than its genetic and transcriptomic landscape. The first study describing the proteome of CLL was conducted by Perrot et al. (2011) who identified differential protein abundances between three U-CLL and three M-CLL patient samples by using quantitative two-dimensional fluorescence difference gel electrophoresis. Differences between protein levels in U-CLL (nine patients) and M-CLL (nine patients) could later be confirmed by Eagle et al. (2015). Through the use of isobaric tags for relative and absolute quantification (iTRAQ) based mass spectrometry, they were able to identify 3 521 proteins and found migratory pathways to be differentially regulated between U-CLL and M-CLL (Eagle et al., 2015). Moreover, the proteome of CLL has been compared to healthy B-cells in small cohorts of CLL patients (nine CLL in Mayer et al. (2018) and 14 CLL in Johnston et al. (2018)). These studies revealed that aged B-cells are more similar to CLL B-cells than B-cells from young individuals. Moreover, proteomic changes affecting the splicing machinery and metabolic pathways were prominent in CLL (Johnston et al., 2018; Mayer et al., 2018). Even though all of these studies highlighted important aspects of the biology of CLL, a systematic analysis of a larger cohort of CLL patients and the integration with other datasets is still lacking.

### 1.6.2 Proteogenomic profiling in other cancer entities

Recent developments in mass spectrometry have enabled the proteomic profiling of multiple samples in parallel, allowing the unbiased comparison of specimen from different cancer patients (Branca et al., 2014). Concurrently, the field of proteogenomics evolved, which tries to integrate

the results obtained from quantitative proteomics with genomics and often also other omics datasets. Through this approach new insights for many different cancer entities have been gained, including solid cancers, like breast (Johansson et al., 2019; Mertins et al., 2016), gastric (Mun et al., 2019), colon and rectal (Vasaikar et al., 2019; Zhang et al., 2014), ovarian (Zhang et al., 2016), liver (Dong et al., 2019) and prostate cancer (Sinha et al., 2019), as well as acute leukemias (Alanazi et al., 2020; Yang et al., 2019) and medulloblastoma (Archer et al., 2018). In general, these investigations showed that mRNA and protein levels are not necessarily well correlated, copy-number alterations impact not only mRNA but also protein levels and that proteins seem to have a more direct impact on functional consequences. Additionally, some studies could identify potential new clinical targets and different clinically relevant subgroups within their entity. As the heterogeneous clinical course between different CLL patients is still not completely understood (Hallek, 2017), proteogenomics could be an interesting approach to further characterise this disease.

## 1.7 Targeted therapies for the treatment of CLL

Chemoimmunotherapy had been the gold standard in the treatment of CLL for many years. However, not all patients profit equally from this therapy, with worse outcome for U-CLL, *SF3B1* and *TP53* mutated CLL and patients with del17p13. Since the approval of the BCR signalling inhibitor ibrutinib for the treatment of CLL in 2014, therapy regimens have drastically changed (Scheffold and Stilgenbauer, 2020). Ibrutinib irreversibly inhibits BTK and is even effective in high-risk CLL patients (Bosch and Dalla-Favera, 2019). Because of its broad activity, it is nowadays used not only for the treatment of chemoimmunotherapy refractory patients and patients who do not respond to chemotherapy (Byrd et al., 2013) but also as front-line therapy (Bosch and Dalla-Favera, 2019). Despite this considerable success, patients on ibrutinib rarely reach complete remission and minimal residual disease often remains in the bone marrow (Byrd et al., 2013). Therefore, ibrutinib has to be administered continuously and many patients are on ibrutinib for many years (Byrd et al., 2013; Woyach and Johnson, 2015). A small proportion of patients develop ibrutinib resistant clones, which often occurs through mutations in the genes for BTK or PLC $\gamma$ 2 (Woyach and Johnson, 2015).

Another targeted drug approved for CLL is idelalisib. It targets the delta isoform of PI3K and has shown great efficacy in the treatment of CLL (Furman et al., 2014), with an overall response rate of 72% in relapsed and refractory CLL patients and a progression free survival of 32 months (Brown et al., 2014). Even though efficiencies are comparable to those of ibrutinib, idelalisib causes more toxicities, which makes ibrutinib the more suitable treatment for most patients (Burger and O'Brien, 2018).

In addition to BCR signalling inhibitors, the approval of the BCL-2 inhibitor venetoclax has greatly improved therapy options for patients. Like ibrutinib and idelalisib it can be administered orally and is an attractive option for patients relapsed on chemotherapy or ibrutinib treatment (Burger and O'Brien, 2018). Relapsed or refractory CLL patients had a two-year progression-free survival rate of 85% under venetoclax treatment and no specific restrictions for any genetic

alteration were observed (Seymour et al., 2018). Interestingly, complete remissions are much more frequent with venetoclax than with the other targeted agents and is observed in  $\sim 20\%$  of patients (Roberts et al., 2016). In line with this, minimal residual disease in the bone marrow is less common (Roberts et al., 2016).

## 1.8 *Ex-vivo* drug sensitivity screening

The investigation of the relationship between genetic factors and responses to therapy has helped to develop valuable biomarkers (Bosch and Dalla-Favera, 2019). However, many associations between cell-intrinsic factors and drug response remain unknown and prediction of how and why a patient reacts to a certain drug is still not completely possible. *Ex-vivo* drug sensitivity screening can help to fill these gaps. For this, tumour cells are perturbed with a set of different drugs in microtiter plates (Letai, 2017). In combination with a profound characterisation of the samples, the measured *ex-vivo* drug response profiles can be used for the discovery of new biomarkers. Multiple screens of large collections of cell-lines from many different tumour entities have been conducted, which were able to correlate genetic features with drug sensitivities (Barretina et al., 2012; Basu et al., 2013; Garnett et al., 2012; Iorio et al., 2016). Instead of using cell lines, which do not fully represent tumour heterogeneity (Goodspeed et al., 2016), also primary tumour cells collected from patients have been used for *ex-vivo* drug screening (Dietrich et al., 2018; Pemovska et al., 2013; Snijder et al., 2017; Tyner et al., 2013). One example is our study in which we combined genetic, transcriptomic and methylomic information from 184 CLL patients with drug response profiling. Thus, the patient samples could be classified into subgroups with vulnerabilities to either BCR, mTOR or MEK inhibitors. Most importantly, *ex-vivo* drug responses were associated to clinical outcome (Dietrich et al., 2018). The usage of *ex-vivo* drug sensitivity profiling has been suggested for personalised medicine. A clinical trial resulting from our study (Dietrich et al., 2018) is currently ongoing (ClinicalTrials.gov Identifier: NCT03488641). Additionally, other results across different haematological malignancies look promising and are currently proving the feasibility of using *ex-vivo* drug screening to guide treatment decisions (Pemovska et al., 2013; Snijder et al., 2017; Tyner et al., 2013).

## 1.9 Importance of the microenvironment in CLL

CLL is not only a disease of the blood, but also comprises other lymphoid compartments, like the lymph node and the bone marrow (Burger and O'Brien, 2018). While CLL cells circulating in the blood are mostly found in a resting state, up to 3% of cancer cells start to proliferate in the lymph nodes (Herndon et al., 2017). The important role of these niches in disease pathogenesis is demonstrated by the fact that CLL cells undergo spontaneous apoptosis *ex-vivo* (Collins et al., 1989). The CLL microenvironment consists of many different cell types, including T-cells, follicular dendritic cells, nurse-like cells and BMSCs. They interact with CLL cells through a range of soluble factors and direct cell-cell contact (Fig. 1.2; Kipps et al. (2017)). By providing these signals from the microenvironment to CLL cells cultured *ex-vivo* spontaneous apoptosis can be prevented. Thus, it has been shown that BMSCs, one of the most important interaction partners of B-cells in the bone marrow niche (Murphy, 2012), can rescue CLL cells

from spontaneous apoptosis (Herbst et al., 2020a; Lagneaux et al., 1998; Panayiotidis et al., 1996)

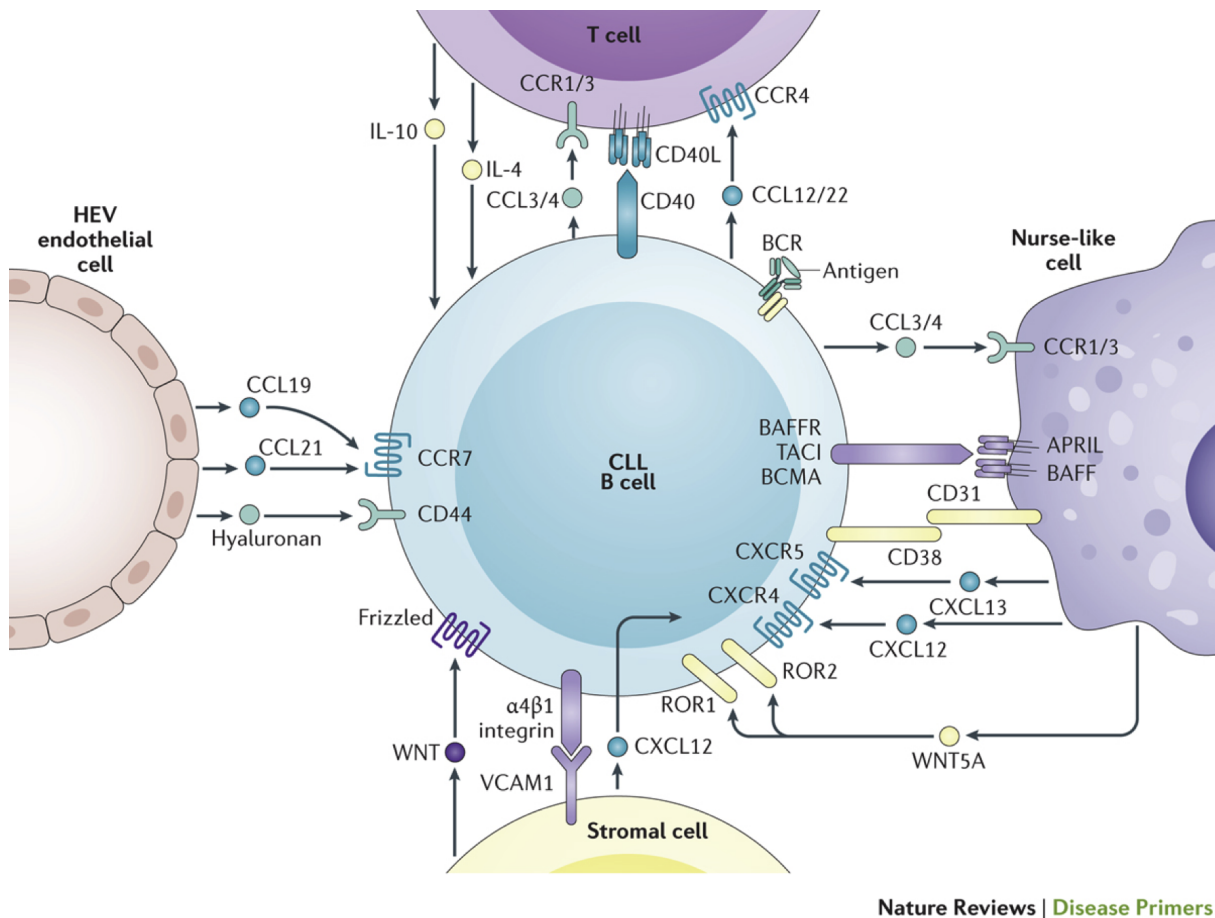


Figure 1.2: **The CLL microenvironment.** CLL cells receive input from various cells of the microenvironment through soluble factors and direct cell-cell contacts. This figure was originally published in Kipps et al. (2017) and reused with permission

### 1.9.1 Models for mimicking the microenvironment in CLL

As the microenvironment plays a crucial role in disease pathogenesis of CLL it is important to further understand the involved compartments and interactions. For this, appropriate model systems are needed. Different approaches for modelling the niches of the bone marrow and the lymph node have been taken. One strategy is to supplement CLL cell mono-cultures with specific signalling molecules known to be present in the respective niches to analyse their impact on cancer cells (Crassini et al., 2017). However, the addition of selected stimuli only probes the influence of specific pathways and cannot recapitulate the complexity of the microenvironment.

A second approach is well suited to study the influence of soluble components on CLL cells. For this, conditioned medium is produced from cells from the microenvironment and transferred to CLL mono-cultures. This model focuses on understanding the influence of the entire soluble microenvironment, rather than on dissecting individual pathways in an isolated setting.

Models using conditioned media take soluble factors into account, yet, they neglect the direct interactions through cell-cell contact, which are essential for leukemia cells (Bakker et al., 2016). Therefore, models using co-cultures of CLL and microenvironmental cells are indispensable to gain a more complete picture on the impact of non-malignant cells on leukemia cells. For this, different components of the cellular microenvironment can be used, depending on the objective of the research. One major interaction partner of CLL cells are T-cells. To decipher the consequences of this interaction, co-cultures of CLL and T-cells can be established. Such studies have revealed that especially stimulation with CD40L and IL-21 contributes to T-cell induced proliferation of CLL cells (Pascutti et al., 2013). Instead of the direct usage of T-cells, CD40L can be expressed on the surface of fibroblasts to induce CD40-mediated signalling in CLL (Crassini et al., 2017). Even though the CD40/CD40L system is commonly used to simulate the microenvironment, it again only relies on a single pathway to activate CLL cells.

Other studies used co-cultures of leukemia cells and so-called nurse-like cells as model system. Nurse-like cells have been first described by Burger et al. (2000) and protect CLL cells from spontaneous apoptosis. The cells spontaneously outgrow from cultures of peripheral blood mononuclear cells (PBMCs) and are of monocytic origin (Ten Hacken and Burger, 2016). Their protective effect on CLL cells has especially been attributed to the activation of BCR and  $\text{NF}\kappa\text{B}$  within CLL cells upon co-culturing with nurse-like cells (Burger et al., 2009).

To recapitulate the interactions of CLL with the bone marrow microenvironment, especially the influence of BMSCs needs to be taken into account. The first approaches into this direction have been taken by co-culturing primary mesenchymal stem cells (MSCs), isolated from bone marrow aspirates of donors, with CLL cells. These experiments have shown that MSCs generally protect CLL cells from spontaneous apoptosis *ex-vivo* through soluble factors and direct cell-cell contact (Lagneaux et al., 1998; Panayiotidis et al., 1996; Plander et al., 2011). As primary material is not readily available for all research groups and primary cells are in general more challenging to handle, multiple bone marrow derived stroma cell lines have been established from murine or human donors (Kurtova et al., 2009). Two of the most commonly used human bone marrow stroma cell lines are HS-5 and NKTert (Kawano et al., 2003; Roecklein and Torok-Storb, 1995). Both cell lines have been shown to provide protection to CLL cells from spontaneous apoptosis, however, the effect of NKTert cells was especially pronounced (Balakrishnan et al., 2015; Cheng et al., 2014; Fiorcari et al., 2013; Guo et al., 2017; Kurtova et al., 2009; Vangapandu et al., 2018; Zhang et al., 2012). The cell lines have been widely used in many research studies and helped to gain valuable insights into how CLL and the bone marrow microenvironment interact. However, investigators should always be aware that these cell lines only represent artificial systems and that the obtained results should always be validated in other models.

### 1.9.2 Influence of the bone marrow niche on drug responses in CLL

During therapy, especially with new targeted agents, clearance of leukemia cells from the blood can often be achieved. However, in most cases minimal residual disease, particularly in the bone

marrow, persists (Burger and O'Brien, 2018). Due to this, it is assumed that the niche of the bone marrow protects CLL cells from drug-induced apoptosis and, thereby, contributes to the emergence of resistant clones (Ten Hacken and Burger, 2016). Few studies exist which have investigated the influence of the bone marrow on the response to selected drugs to further understand the mechanisms of drug resistance. Thus, the chemotherapeutics fludarabine, oxaliplatin, chlorambucil, cyclophosphamide and doxorubicine have been described to have diminished effects in co-cultures with stroma cells (Kay et al., 2007; Kurtova et al., 2009; Mraz et al., 2011; Zhang et al., 2012). Moreover, a reduced efficiency has been shown for the corticosteroid medications hydrocortisone and dexamethasone (Kurtova et al., 2009; Panayiotidis et al., 1996). Furthermore, protection of CLL cells from carilzomib-induced apoptosis has been mentioned (Gupta et al., 2013). Importantly, some studies reported stroma cell mediated resistances to ibrutinib treatment (Cheng et al., 2014; Guo et al., 2017), which might explain why complete eradication of leukemia cells from the bone marrow is rare during therapy with ibrutinib (Byrd et al., 2013). One suggestion for overcoming these resistances is the simultaneous targeting of SYK and JAK with the drug cerdulatinib (Guo et al., 2017). Additionally, the BCL-2 inhibitor AT-101 was able to overcome stroma mediated protection, which might represent an interesting option for avoiding resistance (Balakrishnan et al., 2009). These investigations provide important insights into the effect of stroma cells on drug action. However, to date a systematic investigation of the effect of stroma cells on drug response is lacking. Only a comprehensive evaluation will enable a better understanding of these interactions and allow the development of efficient strategies to overcome the emergence of drug resistances in the bone marrow.

## 1.10 Aims of the thesis

To date the heterogeneous disease course, biology and drug response profiles between CLL patients have not been completely understood. Even though drug response and patient outcome are strongly influenced by numerous cell-intrinsic and extrinsic factors (Fig. 1.3), only certain aspects, like the genetic landscape of CLL, have been thoroughly characterised. So far, an integration also with other cell-intrinsic layers, like the proteome, and a systematic description of the influence of the microenvironment is lacking. Thus, the most important goal of this thesis is to obtain a more complete picture of the different factors influencing drug response and outcome in CLL. This is achieved by addressing the following three main aims.

### 1.10.1 Aim 1: Establishment of a system for co-culture drug sensitivity screening in CLL

Drug-sensitivity screens have been established and conducted for mono-cultures of primary CLL patient samples. However, cell-extrinsic stimuli supplied by the bone marrow microenvironment play an important role in CLL. Even though the effect of the microenvironment on responses to individual drugs has been shown, a systematic analysis is lacking. This is mainly because setups to systematically probe drug responses in the context of cellular components of the bone marrow microenvironment do currently not exist. Therefore, the first aim of this thesis is to set up a platform which allows systematic testing of drug response profiles of primary CLL cells co-

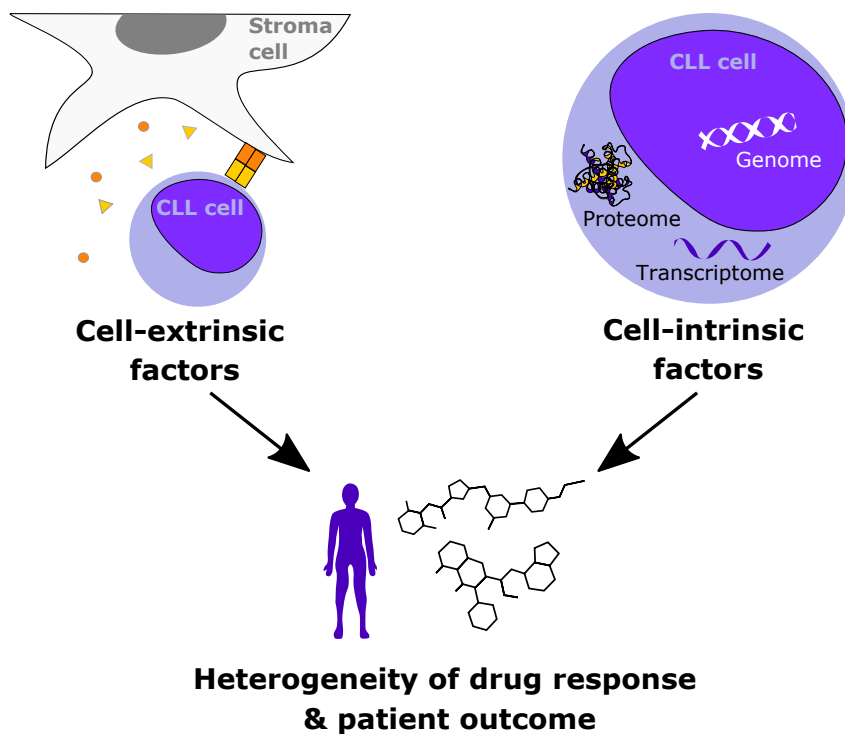


Figure 1.3: **Factors influencing outcome and drug response.** Cell-extrinsic factors, like the interaction with the microenvironment, and cell-intrinsic factors, like the proteome, genome and transcriptome, determine drug response and outcome of CLL.

cultured with bone marrow stroma cells. For this, careful evaluation of the bone marrow stroma cells used as model is crucial. Moreover, culture conditions, like the assay format, cell densities and the work-flow need to be optimised. Finally, the optimal screening setup will be used to perform a systematic co-culture drug-screen in a cohort comprising 81 CLL patient samples.

### 1.10.2 Aim 2: Analysis of cell-intrinsic factors by proteogenomic characterisation of primary CLL patient samples

The molecular background of the cells of every leukemia patient is unique. To thoroughly evaluate the impact of these cell-intrinsic factors on drug response and outcome, the second aim of this thesis is to perform a proteogenomics analysis of the primary CLL patient samples used in the co-culture drug screen. This comprehensive proteogenomic approach involves the measurement of proteomic, transcriptomic and genetic profiles from 68 CLL patient samples. In order to link molecular alterations to functional consequences the proteogenomic dataset will be connected with the mono-culture drug-sensitivity data and clinical parameters of CLL samples. Even though the value of proteogenomics has recently been demonstrated for multiple, mainly solid, cancer entities, the proteome of CLL has so far only been described in small cohorts. Additionally, systematic integration with other omics datasets and functional consequence is lacking. This work will reveal the potential of integrating proteogenomics of primary cancer patient samples with functional screening and represent the first proteogenomic characterisation of CLL.

### **1.10.3 Aim 3: Analysis of cell-extrinsic factors by systematic description of the influence of bone marrow stroma cells on drug response in CLL**

The third aim is to understand the influence of cell-extrinsic factors on drug response in CLL and to investigate the interplay with cell-intrinsic factors. For this, a systematic comparison of mono- and co-culture drug response profiles will be performed. Where appropriate, information from the proteogenomic characterisation will be integrated with the drug response profiles to obtain a more complete picture.

Overall, this study will provide a systematic insight into how cell-intrinsic and extrinsic factors influence CLL drug responses and describe the biological and clinical heterogeneity between CLL patients.

## 2 Materials and methods

*Most of the methods presented here have been submitted for publication or are in preparation for publication in Herbst et al. (2020a), Herbst et al. (2020b) and Herbst et al. (2020c). The text was originally written by me. Paragraphs without quotation marks have been rewritten for this thesis.*

### 2.1 Cell culture

HS-5 cells were a kind gift by Martina Seiffert, DKFZ, Heidelberg, and were maintained in DMEM (Thermo Fisher Scientific) supplemented with 10 % fetal bovine serum (FBS; Thermo Fisher Scientific), 1 % penicillin/streptomycin (Thermo Fisher Scientific) and 1 % glutamine (Thermo Fisher Scientific) in a humidified atmosphere at 37 °C and 10 % CO<sub>2</sub>. NKTert cells were a kind gift by Marco Herling, University of Cologne, and were maintained in RPMI (Thermo Fisher Scientific) supplemented with 10 % FBS (Thermo Fisher Scientific), 1 % penicillin/streptomycin (Thermo Fisher Scientific) and 1 % glutamine (Thermo Fisher Scientific) in a humidified atmosphere at 37 °C and 5 % CO<sub>2</sub>. To confirm the correct identity of the cell lines genomic DNA was extracted with the DNeasy Blood & Tissue Kit (Qiagen) and send to Multiplexion GmbH for authentication. The HS-5 cell line could be correctly identified. As the NKTert cell line is neither sold by ATCC, nor by DSMZ, and, therefore, not present in their databases, it could not clearly be identified. However, authentication showed no match against any other cell line. In addition, cell lines were regularly tested for contamination with mycoplasma by PCR and were always negative.

### 2.2 Patient samples

Written consent was obtained from CLL patients according to the declaration of Helsinki. Peripheral blood mononuclear cells were isolated from blood using Ficoll density gradient centrifugation. Cells were viably frozen in RPMI (Thermo Fisher Scientific) containing 45 % FBS (Thermo Fisher Scientific) and 10 % DMSO (SERVA Electrophoresis GmbH) and kept on liquid nitrogen until use. Cells were thawed freshly before the experiment and rolled in serum containing medium for 3 hours on a roll mixer at room temperature to allow cells to recover. To deplete dead cells, which form clumps during this procedure, the suspension was filtered through a 40 µm cell strainer (Sarstedt). Cell viability and counts were analysed using Trypan Blue (Thermo Fisher Scientific). Percentages of alive CLL cells always exceeded 90 % at culture start or freezing of pellets for multi-omics characterisation. (Herbst et al., 2020c)

## 2.3 Assays for the analysis of phagocytosis by stroma cells

### 2.3.1 Comparing numbers and percentages of alive and dead cells in mono- and co-cultures using microscopy and flow cytometry

*The text for this section (2.3.1) was in parts written by Marta Stolarczyk.*

This section describes the experiment shown in Fig. 3.1. "Cancer cells from four different patients with CLL were cultured ( $2 \times 10^5$  cells/well) either alone or in co-culture with NKTert stroma cells ( $1 \times 10^4$  cells/well) in 96-well glass bottom microscopy plates (zell-kontakt GmbH). Stroma cells were seeded 24 hours before the addition of leukemia cells. The samples were treated with solvent control (DMSO; SERVA Electrophoresis GmbH), 63 nM venetoclax or 10  $\mu$ M fludarabine. After 72 hours the cultures were stained with the nuclear dye SiR-DNA (1  $\mu$ M, Spirochrome), the viability dye Calcein AM (1  $\mu$ M; Invitrogen) and the dead cell marker propidium iodide (PI; 5  $\mu$ g/ml, Sigma-Aldrich). Images were taken with the confocal LSM710 microscope (Zeiss) equipped with climate control (37 °C, 5 % CO<sub>2</sub>) using a 20x objective lens. Z-stack images were acquired in triplicate wells, and within one well four adjacent fields were imaged." (Herbst et al., 2020b)

"Image analyses were performed with the KNIME software (Berthold et al., 2009). Viability of the lymphocytes was calculated based on Calcein AM and PI signals in the Z-stack images that correspond to live and dead cells, respectively. After background subtraction using a 'rolling ball' method (radius: 10) a global threshold was applied (Huang method). Objects were separated using watershed. Total cell counts were obtained based on SiR-DNA signal (labelling filter: 25-250 pixels). Live/dead cell populations were classified based on the intensity histogram of Calcein and PI signal with a selection of the threshold separately for each cell culture condition: CLL cell culture, and co-culture of CLL cells with NKTert cells or HS-5 cells." (Herbst et al., 2020b)

"Directly after acquisition of the confocal microscopy pictures, lymphocytes previously labelled with SiR-DNA, Calcein and PI were pipetted from each cultural condition to a 96-well round bottom plate (Greiner) for further analysis with an iQue Screener (Intellicyt). Calcein and PI signals were recorded. The following gating strategy was pursued: Exclusion of potentially remaining stroma cells, by setting of a lymphocyte gate and exclusion of singlets. The percentage of alive cells was determined by gating on Calcein positive and PI negative cells." (Herbst et al., 2020b)

### 2.3.2 Visualisation of disappearance of leukemia cells and presence of phagosomes by CellTracker and lysosomal staining

This section describes the experiment shown in Fig. 3.2 and 3.3a. CLL cells from four patients were labelled with CellTracker Green (10  $\mu$ M, Invitrogen) according to the manufacturer's protocol and pretreated with solvent control or 63 nM venetoclax for 24 hours. NKTert or HS-5 stroma cells were labelled with CellTracker Blue (10  $\mu$ M, Invitrogen) according to the manu-

facturer’s protocol. Co-cultures of CLL cells and stroma cells were established. After 16 hours the cultures were additionally stained with lysosomal dye NIR ( $1 \mu\text{l}/\text{ml}$ , Abcam) and PI ( $5 \mu\text{g}/\text{ml}$ , Sigma-Aldrich). The samples were imaged on an Opera Phenix microscope (Perkin Elmer) in confocal mode. For clearer visualisation, the signal from the lysosomal dye is not shown in Fig. 3.2, while Cell Tracker Green signal and PI staining are not shown Fig. 3.3a. The images shown are representative of all experiments performed. (Herbst et al., 2020b)

### 2.3.3 Quantification of the amount of phagosomes

This section describes the experiment shown in Fig. 3.3b. NKTert cells were seeded at a density of  $2.5 \times 10^3$  cells/well, HS-5 at a density of  $5 \times 10^3$  cells/well into wells of a 384  $\mu$ -Clear microscopy plate (Greiner) in technical triplicates. After 4 hours CLL patient cells were added at a density of  $5 \times 10^4$  cells/well to co-culture wells, while additional medium was added to stroma mono-culture wells. Cells were cultured in RPMI (Thermo Fisher Scientific) supplemented with 10 % human serum (male AB, H6914-100ml Batch SLBT2873, Sigma-Aldrich), 1 % penicillin/streptomycin (Thermo Fisher Scientific) and 1 % glutamine (Thermo Fisher Scientific). The cultures were treated with 10 nM venetoclax or were left untreated. After co-culturing for 48 hours staining with Hoechst 33342 ( $4 \mu\text{g}/\text{ml}$ , Invitrogen), Calcein AM ( $1 \mu\text{M}$ , Invitrogen), PI ( $5 \mu\text{g}/\text{ml}$ , Sigma-Aldrich) and lysosomal dye NIR ( $0.05 \mu\text{l}/\text{well}$ , Abcam) was performed. The samples were imaged on a CellObserver microscope (Zeiss). The number of phagosomes was quantified using a custom script written in R, with the help of the EBImage package (Pau et al., 2010). In brief, a global threshold was applied on the signal from the lysosomal channel, followed by a filling of holes with the *fillHull* function. To separate objects in close proximity a watershed operation was performed on the distance map of foreground and background pixels. Only objects ranging between 100 and 1500 pixels in size and a circularity of more than 0.8 were classified as phagosomes. The experiment was conducted three times with different CLL patient samples. (Herbst et al., 2020b)

### 2.3.4 Co-cultures of NKTert and apoptotic cells of different origins

This section describes the experiment shown in Fig. 3.4. To investigate whether phagocytosis by NKTert was specific for dead CLL cells, the mantle cell lymphoma cell line HBL-2, the carcinoma cell line HELA or the benign epithelial cell line HEK-293T were labelled with CellTracker Green ( $10 \mu\text{M}$ , Invitrogen) and treated for 24 hours with  $10 \mu\text{M}$  doxorubicine to induce apoptosis, or solvent control (DMSO; SERVA Electrophoresis GmbH). NKTert cells were stained with CellTracker Blue ( $10 \mu\text{M}$ , Invitrogen) according to the manufacturer’s instructions. Subsequently, the target cells were co-cultured with NKTert cells in wells of a 384  $\mu$ -Clear microscopy plate (Greiner). After 16 hours the cultures were stained with PI ( $5 \mu\text{g}/\text{ml}$ , Sigma-Aldrich) and lysosomal dye NIR ( $0.05 \mu\text{l}/\text{well}$ ). Co-cultures of NKTert and CLL cells were used as positive control. The samples were imaged on an Opera Phenix microscope (Perkin Elmer) in confocal mode. Representative images are shown in Fig. 3.4. (Herbst et al., 2020b)

### 2.3.5 Flow cytometry of CD45 stained cells

This section describes the experiment shown in Fig. S2. "HEK-293T, HS-5, and NKTert cells were harvested with Accutase (Innovative Cell Technologies) to avoid cleavage of surface epitopes. MCL-2 cells were resuspended. Cells were stained with CD45 (BD Pharmingen FITC Mouse Anti-Human CD45, Clone: HI30; BD Biosciences) and analysed on a LSRII flow cytometer (BD Biosciences)." (Herbst et al., 2020b)

### 2.3.6 Experiment assessing phagocytosis by primary MSCs

This section describes the experiment shown in Fig. 3.5 and S3. "Primary CLL cells were labelled with CellTracker Green (10  $\mu$ M, Invitrogen). Apoptosis was induced by treatment with 63 nM venetoclax. After 24 hours the cells were added to primary MSCs of four different healthy donors, labelled with CellTracker Blue (10  $\mu$ M, Invitrogen) into 96-well glass bottom microscopy plates (zell-kontakt GmbH). After incubation for 16 hours the cultures were stained with lysosomal dye NIR (1  $\mu$ l/ml, Abcam) and PI (5  $\mu$ g/ml, Sigma-Aldrich). The samples were imaged on an Opera Phenix microscope (Perkin Elmer) in confocal mode. Representative images are shown in Fig. 3.5 and S3." (Herbst et al., 2020b)

### 2.3.7 Proteomics of HS-5 and NKTert

This section describes the experiment shown in Fig. S4. "HS-5 or NKTert cells were trypsinized (Thermo Fisher Scientific), washed with PBS (Thermo Fisher Scientific) and snap frozen in liquid nitrogen. Analysis of the whole proteome using mass spectrometry was performed by the EMBL proteomics core facility. Differentially abundant proteins were analyzed using limma (Ritchie et al., 2015). Gene set enrichment analysis for the KEGG pathways (Kanehisa et al., 2019) was performed using GSEA (Subramanian et al., 2005). A heatmap of the protein abundance of proteins in the lysosomal pathway was visualised using R." (Herbst et al., 2020b)

## 2.4 Proteogenomic profiling of CLL cells

### 2.4.1 Preparation of samples for proteomics, RNA and panel sequencing

"Cells were thawed, allowed to recover in RPMI medium (Thermo Fisher Scientific) containing 10% FBS (Sigma Aldrich) for 3 hours and filtered through a 40  $\mu$ m cell strainer (Sarstedt). Tumor cells were collected by Magnetic-activated cell sorting (MACS) using CD19 beads (Miltenyi Biotec). Samples were split into aliquots for proteomics analysis ( $1 \times 10^7$  cells), RNA sequencing ( $5 \times 10^6$  -  $1 \times 10^7$  cells) and panel sequencing ( $5 \times 10^6$  cells). Pellets for proteomic analysis were washed twice with ice cold PBS (Thermo Fisher Scientific) and snap frozen in liquid nitrogen. Samples for panel sequencing were washed once with PBS (Thermo Fisher Scientific) and snap frozen in liquid nitrogen. DNA was extracted using the DNeasy Blood & Tissue Kit (Qiagen) according to the manufacturer's instructions. Cell pellets for RNA sequencing were resuspended in QIAzol Lysis Reagent (Qiagen) and homogenized using a QIAshredder (Qiagen). RNA was isolated using the RNeasy Mini Kit (Qiagen) according to the manufacturer's instructions." (Herbst et al., 2020c)

## 2.4.2 Proteomics profiling of CLL samples

*This method section 2.4.2 was originally written by our collaborators from Janne Lehtiö's group, Karolinska Institute, Stockholm but was, nevertheless, included in the thesis for the sake of completeness.*

"Cell pellets were dissolved in Lysis buffer (4% SDS, 50 mM HEPES pH 7.6, 1 mM DTT), heated to 95 °C and sonicated. The total protein amount was estimated (DC Protein Assay, Bio-Rad Laboratories). Samples were then prepared for mass spectrometry analysis using a modified version of the SP3 protein clean-up and a digestion protocol (Hughes et al., 2014; Moggridge et al., 2018), where proteins were digested by LysC and trypsin (sequencing grade modified, Pierce). In brief, up to 250 µg protein from each sample was alkylated with 4 mM Chloroacetamide. Sera-Mag SP3 bead mix (20 µl) was transferred into the protein sample together with 100% acetonitrile to a final concentration of 70%. The mix was incubated under rotation at room temperature for 18 min. The mix was placed on the magnetic rack and the supernatant was discarded, followed by two washes with 70% ethanol and one with 100% acetonitrile. The beads-protein mixture was reconstituted in 100 µl LysC buffer (0.5 M Urea, 50 mM HEPES pH: 7.6 and 1:50 enzyme (LysC) to protein ratio) and incubated overnight. Finally, trypsin was added in 1:50 enzyme to protein ratio in 100 µl 50 mM HEPES pH 7.6 and incubated overnight. The peptides were eluted from the mixture after placing the mixture on a magnetic rack, followed by peptide concentration measurement (DC Protein Assay, Bio-Rad Laboratories). The samples were then pH adjusted using TEAB pH 8.5 (100 mM final concentration), 65 µg of peptides from each sample were labelled with isobaric TMT-tags (TMT10plex reagent) according to the manufacturer's protocol (Thermo Fisher Scientific). Each set consisted of nine individual patient samples and the tenth channel contained the same sample pool in each set, consisting of a mixture of patient samples. Sample pools were used as denominators when calculating TMT-ratios and thus served to link the eight sets together. The tryptic peptides for each set were separated by immobilized pH gradient - isoelectric focusing (IPG-IEF) on 3–10 strips as described previously (Branca et al., 2014)." (Herbst et al., 2020c)

"Of note, the labelling efficiency was determined by LC-MS/MS before pooling of the samples. For the sample clean-up step, a solid phase extraction (SPE strata-X-C, Phenomenex) was performed and purified samples were dried in a SpeedVac. An aliquot of approximately 10 µg was suspended in LC mobile phase A and 1 µg was injected on the LC-MS/MS system." (Herbst et al., 2020c)

"Online LC-MS was performed as previously described (Branca et al., 2014; Johansson et al., 2019) using a Dionex UltiMate<sup>TM</sup> 3000 RSLCnano System coupled to a Q-Exactive-HF mass spectrometer (Thermo Fisher Scientific). Each of the 72 plate wells was dissolved in 20 µl solvent A and 10 µl were injected. Samples were trapped on a C18 guard-desalting column (Acclaim PepMap 100, 75 µm x 2 cm, nanoViper, C18, 5 µm, 100 Å), and separated on a 50 cm long C18 column (Easy spray PepMap RSLC, C18, 2 µm, 100 Å, 75 µm x 50 cm). The nano capillary solvent A was 95% water, 5% DMSO, 0.1% formic acid; and solvent B was 5% water, 5% DMSO,

95 % acetonitrile, 0.1 % formic acid. At a constant flow of 0.25  $\mu\text{l}/\text{min}$ , the curved gradient went from 6-8 % B up to 40 % B in each fraction in a dynamic range of gradient length, followed by a steep increase to 100 % B in 5 min. FTMS master scans with 60 000 resolution (and mass range 300-1500  $m/z$ ) were followed by data-dependent MS/MS (30 000 resolution) on the top 5 ions using higher energy collision dissociation (HCD) at 30 % normalized collision energy. Precursors were isolated with a 2  $m/z$  window. Automatic gain control (AGC) targets were  $1 \times 10^6$  for MS1 and  $1 \times 10^5$  for MS2. Maximum injection times were 100 ms for MS1 and 100 ms for MS2. The entire duty cycle lasted  $\sim 2.5$  seconds. Dynamic exclusion was used with 30 seconds duration. Precursors with unassigned charge state or charge state 1 were excluded. An underfill ratio of 1 % was used.” (Herbst et al., 2020c)

”Protein and peptide identification and quantification was carried out as previously described (Branca et al., 2014; Johansson et al., 2019). Briefly, Orbitrap raw MS/MS files were converted to mzML format using msConvert from the ProteoWizard tool suite (Chambers et al., 2012). Spectra were then searched using MSGF+ (v10072) and Percolator (v2.08), where search results from 8 subsequent fraction were grouped for Percolator target/decoy analysis. All searches were done against the human protein subset of Ensembl 75 in the Galaxy platform (Herbst et al., 2020c). MSGF+ settings included precursor mass tolerance of 10 ppm, fully-tryptic peptides, maximum peptide length of 50 amino acids and a maximum charge of 6. Fixed modifications were TMT-10plex on lysines and peptide N-termini, and carbamidomethylation on cysteine residues, a variable modification was used for oxidation on methionine residues. Quantification of TMT-10plex reporter ions was done using OpenMS project’s IsobaricAnalyzer (v2.0). PSMs found at 1 % FDR were used to infer gene identities.” (Herbst et al., 2020c)

”Protein quantification by TMT10plex reporter ions was calculated using TMT PSM ratios to the entire sample set (all 10 TMT-channels) and normalized to the sample median. The median PSM TMT reporter ratio from peptides unique to a gene symbol was used for quantification. Protein FDRs were calculated using the picked-FDR method using gene symbols as protein groups and limited to 1 % FDR.” (Herbst et al., 2020c)

### 2.4.3 IGHV status analysis

”RNA was isolated from  $1 \times 10^7$  cells using TRIZOL reagent (Thermo Fisher Scientific) according to the manufacturer’s instructions. cDNA was synthesized from 2  $\mu\text{g}$  RNA using High-capacity cDNA Reverse Transcription Kit (Thermo Fisher Scientific) according to manufacturer’s instructions. PCR reactions as well as the analyses were performed as previously described with minor modifications (Szankasi and Bahler, 2010). For PCR reactions AmpliTaq Gold DNA polymerase (Thermo Fisher Scientific) with 0.2  $\mu\text{M}$  of each primer and 0.2 mM of each dNTP was used. VH1-, VH3- and VH4- segments were amplified in single reactions whereas primers for VH2, VH3-21, VH5 as well as VH6-segments were run in a multiplex PCR reaction as described (Szankasi and Bahler, 2010). The PCR program was as follows: initial denaturation at 94  $^\circ\text{C}$  for 2 minutes, followed by 40 cycles of denaturation (94  $^\circ\text{C}$ , 20 seconds), annealing (52  $^\circ\text{C}$ , 10 seconds) and elongation (72  $^\circ\text{C}$ , 30 seconds) and a final elongation step of 2 minutes at 72  $^\circ\text{C}$ .

PCR products were sent for Sanger Sequencing (GATC Biotech) using the appropriate forward and the JH-1 reverse primer for the sequencing reaction. In the multiplex PCR reaction both JH-rev as well as JH-1 rev were used for sequencing. After sequencing forward and reverse sequencing results were aligned. To determine the closest matching germline VH-sequence as well as the mutation status, i.e. the percentage of sequence identity, of the VH-segment determined the IMGT/V-Quest-Database (IMGT team) was used. The primers for individual PCRs were as follows: PCR1: VH1, JH, JH-1; PCR2: VH3, JH, JH-1; PCR3: VH4, JH, JH-1; PCR4: VH2, VH3-21, VH5, VH6, JH, JH-1 (Szankasi and Bahler, 2010).” (Herbst et al., 2020c)

#### 2.4.4 DNA panel sequencing

”For gene mutation analysis of CLL candidate genes we designed a customized Illumina TruSeq Custom Amplicon (TSCA) panel with two independent primer sets for a redundant coverage of *NOTCH1*, *SF3B1*, *ATM*, *TP53*, *RPS15*, *BIRC3*, *MYD88*, *FBXW7*, *POT1*, *XPO1*, *NFKBIE*, *EGR2* and *BRAF*. For *ATM*, *BIRC3*, *EGR2*, *FBXW7*, *MYD88*, *NFKBIE*, *POT1* and *TP53* the full gene was covered. For *BRAF* (exons 11-18), *NOTCH1* (exon 34 +3’UTR), *RPS15* (exons 3-4), *SF3B1* (exons 14-16) and *XPO1* (exons 14-17) the most commonly affected exons were covered. The selection of these targets comprises the 11 most frequently mutated genes in CLL identified via unbiased whole exome sequencing of 528 CLL patients (Landau et al., 2015). Library preparation was performed using TruSeq Custom Amplicon Assay Kit v1.5 including extension and ligation steps between custom probes. Samples were indexed, pooled and loaded on a Illumina MiSeq flowcell in 32 sample batches.” (Herbst et al., 2020c)

”The cumulative target size was 41 352 bp covered with 304 amplicons in each panel with an amplicon length up to 250 bp. Adjacent 5 intron bp were included to cover splice site mutations. Input of 250 ng DNA from peripheral blood mononuclear cells was sufficient for libraries according to the Illumina TSCA protocol.” (Herbst et al., 2020c)

”We used a custom bioinformatics pipeline including BWA and Samtools (alignment; (Li, 2011)), and Varscan (variant calling and annotation; (Koboldt et al., 2012)). Current databases (COSMIC (Tate et al., 2019), 1000G (1000 Genomes Project Consortium et al., 2015), dbSNP145, ClinVar (Landrum et al., 2018)) were taken into consideration to evaluate and report variants above a threshold of 5% mean variant allele fraction (VAF) as pathogenic/non pathogenic. Only mutations which occurred in at least three patients were considered for further analyses.” (Herbst et al., 2020c)

#### 2.4.5 DNA copy number variants

”DNA copy numbers were assessed using Illumina CytoSNP-12 and HumanOmni2.5-8 microarrays. DNA (200 ng) was processed according to the manufacturer’s instructions. Arrays were read out using the iScan array scanner (Illumina). Fluorescence in situ hybridization (FISH) analysis was performed for del11q22.3, del17p13, del13q14, trisomy 12, gain8q24 and gain14q32. Only alterations which were found to be present in at least three patients and absent in at least three patients were considered for further analyses.” (Herbst et al., 2020c)

## 2.4.6 RNA Sequencing

"mRNA sequencing libraries were prepared according to the manufacturer's protocol (TruSeq Stranded Total RNA Library Preparation Kit). Sequencing was performed on Illumina NextSeq 500 platform with 10-12 samples multiplexed per lane. After demultiplexing, the RNA-Seq reads were aligned to the human reference genome (GRCh 37.75/hg 19) using STAR (version 2.6.0c) with default parameters (Dobin et al., 2013). Read counts per gene were obtained with htseq-count (Anders et al., 2015) using the default overlap resolution mode-union. Library size normalization, variance stabilizing transformation and differential expression calling were performed using R/Bioconductor package DESeq2 (Love et al., 2014)." (Herbst et al., 2020c)

## 2.5 Co-culture drug screen

### 2.5.1 Optimisation of seeding conditions for co-culture screen

HS-5 cells were seeded at different densities, described in section 3.1.3.1, into wells of a 384  $\mu$ -Clear microscopy plate (Greiner). Cultures were treated with solvent control (DMSO; SERVA Electrophoresis GmbH) or 10 nM venetoclax. For visualisation of the densities, samples were stained with Calcein AM (1  $\mu$ M, Invitrogen), PI (5  $\mu$ g/ml, Sigma-Aldrich) and lysosomal dye NIR (0.05  $\mu$ l/well, Abcam) and imaged on a CellObserver microscope (Zeiss).

### 2.5.2 Preparation of screening plates

In total 81 CLL samples were examined in the screen. Samples were selected based on availability of material. 43 drugs in 3 concentrations were used for the screen (table 2.1). Drug concentrations ranged from subnanomolar to low micromolar and were chosen based on previous experience with the drugs. Increase of the concentration was 15 fold per step to cover a broad spectrum of concentrations. Drugs were obtained from different distributors (see table 2.1) and diluted according to the manufacturer's instructions. Further dilution was carried out in DMSO (SERVA Electrophoresis GmbH) and masterplates containing 4  $\mu$ l of diluted drugs were frozen at -20 °C for direct use on the screening days. On the screening day HS-5 stroma cells were detached and seeded at a density of  $1 \times 10^4$  cells/well in 20  $\mu$ l into the columns with even numbers of CellCarrier-384 Ultra Microplates (Perkin Elmer). The high cell count enables even distribution of cells across the well. The columns with uneven numbers were filled with the same amount of medium. The cells were left at 37 °C for 3-4 hours to permit attachment. In the meantime leukemia cells were thawed and allowed to recover, as described above. Per screening day either 5 or 10 patient samples were screened. Drug masterplates were thawed and the content diluted in 96  $\mu$ l serum free medium per well. 2.5  $\mu$ l of drugs were transferred to the attached stroma cells, before adding 17.5  $\mu$ l containing  $2 \times 10^4$  patient cells per well. The whole screen was carried out in DMEM (Thermo Fisher Scientific) supplemented with 10 % human serum (male AB, H6914-100ml Batch SLBT2873, Sigma-Aldrich), 1 % penicillin/streptomycin (Thermo Fisher Scientific) and 1 % glutamine (Thermo Fisher Scientific) at a final volume of 40  $\mu$ l in the culture plates. Cells were incubated at 37 °C in a humidified atmosphere and 10 % CO<sub>2</sub> for 3 days. (Herbst et al., 2020a)

Table 2.1: **Drugs and concentrations used in high-throughput drug screen.**

Drug	1st concentration [ $\mu$ M]	Con- centration [ $\mu$ M]	2nd concentration [ $\mu$ M]	Con- centration [ $\mu$ M]	3rd concentration [ $\mu$ M]	Con- centration [ $\mu$ M]	Supplier
Bafilomycin A1	0.04		0.6		9		Selleckchem
BAY11-7085	0.04		0.6		9		Selleckchem
BAY61-3606	0.04		0.6		9		Sigma-Aldrich
Carfilzomib	0.001		0.015		0.225		Selleckchem
CPI-169	0.04		0.6		9		Selleckchem
Cytarabine	0.1		1.5		22.5		Sigma-Aldrich
Dasatinib	0.004		0.06		0.9		Selleckchem
Dexamethasone	0.001		0.015		0.225		Sigma-Aldrich
Doxorubicine	0.002		0.03		0.45		Selleckchem
Duvelisib	0.02		0.3		4.5		Selleckchem
Enasidenib	0.04		0.6		9		Selleckchem
Everolimus	0.04		0.6		9		Selleckchem
EVP4593	0.04		0.6		9		Selleckchem
Fludarabine	0.04		0.6		9		Selleckchem
Ganetespib	0.04		0.6		9		Selleckchem
I-BET-762	0.02		0.3		4.5		Selleckchem
Ibrutinib	0.04		0.6		9		Selleckchem
Idelalisib	0.04		0.6		9		Selleckchem
IRAK1/4 Inhibitor I	0.04		0.6		9		Sigma-Aldrich
IRAK4 Inhibitor, Compound 26	0.02		0.3		4.5		Merck Chemicals
Ixazomib	0.1		1.5		22.5		Selleckchem
JQ1	0.1		1.5		22.5		Selleckchem
Lenalidomide	0.04		0.6		9		Sigma-Aldrich
LY2228820	0.04		0.6		9		Selleckchem
Midostaurin	0.04		0.6		9		Sigma-Aldrich
MK2206	0.04		0.6		9		Selleckchem
Nutlin 3a	0.04		0.6		9		Selleckchem
Palbociclib	0.04		0.6		9		Selleckchem
Plerixafor	0.1		1.5		22.5		Selleckchem
Pomalidomide	0.02		0.3		4.5		Selleckchem
PRT062607	0.02		0.3		4.5		Selleckchem
Pyridone 6	0.04		0.6		9		MedChemExpress
Quizartinib	0.04		0.6		9		Selleckchem
Rapamycin	0.1		1.5		22.5		Selleckchem
Ruxolitinib	0.04		0.6		9		Selleckchem
Selinexor	0.04		0.6		9		Selleckchem
Selumetinib	0.04		0.6		9		Selleckchem
Sotrastaurin	0.04		0.6		9		Selleckchem

Thioguanine	0.04	0.6	9	Selleckchem
Tofacitinib	0.1	1.5	22.5	Selleckchem
UMI-77	0.1	1.5	22.5	Selleckchem
Venetoclax	0.001	0.015	0.225	Selleckchem
Vorinostat	0.04	0.6	9	Selleckchem

### 2.5.3 Screen readout by spinning disk confocal microscopy

As readout high-throughput, high-content microscopy was chosen. CLL screening plates were stained with  $4 \mu\text{g}/\text{ml}$  Hoechst 33342 (Invitrogen) and  $1 \mu\text{l}/\text{ml}$  lysosomal dye NIR (abcam). Using an Opera Phenix High Content Screening System (Perkin Elmer) three positions per well with a stack of ten images at a distance of  $1.2 \mu\text{m}$  were acquired with a 40x water objective in confocal mode. This amounted to the acquisition of  $\sim 22\,000$  images per patient. (Herbst et al., 2020a)

### 2.5.4 Processing of images

Images of CLL samples were processed using the image analysis software Harmony (Perkin Elmer). Stacks were processed by using maximum intensity projection. CLL nuclei were identified by segmentation on the Hoechst channel and separated from stroma cell nuclei based on the area of the nucleus. Results per cells were exported and further analysis was conducted in the statistical programming language R (R Core Team, 2018). To assess whether a cell was alive or dead, the area of the nucleus of each individual cell was determined. When CLL cells die the nucleus condenses and, therefore, gets smaller and brighter. By plotting a histogram of nuclear area across all plates and patients I determined that a threshold of  $23.8 \mu\text{m}^2$  can distinguish the two populations of alive and dead cells most accurately. This method had previously been validated by concurrent staining with the viability dye Calcein AM (Invitrogen) and the dead cells stain PI (Sigma-Aldrich). Using this threshold cells were classified into alive and dead and the percentage of alive cells was calculated for each well. (Herbst et al., 2020a)

### 2.5.5 Validation of screening results in primary MSC co-cultures

Primary MSCs of three different donors were used.  $1\,000 \text{ cells}/\text{well}$  were seeded into 96-well glass bottom plates (zell-kontakt GmbH) in Bulletkit medium (Lonza). The plates were cultured in a humidified atmosphere at  $37^\circ\text{C}$  and  $5\%$   $\text{CO}_2$  for 2 days to allow MSCs to adhere and recover. CLL cells were thawed, allowed to recover in medium for 3 hours and filtered through a  $40 \mu\text{m}$  cell strainer (Sarstedt) to get rid of dead cells. The medium was removed from MSCs and  $2 \times 10^5 \text{ CLL cells}/\text{well}$  added to the stroma cells in Bulletkit medium (Lonza). Apart from co-cultures also mono-cultures of only CLL cells were established. Cultures were treated with  $9 \mu\text{M}$  idelalisib,  $1.5 \mu\text{M}$  JQ1,  $0.6 \mu\text{M}$  fludarabine,  $22.5 \mu\text{M}$  tofacitinib,  $9 \mu\text{M}$  ruxolitinib or solvent control (DMSO; SERVA Electrophoresis GmbH) and incubated in a humidified atmosphere at  $37^\circ\text{C}$  and  $5\%$   $\text{CO}_2$  for 3 days. Each condition was assessed in technical duplicates. The cultures were stained with Hoechst 33342 ( $4 \mu\text{g}/\text{ml}$ , Invitrogen), Calcein AM ( $1 \mu\text{M}$ , Invitrogen), PI ( $5 \mu\text{g}/\text{ml}$ , Sigma-Aldrich) and lysosomal dye NIR ( $1 \mu\text{l}/\text{ml}$ , Abcam) and the whole wells were

imaged on an Opera Phenix microscope (Perkin Elmer) with a 10x objective in confocal mode. Using the image analysis software Harmony (Perkin Elmer) CLL cells were segmented based on Hoechst signal and Calcein and PI intensities were measured. All further analysis steps were conducted in R (R Core Team, 2018). Cells with a Calcein intensity above a certain threshold and with PI intensities below a certain threshold were classified as alive. To avoid a possible influence of phagocytosis on relative percentages of alive cells, absolute counts of alive CLL cells were used for all further analyses. (Herbst et al., 2020a)

### 2.5.6 Western blots STAT3

For assessing the impact of stroma co-culture on STAT3 phosphorylation in CLL cells DMEM medium supplemented with 10 % human serum (male AB, H6914-100ml Batch SLBT2873, Sigma-Aldrich), 1 % penicillin/streptomycin (Thermo Fisher Scientific) and 1 % glutamine (Thermo Fisher Scientific) or  $5 \times 10^6$  HS-5 cells were pre-plated into 10 cm dishes. After 3 hours CLL cells were added at  $1.5 \times 10^7$  cells/dish to establish mono- and co-cultures. DMSO (0.22 %; SERVA Electrophoresis GmbH), ruxolitinib (10  $\mu$ M) or tofacitinib (22  $\mu$ M) were added. After incubation for 48 hours CLL cells were carefully harvested. Cells were counted using Trypan Blue (Thermo Fisher Scientific) and contamination with HS-5 cells was excluded by visual inspection. (Herbst et al., 2020a)

For assessing the impact of soluble factors produced by stroma, HS-5 cells or primary MSCs were cultured in DMEM medium supplemented with 10 % FBS (Thermo Fisher Scientific), 1 % penicillin/streptomycin (Thermo Fisher Scientific) and 1 % glutamine (Thermo Fisher Scientific) or Bulletkit medium (Lonza) respectively. Conditioned medium was harvested after 3 days of culture. After the removal of cellular debris by centrifugation at 1000 g, aliquots of conditioned medium were frozen.  $7.5 \times 10^6$  CLL patient cells in DMEM medium supplemented with 10 % FBS (Thermo Fisher Scientific), 1 % penicillin/streptomycin (Thermo Fisher Scientific), 1 % glutamine (Thermo Fisher Scientific) and 25 % conditioned medium were seeded into 10 cm dishes. Cells were harvested after culturing for 48 hours. (Herbst et al., 2020a)

Samples for Western Blot were prepared by washing once with ice-cold PBS (Thermo Fisher Scientific) and lysed in 100  $\mu$ l RIPA buffer (Sigma-Aldrich) containing PhosSTOP (Sigma-Aldrich) and cOmplete, Mini Protease Inhibitor Cocktail (Sigma-Aldrich). After incubation on ice for 30 min the samples were centrifuged at 15 000 g for 20 min at 4 °C. The supernatant was aliquoted and frozen at -80 °C until use. Samples were run on 10 % acrylamide gels (SERVA Electrophoresis GmbH) at 45 mA. As marker, the dual color Precision Plus (Bio-Rad Laboratories) ladder was used. Transfer to PVDF membranes (Thermo Fisher Scientific) was performed at 400 mA. Primary antibodies were incubated over night. Primary and secondary antibodies are listed in table 2.2. (Herbst et al., 2020a)

Table 2.2: **Antibodies used for Western Blots.**

Target	Clone	Host Animal	Antibody type	Provider	Number
Phospho-Stat3 Tyr705	D3A7	Rabbit	mAb	Cell Signaling Technology	9145
Stat3	D1B2J	Rabbit	mAb	Cell Signaling Technology	30835
$\beta$ -actin	2D4H5	Mouse	mAB	Proteintech Group	66009-1- Ig
Anti-mouse IgG (H+L), HRP conjugate		Goat	secondary	Proteintech Group	SA00001- 1
Anti-rabbit IgG (H+L), HRP conjugate		Goat	secondary	Proteintech Group	SA00001- 2

## 2.6 Statistical analyses

”All statistical analyses were performed in the statistical programming language R (R Core Team, 2018) using the RStudio interface (RStudio Team, 2016). Formatting and plotting of data was in most cases done with the help of the tidyverse package (Wickham et al., 2019). Statistical tests were performed as indicated in the text and figures” (Herbst et al., 2020c). Correction for multiple testing was performed with the Benjamini-Hochberg procedure. ”For easy handling of this multi-omics dataset the R package MultiAssayExperiment was used (Ramos et al., 2017).” (Herbst et al., 2020c)

### 2.6.1 Analysis of differential proteins and mRNA

”Differential protein abundance between samples with different genetic alterations was assessed by performing limma (Ritchie et al., 2015) and DEqMS (Zhu, 2019) on the log<sub>2</sub> transformed protein abundances. Proteins were considered as differential if the adjusted p-value was below 0.001 and the absolute log<sub>2</sub> fold change exceeded 0.5. Differential gene expression was performed on the raw count values using DESeq2 (Love et al., 2014). Genes were considered as differential if the adjusted p-value was below 0.001 and the absolute log<sub>2</sub> fold change exceeded 1.5.” (Herbst et al., 2020c)

### 2.6.2 Protein-mRNA correlation

”Spearman correlation for protein-mRNA pairs was calculated with the *cor.test* function from the stats package (R Core Team, 2018). Cumulative distribution functions of the correlation coefficients were compared using a two-sided Kolmogorov-Smirnov test with the function *ks.test* from the stats package.” (Herbst et al., 2020c)

### 2.6.3 Analysis of time to next treatment

”Time to next treatment (TTT) was calculated from the date of sample collection to subsequent treatment initiation. Patients without treatment initiation during the observation time and patients who died before treatment initiation were censored at the latest follow-up contact.

Proportional hazards regression (Cox regression) was used to explore the potential impact of protein abundances, gene expression and latent factors from MOFA analysis on TTT. Therefore, the *coxph* function of the R package *survival* (Therneau, 2020) was used. To draw Kaplan-Meier curves maximally selected rank statistics was performed using the R package *maxstat* (Hothorn, 2017). For drawing Kaplan-Meier curves the *survminer* package (Kassambara et al., 2019) was used.” (Herbst et al., 2020c)

#### 2.6.4 Dimensionality reduction and consensus clustering

”Consensus clustering on proteins or transcripts was performed using the *ConsensusClusterPlus* function from the *ConsensusClusterPlus* package (Wilkerson et al., 2010). For this 1-Pearson correlations were clustered hierarchically and resampling was performed 1000 times. The optimal number of clusters was determined based on the cluster stabilities shown in the consensus matrix, the consensus CDF and the delta area and tracking plots. The above measures supported clustering of proteomic data into 4-6 clusters. As the increase from 5 to 6 clusters lead to the subdivision of trisomy 12 patients into U-CLL and M-CLL and, therefore, indicated biological meaningfulness of the clusters, we chose 6 clusters as optimal value. On mRNA level clustering into less than 5 groups was not justifiable from the relative change in area under the CDF curve. Additionally, clustering into more than 5 subgroups only lead to splitting off of individual patients. Therefore, 5 clusters were chosen as the optimal number of clusters.” (Herbst et al., 2020c)

”T-distributed stochastic neighbor embedding (t-SNE) was performed with the *Rtsne* function from the *Rtsne* package (Krijthe, 2015). Principal component analysis was performed using the *prcomp* function from the *stats* package. Visualisation of clustered heatmaps was done using the *pheatmap* function from the *pheatmap* package (Kolde, 2019).” (Herbst et al., 2020c)

#### 2.6.5 Association of proteomics groups with genetic alterations

”To assess the association between the proteomics groups (PGs) and genetic alterations Fisher’s exact test was used. P-values were adjusted using the Benjamini–Hochberg procedure.” (Herbst et al., 2020c)

#### 2.6.6 *In-vivo* lymphocyte growth rate

”Patients which had lymphocyte counts available for less than 4 timepoints between the sample collection date and the time of the next treatment and patients currently in treatment were excluded. Thus, 35 patients with enough data remained. No data was available for patients within proteomics subgroup PG6. Lymphocyte growth rates were calculated by fitting a linear model to the log10 transformed lymphocyte counts of all timepoints between the sample collection date and the time of the next treatment versus the period of time.” (Herbst et al., 2020c)

#### 2.6.7 Analysis of differential splicing

”Due to its short computational time the julia-based tool *whippet* (Sterne-Weiler et al., 2018) was used for visualisation of specific splicing events, following the recommended workflow. In brief,

an index was created from the human reference genome (GRCh37). Fastq files were quantified using the options for single-end reads. PG5 was compared to all other samples, or *SF3B1* mutated samples were compared to wild type samples, by using the *whippet-delta* function and setting the parameters of *-r* to 20 and *-s* to 3. For visualisation, delta percent-spliced-in values were plotted in R.” (Herbst et al., 2020c)

### 2.6.8 Gene ontology and KEGG gene set enrichment analyses

”Gene sets were downloaded from KEGG (Kanehisa et al., 2019). Enrichment analysis was performed using GSEA (Mootha et al., 2003; Subramanian et al., 2005). To not confound the analysis, PG5 was compared only to the other non-trisomy 12 groups (PG3, PG4, PG6), as consensus clustering determined trisomy 12 to be the strongest driver of clustering.” (Herbst et al., 2020c)

### 2.6.9 Analysis of association between PG5 and drug response

For calculation of associations between drug response and PG5, the normalised drug response values of the mono-culture *ex-vivo* drug sensitivity screen were used. Differences between drug responses of patient samples belonging to PG5 and all other samples was assessed by Wilcoxon signed-rank test. Correction for multiple testing was applied using the Benjamini-Hochberg procedure. The false discovery rate was set to 25 %. (Herbst et al., 2020c)

### 2.6.10 Validation of PG5 in published cohort

The symbols for the C2 module of the curated canonical pathways from KEGG were downloaded from MSigDB (Liberzon et al., 2011). The pathways for the ‘Spliceosome’, ‘B-cell receptor signalling’, ‘Valine, leucine and isoleucine degradation’ and the ‘Proteasome’ (v7.0) were downloaded from MSigDB (Liberzon et al., 2011). The published proteomics dataset of 9 U-CLL and 9 M-CLL samples by Eagle et al. (2015) was used as cohort for validation. Information about the presence of trisomy 12 was not available for the cohort by Eagle et al. (2015), therefore, its presence was estimated by calculating the mean abundance of proteins located on chromosome 12. (Herbst et al., 2020c)

All available proteins in the spliceosome and BCR signalling pathways were used to perform unsupervised hierarchical clustering on the proteomics data from this study and the validation dataset. For this, the *pheatmap* function from the *pheatmap* package (Kolde, 2019) was used and one cluster was split off automatically by setting the *cutree* option to 2. In both cases a subgroup with low BCR and high spliceosome abundance was split off. This cluster contained mainly PG5 patients in the cohort analysed in this thesis. As the cluster which formed in the cohort by Eagle et al. (2015) had a similar size as PG5 and contained both, U-CLL, as well as M-CLL patients it was defined as ‘PG5-like’. None of the patients in the PG5-like cluster belonged to the patients with the top 20 % abundances of proteins on chromosome 12, which is the average occurrence of trisomy 12 in a representative cohort (Abruzzo et al., 2018). Mean protein abundances for the genes in the KEGG gene sets ‘Proteasome’ and ‘Valine, leucine and

isoleucine degradation' were calculated and compared between the PG5-like cluster and all other patients by Wilcoxon signed-rank test. (Herbst et al., 2020c)

### 2.6.11 Analysis of spontaneous apoptosis

For the analysis of spontaneous apoptosis and the protection from it only the wells containing solvent control (DMSO; SERVA Electrophoresis GmbH) were considered. For evaluation of an edge effect, the percentages of alive cells per well were used. For all other analyses, wells on the edges of the culture plates were excluded and the mean percentages of alive cells were averaged across wells for each patient. The values were normalised to the mean of the inner-well controls per patient only for the analysis of an edge effect. For all other analyses the values were directly used without prior normalisation. This allowed the determination of the rate of spontaneous apoptosis. (Herbst et al., 2020a)

### 2.6.12 Calculation of drug-drug correlations

For calculating the correlations between drug responses within mono- or co-cultures the concentration with the largest variance was chosen for each drug, to capture the largest heterogeneity between patient responses. Pairwise Spearman correlation coefficients were calculated using the *rcorr* function from the Hmisc package (Harrell Jr et al., 2020). For mono- and co-cultures drug-drug correlations were clustered separately using the *heatmap* function from the heatmap package (Kolde, 2019). (Herbst et al., 2020a)

### 2.6.13 Assessment of association between genetic alterations and co-culture drug response

For assessing the association between IGHV status and response to ibrutinib and the association between *TP53* mutations and response to nutlin 3a in mono- and co-cultures, percentages of alive cells normalised to the solvent control wells of the respective culture conditions (mono-culture to mono-culture controls and co-cultures to co-culture controls) were used to minimize confounding by the effect of and protection from spontaneous apoptosis. Differences between responses of U-CLL and M-CLL to treatment with 40 nM ibrutinib were assessed by Wilcoxon signed-rank test for both mono- and co-cultures. Differences between responses of wild type and *TP53* mutated CLL to treatment with 9  $\mu$ M nutlin 3a were assessed by Wilcoxon signed-rank test for both mono- and co-cultures. (Herbst et al., 2020a)

### 2.6.14 Linear model to describe the interaction of stroma cells with drug response

To assess the effect of stroma cells on drug-induced apoptosis of CLL, some drug conditions were excluded according to the following criteria. Drug concentrations which were toxic to stroma cells were excluded, as these do not represent proper co-cultures. The degree of stroma cell death was assessed by measuring the percentage of area covered by stroma cells using the image analysis software Harmony (Perkin Elmer). For this, all nuclei were segmented in the Hoechst channel and CLL nuclei were excluded by setting a size threshold. Next, the cytoplasm

of stroma cells was found using the signal from the lysosomal dye as proxy. Conditions in which less than 40 % of the image area was covered by stroma were classified as too toxic conditions. Moreover, concentrations which did neither impact mono- nor co-culture responses significantly across all patients were excluded. This ensured that conditions with equal effects in mono- and co-cultures were only classified as such if the drug was in any way active in CLL cells. In some cases drugs did not diminish but increase the percentage of alive CLL cells. These conditions would confound the analysis with the linear model and were therefore excluded. Finally, drug concentrations in which the mean percentage of alive cells across all patients was diminished to levels below 15 % in mono- and co-cultures were excluded, as these conditions were considered as too toxic to obtain any meaningful results. (Herbst et al., 2020a)

To distinguish the effect of stroma cells on spontaneous apoptosis from their effect on drug-induced apoptosis, a linear model was established:

*Percentage alive CLL cells*  $\sim$  *effect<sub>culture model</sub> + effect<sub>drug</sub> + effect<sub>culture model</sub> : effect<sub>drug</sub>*.

The absolute percentages of alive cells of all remaining conditions were used as input values. A Z-score from the interaction term was calculated. Moreover, statistical significance or equivalence of the interaction was tested by applying a two-sided t-test and the 'two-one-sided t-tests' (TOST) procedure with the *TOSTone.raw* function from the TOSTER package (Lakens, 2017). Alpha was set to 0.05 and equivalence bounds were set to an increase or decrease of the percentage of alive cells by 10 %. (Herbst et al., 2020a)

## 3 Results

### 3.1 Establishment of a system for co-culture drug sensitivity screening in CLL

To systematically investigate the influence of the bone marrow microenvironment on drug response of primary CLL patient cells a robust setup suitable for high-throughput drug sensitivity screening is required. Therefore, all necessary steps and components were carefully evaluated.

#### 3.1.1 General design considerations for the high-throughput drug sensitivity screen

First, general considerations about the layout of the screen needed to be taken. Due to limited availability of patient cells, costs of reagents and scalability of the experiment an experimental setup in 384-well plates was chosen. The small size of these wells permits small working volumes, reducing amounts of cells and reagents needed per well and thereby enabling the screening of a larger number of conditions.

To be able to directly compare between cultures with and without microenvironmental support, a layout in which mono- and co-culture wells are located on the same plate was chosen. Wells with the same treatment conditions were located directly next to each other to ensure that the mono- and co-culture conditions are exposed to similar fluctuations occurring during the incubation period within the cell culture incubator.

To not confound the influence of the microenvironment by the addition of serum from a different species, human serum was chosen as supplement to the culture medium. The usage of serum of human origin mimics the soluble microenvironment *in-vivo* more closely. In addition it has been shown, that human serum can support the survival of CLL cells *ex-vivo* better than fetal bovine serum (Primo et al., 2018).

#### 3.1.2 Characterisation of bone marrow stroma cell model

*The results described in this section (3.1.2) have been submitted for publication (Herbst et al., 2020b). The text was originally written by me and has been modified for this thesis.*

Most importantly appropriate culture conditions need to be chosen to model the niche of the bone marrow microenvironment. One of the most abundant interaction partners of CLL cells in the bone marrow are stroma cells. For some drugs this interaction has been shown to cause resistances to treatment (Kurtova et al., 2009; Lagneaux et al., 1998). To stay as close

as possible to the *in-vivo* situation in patients, bone marrow stroma cells of human origin were chosen as microenvironmental support for primary CLL cells. Three bone marrow stroma cell types have been widely used for leukemia - stroma cell co-cultures: primary mesenchymal stem cells (MSCs) and the bone marrow stroma cell lines NKTert and HS-5 (Kawano et al., 2003; Panayiotidis et al., 1996; Roecklein and Torok-Storb, 1995).

In theory the usage of primary MSCs and primary CLL cells for *ex-vivo* experiments would mimic the interaction *in-vivo* most accurately. However, the number of MSCs which can be collected from the bone marrow of donors is limited. To perform robust high-throughput screens, the experimental conditions need to be as reproducible as possible. The usage of primary MSCs would restrict feasibility and reproducibility of the high-throughput screen.

An alternative model are bone marrow stroma cell lines. These have the advantage that they can be expanded to obtain sufficient amounts of cells and, therefore, the stroma cell's phenotype can be kept constant during the course of the drug screen. To date, two widely used human bone marrow stroma cell lines exist: HS-5 and NKTert. The behaviour of both cell lines in co-cultures with primary CLL cells was evaluated to select the most appropriate model for high-throughput co-culture drug sensitivity screening.

### **3.1.2.1 Evaluation of NKTert and HS-5 as suitable feeder cell layer for high-throughput co-culture screening**

First, the behaviour of NKTert cells in co-culture with primary CLL cells was characterised. For this, cancer cells from four different CLL patients were cultured either alone or in co-culture with NKTert. To additionally include the influence of drugs, the samples were treated with solvent control, 63 nM venetoclax or 10  $\mu$ M fludarabine. The cultures were stained with the nuclear dye SiR-DNA, the viability dye Calcein-AM and the dead cell marker propidium iodide (PI) after 72 hours. Using microscopy or flow cytometry, a higher percentage of alive cells in the co-cultures than in the mono-cultures could be confirmed, as reported previously for NKTert co-cultures (Kurtova et al., 2009). This suggests a protective effect by the stroma cells (Fig. 3.1a,b).

In addition to these relative numbers, the amount of total (Fig. 3.1c), alive (Fig. 3.1d; Calcein positive) and dead (Fig. 3.1e; PI positive) leukemia cells was quantified in the microscopy images. Surprisingly, much lower absolute leukemia cell counts were observed in NKTert co-cultures than in mono-cultures. Absolute counts of alive cells in the cultures did not differ between mono- and co-cultures. However, the number of dead cells drastically decreased in NKTert co-cultures, explaining the decline in absolute leukemia cells counts. (Herbst et al., 2020b)

To further investigate this surprising behaviour, leukemia cells from four other patients were labelled with CellTracker Green and co-cultured with CellTracker Blue labelled NKTert (Fig. 3.2). CLL cells were pretreated with solvent control or 63 nM venetoclax for 24 hours to induce apoptosis. Already after co-culturing for 16 hours, leukemia cells disappeared from venetoclax treated NKTert co-cultures. No noticeable decrease of leukemia cells in mono-cultures of CLL was de-

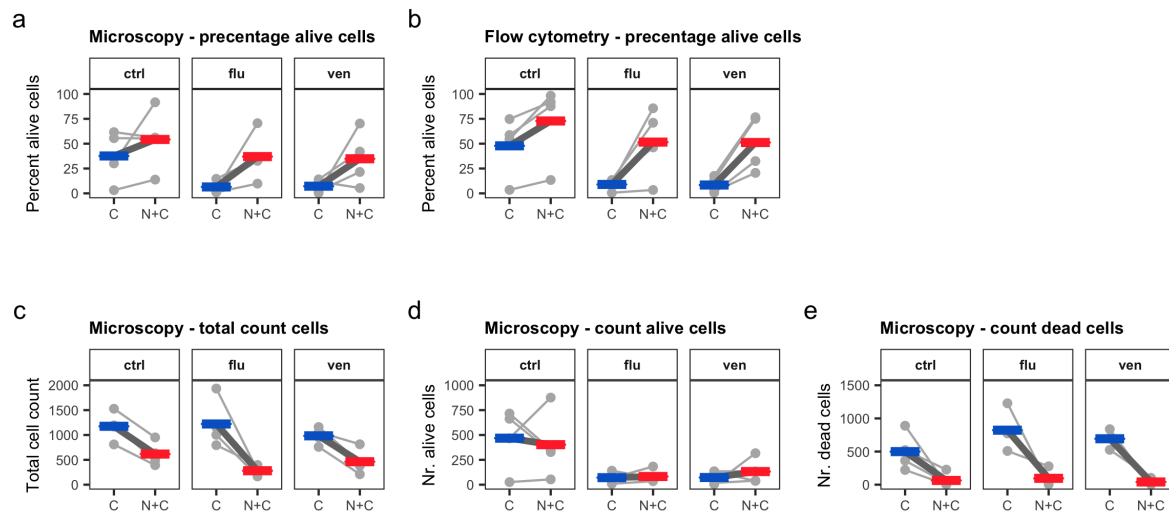


Figure 3.1: **Dead CLL disappeared from NKTert co-cultures, artificially increasing the percentage of alive cells.** **a & b**, The percentage of alive CLL cells was higher in solvent control, fludarabine and venetoclax treated co-cultures of CLL and NKTert than in mono-cultures of CLL alone. The readout was either performed with microscopy (**a**) or flow cytometry (**b**). **c**, Total cell counts decreased in co-cultures of CLL and NKTert in comparison to mono-cultures of CLL. **d**, The total number of alive cells was comparable between the culture conditions. **e**, Dead CLL cells disappeared from co-cultures with NKTert; ctrl = solvent control treated (DMSO), flu = 10  $\mu$ M fludarabine treated, ven = 63 nM venetoclax treated, C = mono-cultures of CLL, N+C = co-cultures of CLL and NKTert; paired t-test, \*\* =  $p < 0.01$ , \* =  $p < 0.05$ , points and lines = individual patients, coloured bars = mean. (Herbst et al., 2020b)

tected. To investigate whether HS-5 cells behave similarly, the same experiment was conducted with this bone marrow stroma cell line. For HS-5 co-cultures no decrease in dead cell counts could be seen (Fig. 3.2). (Herbst et al., 2020b)

These experiments show that apoptotic CLL cells disappear from NKTert co-cultures. This behaviour was not observed for HS-5 bone marrow stroma cells. (Herbst et al., 2020b)

### 3.1.2.2 NKTert cells phagocytose dead CLL cells

To understand why apoptotic cells disappear, NKTert co-cultures were additionally stained with lysosomal dye NIR. Using confocal microscopy, large lysosomal bodies inside NKTert cells were observed (Fig. 3.3a). These had the size and shape of CLL cells. Lysosomal bodies often co-localized with CellTracker Green and PI staining and were surrounded by, but did not include, CellTracker Blue staining (Fig. S1). The amount of these phagosomes was quantified automatically in three additional and independent experiments comprising three patients in total (Fig. 3.3b). A high number of phagosomes in venetoclax treated NKTert co-cultures could be confirmed, while large lysosomal bodies were absent in CLL mono-cultures, NKTert mono-

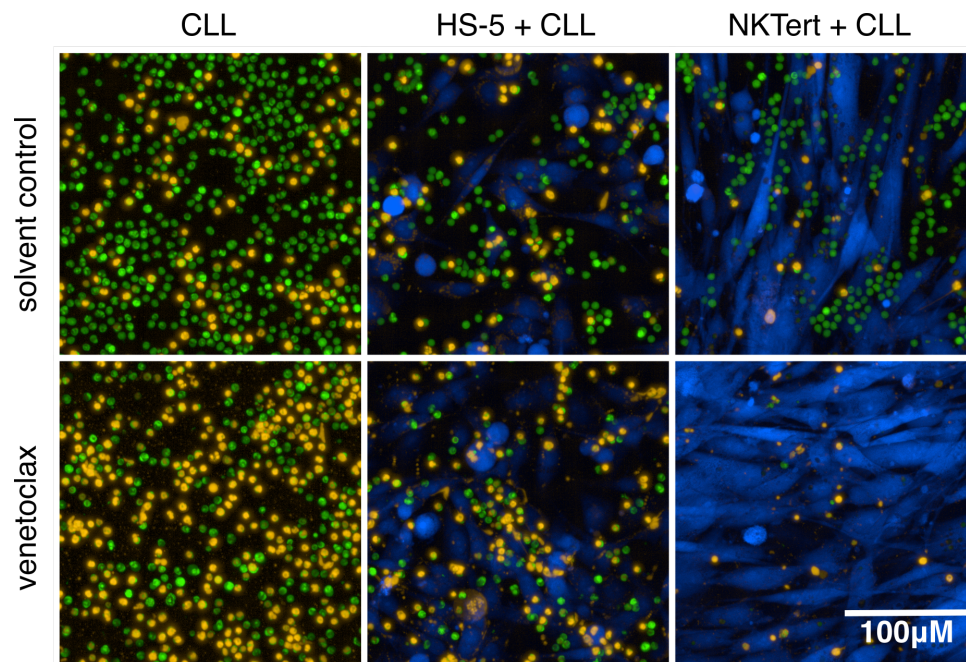


Figure 3.2: **Microscopy images showing disappearance of dead CLL cells from drug treated co-cultures with NKTert.** Representative confocal microscopy images of CLL mono-cultures or co-cultures of CLL and NKTert or HS-5, treated with solvent control (DMSO) or 63 nM venetoclax. Initially leukemia cells had been seeded at equal amounts to all cultures; Green = CellTracker Green labelled CLL, blue = CellTracker Blue labelled stroma cells, yellow = dead cells stained with propidium iodide. (Herbst et al., 2020b)

cultures or co-cultures of CLL and HS-5 cells. Hence, NKTert phagocytose apoptotic CLL cells and, thereby, clear these cells from the cultures. (Herbst et al., 2020b)

### 3.1.2.3 NKTert cells also phagocytose other dead cells than CLL

To investigate whether phagocytosis by NKTert was specific for dead CLL cells, the mantle cell lymphoma cell line HBL-2, the carcinoma cell line HELA or the benign epithelial cell line HEK-293T were treated with solvent control or 10  $\mu$ M doxorubicine for 24 hours, to induce apoptosis, and subsequently co-cultured with NKTert cells. As in previous experiments the target cells had been labelled with CellTracker Green, while NKTert cells had been labelled with CellTracker Blue. The cultures were stained with PI and lysosomal dye NIR after co-culturing for 16 hours. Co-cultures of NKTert and CLL cells were used as positive control. NKTert did not only massively phagocytose dead CLL cells, but also apoptotic cells of all other tested cell lines, regardless of their origin (Fig. 3.4). Consequently, the phagocytic activity by NKTert is not specific for CLL cells, but is a general phenomenon. (Herbst et al., 2020b)

### 3.1.2.4 NKTert cells are not of macrophagic origin

The observation of the massive phagocytic activity exhibited by NKTert raised the question whether the cells are of macrophagic origin. Kawano et al. (2003) had shown that NKTert

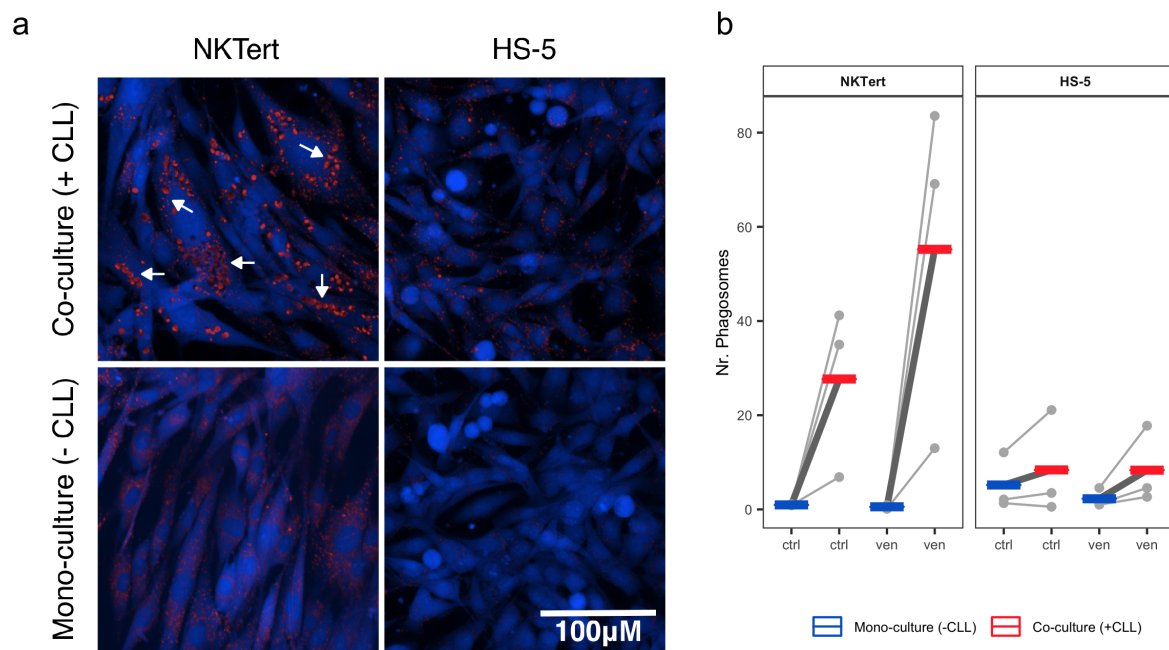


**Figure 3.3: Phagosomes observed in CLL-NKTert co-cultures.** **a**, Representative confocal microscopy images of NKTert or HS-5 in mono-culture or co-cultured with primary CLL cells and treated with 63 nM venetoclax; blue = CellTracker Blue labelled stroma cells, red = lysosomal dye NIR. Arrows only highlight some of the numerous phagosomes. **b**, Automated quantification of the number of phagosomes in NKTert or HS-5 mono-cultures or CLL-NKTert and CLL-HS-5 co-cultures, treated with solvent control (DMSO; ctrl) or 63 nM venetoclax (ven); points and lines = individual patients, analysed in separate experiments, coloured bars = mean. (Herbst et al., 2020b)

are negative for the hematopoietic cell marker CD45 and, thus, cannot be macrophages. By performing staining against CD45 and flow cytometry this finding could be confirmed (Fig. S2). Therefore, the extensive phagocytosis by NKTert cannot be explained by a macrophagic phenotype of NKTert. (Herbst et al., 2020b)

### 3.1.2.5 Some mesenchymal stem cells also phagocytose dead CLL cells

As NKTert cells are an immortalised cell line they are to some extent an artificial system. The question arises whether the ability to phagocytose apoptotic cells is restricted to the cell line NKTert or whether it also occurs in primary MSCs. To answer this question primary CLL cells were labelled with CellTracker Green and apoptosis was induced by treatment with 63 nM venetoclax. After 24 hours the cells were added to primary MSCs from four different healthy donors, labelled with CellTracker Blue. After co-culturing for 16 hours, the cultures were stained with lysosomal dye NIR and PI and imaged with a confocal microscope. Phagocytosed CLL were observed inside MSCs from two out of the four donors (Fig. S3). Phagocytosis was especially high in MSC culture 1 (Fig. 3.5), while MSC 2 only exhibited an intermediate amount of phagocytosis

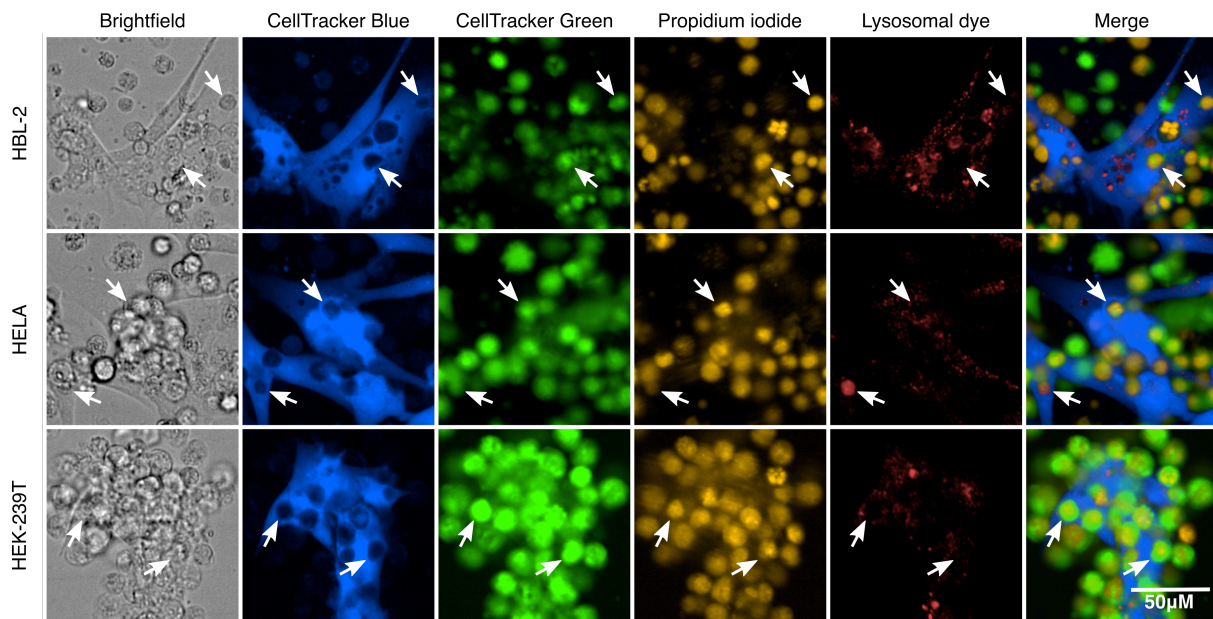


Figure 3.4: **NK TERT cells also phagocytose dead cells of other origins.** Representative confocal microscopy images of co-cultures of CellTracker Blue labelled NK TERT and CellTracker Green labelled HBL-2, HELA or HEK-293T cell lines, previously treated with  $10 \mu\text{M}$  doxorubicine and stained with propidium iodide and lysosomal dye NIR. White arrows highlight some examples in which apoptotic target cells have been phagocytosed by NK TERT. (Herbst et al., 2020b)

(Fig. S3). This shows that not only NK TERT, but also some primary MSCs are able to extensively phagocytose apoptotic cells and that a large heterogeneity between stroma cells exists. (Herbst et al., 2020b)

### 3.1.2.6 Lysosomal pathway is upregulated in NK TERT in comparison to HS-5 cells

Only one out of the two tested human bone marrow stroma cell lines and two out of the four tested MSCs phagocytosed apoptotic cells. To explore which pathways influence this phenomenon, RNA sequencing and proteomics of HS-5 and NK TERT cells was performed. Differentially expressed genes in RNA sequencing correlated with differentially abundant proteins in proteomics (Fig. S4a). Within the differentially abundant proteins the lysosomal gene set was most significantly enriched. Most proteins in this pathway were upregulated in NK TERT in comparison to HS-5 (Fig. S4b). This indicates that NK TERT are able to phagocytose apoptotic cells due to upregulation of proteins in the lysosomal pathway. (Herbst et al., 2020b)

### 3.1.2.7 HS-5 cells represent the better model for a co-culture drug sensitivity screen

The results presented above show that NK TERT cells phagocytose apoptotic cells. Even though this finding is very interesting, the observed behaviour could lead to a misinterpretation of the results from a co-culture drug screen. Phagocytosis of dead cells leads to a higher percentage of alive cancer cells in co-cultures which can falsely be interpreted as protection of CLL cells from

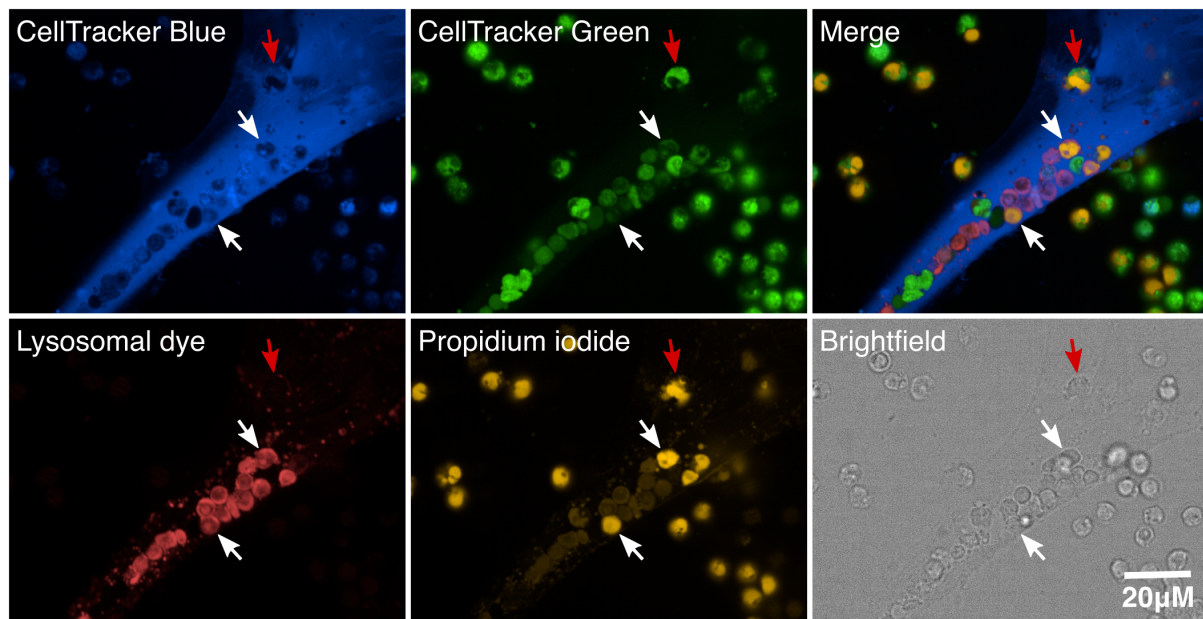


Figure 3.5: **Some MSCs also phagocytose apoptotic CLL.** Representative confocal microscopy images of co-cultures of CellTracker Blue labelled MSCs from one donor (MSC1) and CellTracker Green labelled CLL cells, previously treated with 63 nM venetoclax and stained with propidium iodide and lysosomal dye NIR. White arrows highlight some examples in which apoptotic CLL have been phagocytosed by MSC. The red arrow highlights an apoptotic CLL cell in the process of being phagocytosed by MSC. (Herbst et al., 2020b)

spontaneous and drug-induced apoptosis by stroma cells. In the well established bone marrow stroma cell line HS-5 this extensive phagocytic activity was not observed. Therefore, HS-5 cells were chosen as suitable model for the co-culture screen. However, it needs to be kept in mind, that this system only represents a model to enable high-throughput screening and all obtained results should be further validated in co-culture models with primary stroma cells from the bone marrow.

### 3.1.3 Optimisation of seeding conditions for co-culture screen

#### 3.1.3.1 Optimal cell count for seeding of cells

To further optimise the culture conditions for the high-throughput screen different seeding densities of the HS-5 stroma cells were tested. Either  $0.5 \times 10^4$ ,  $1.6 \times 10^4$  or  $5 \times 10^4$  HS-5 cells were seeded into wells of a 384-well plate. In addition, cells were treated with solvent control or 10 nM venetoclax. No difference was observed between the control wells and drug treated cultures, as HS-5 do not seem to be susceptible to venetoclax treatment. The highest density of cells led to growth of HS-5 cells on top of each other. In the lowest density an uneven distribution of HS-5 cells across the well was observed (Fig. 3.6a). Uneven growth could potentially lead to problems in the analysis of images, as local effects of stroma cells on CLL cells would need to be accounted for by including the local densities of stroma cells in the calculations. Wells with seeding densities of  $1.6 \times 10^4$  cells/well were densely but evenly covered (Fig. 3.6b). To avoid the

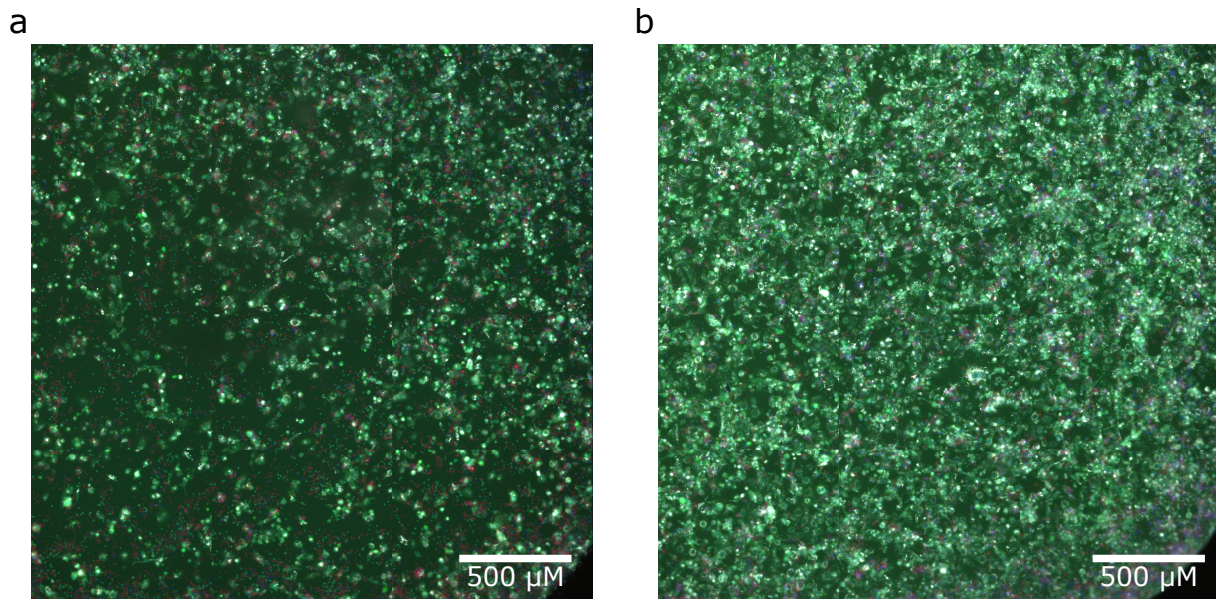


Figure 3.6: **Optimisation of HS-5 cell counts.** HS-5 cells seeded at **a**,  $0.5 \times 10^4$  cells/well or **b**,  $1.6 \times 10^4$  cells/well into a 384-well plate and co-cultured with CLL. Representative images are shown (in these cases venetoclax treated conditions). Green = Calcein AM, blue = Hoechst 33342, red = propidium iodide, white = lysosomal dye NIR.

occurrence of local effects,  $1 \times 10^4$  cells/well were chosen as optimal seeding density for HS-5 cells. It has been reported that the ratio between stroma cells and CLL cells does not affect viability within co-cultures (Kurtova et al., 2009). Due to the limited availability of patient cells a CLL to stroma ratio of 2:1 ( $2 \times 10^4$  CLL cells/well) was chosen.

### 3.1.3.2 Irradiation of stroma cell line for co-culture screen

To avoid local effects within the co-culture wells, a high density of stroma cells was chosen. Yet, this causes the problem that stroma cells overgrow during the three day incubation period of the drug screen assay. A way to overcome this issue is the irradiation of stroma cells at sub-lethal doses to prevent proliferation of cells, but to maintain at the same time metabolic activity to allow the expression of cytokines and cell surface ligands (Roy et al., 2001). At a dose of 10 Gray (Gy) HS-5 cells did not significantly proliferate but remained viable for several days, judging by their morphology and clear Calcein signal. Furthermore, after freezing of stroma cells, which is a crucial step to facilitate the screening workflow, HS-5 cells irradiated with 10 Gy recovered equally well as untreated cells.

Consequently, HS-5 cells irradiated with 10 Gy were selected as suitable microenvironmental model to mimic the bone marrow niche accurately and to ensure the feasibility of the high-throughput co-culture drug screen at the same time.

### 3.1.4 Readout for co-culture drug screen

#### 3.1.4.1 Theoretical considerations for choosing an assay readout

When performing drug screening the viability of cells needs to be determined at the end of the assay to read out drug responses. Different methods for this task exist. The easiest and most widely used assay is a measurement of ATP levels (Friedman et al., 2015; Wood et al., 2006). For this, cells are lysed to release intracellular ATP. A luciferase based measurement can then quantify ATP levels. The assay can be read out using a microplate reader, which makes it quick and convenient. Yet, this assay is not suited for co-culture drug screening. All cells, stroma as well as leukemia cells, are lysed during this process, which prevents the distinction between leukemia and stroma viabilities. As stroma cells are more metabolically active than CLL cells, the signal from the stroma cells would additionally dominate the signal from the leukemia cells.

Another option for reading out the percentages of alive cells in the cultures would be a flow cytometry based assay. For this, CLL cells either need to be washed off from the stroma layer, or all cells need to be detached, for example with trypsin. This process raises some issues. The detachment procedure can have a negative impact on cell viability, leading to an additional source of error. On the other hand, some leukemia cells might not detach from HS-5 cells when removing leukemia cells by washing. This could lead to a systematic bias.

The least invasive way of measuring leukemia cell drug responses is the usage of microscopy. This technique allows the direct readout of the percentages of alive cells, leaving the architecture of the culture system intact. Additionally, the percentages of alive stroma cells and leukemia cells can be determined separately allowing a better monitoring of the culture system. The possibility of looking at the images manually, once the screen has been completed, moreover provides the option to identify potential errors retrospectively if irregularities within the data are observed during analysis. Finally, a microscopy-based assay is not limited to the assessment of percentages of alive cells, but can in addition extract other features, like cell morphology or distances between cells. These advantages led to the conclusion that an image-based setup would be best suited for a co-culture drug sensitivity screen.

#### 3.1.4.2 Comparison of staining panels for detection of alive cells

The presence of apoptosis can be measured in different ways using a microscopy-based system. The least invasive method is the usage of bright-field images and complex image analysis methods to detect morphological changes. However, this is a very challenging task, as contrast is low in bright-field images and a change in CLL morphology during apoptosis is barely detectable. Thus, the usage of a fluorescent staining panel to determine the percentage of apoptotic CLL cells in the screen was evaluated. To leave the architecture of the culture system as unperturbed as possible, dyes which do not require washing steps were favoured.

Apoptosis is a multi-step process, which can be detected with fluorescent dyes at multiple stages (Vorobjev and Barteneva, 2017). One of the earlier stages involves the decrease of

metabolic activity, including decreased ATP production and esterase activity. Calcein AM is a dye which turns green in alive cells upon cleavage by esterases and, thus, alive cells can be detected (Johnson, 2010). Towards the end of the apoptotic sequence, the plasma membrane gets perforated, which allows the entry of membrane-impermeable dead cell stains, like PI, into the cell (Vorobjev and Barteneva, 2017). PI binds to DNA and consequently labels dead cells (Johnson, 2010). Other DNA binding dyes exist which can also permeate the membrane of alive cells and enter the nucleus. Examples are Hoechst 33342 (Hoechst) (Johnson, 2010) or SiR-DNA (Lukinavičius et al., 2015). These dyes are commonly used in microscopy to perform the initial segmentation step which computationally separates cells in image analysis. In addition, the nucleus and its DNA content also undergo morphological changes in the late stages of apoptosis which can be monitored using these cell-permeable dyes (Vorobjev and Barteneva, 2017).

To select a suitable staining panel Calcein AM, PI and Hoechst were tested for their ability to stain CLL cells without the need for a washing step. For all of these dyes direct addition to the cultures, followed by an incubation time of 90 min at 37 °C, resulted in a clear and stable signal with good contrast. During these experiments clear morphological differences between the nucleus of alive and dead CLL cells could be observed in the Hoechst channel. For dead CLL cells, the Hoechst signal was brighter and occupied a smaller area, suggesting a condensation of DNA during apoptosis (Fig. S5). The usage of Hoechst in the final staining panel is required to correctly segment cells. If Hoechst could, based on these morphological changes, in addition, be used to determine whether a CLL cell is alive or dead, the triple staining panel of Hoechst, Calcein AM and PI could be reduced to a single staining with only Hoechst. This would reduce acquisition time, costs and spectral crosstalk between dyes. To evaluate this option, percentages of alive CLL cells in mono-cultures, calculated from Hoechst area or Calcein AM intensities, were compared in a joined effort with Tobias Roeder. The percentage of alive CLL cells determined using Calcein AM intensities or Hoechst area correlated well (Pearson correlation,  $r = 0.92$ , Fig. 3.7). In general, the usage of morphological features instead of intensities should be favoured for microscopy-based readouts. This is because fluorescent intensities are susceptible to experimental or technical variations and can shift over time and are, therefore, not very robust. Consequently, the area of a Hoechst single-stain was chosen as the best readout to determine drug responses.

### 3.1.5 Selection of the drug panel for the co-culture screen

To perform an informative drug sensitivity screen the choice of appropriate drugs and concentrations is crucial. In total, a panel of 43 different drugs was selected. This included ibrutinib, venetoclax, idelalisib and fludarabine, which are drugs frequently used in the treatment of CLL. Most of the other drugs chosen for the screen are FDA approved or currently in clinical trial. For a comprehensive list see table 2.1. Moreover, if possible, multiple drugs targeting the same pathway were included in the screen, e.g. the JAK inhibitors ruxolitinib, tofacitinib and pyridone 6, the PI3K inhibitors idelalisib and duvelisib or the chemotherapeutic agents fludarabine, cytarabine and doxorubicine. Due to a limited number of wells on 384-well plates, three concentrations for each drug were chosen. Our group previously published a drug screen in

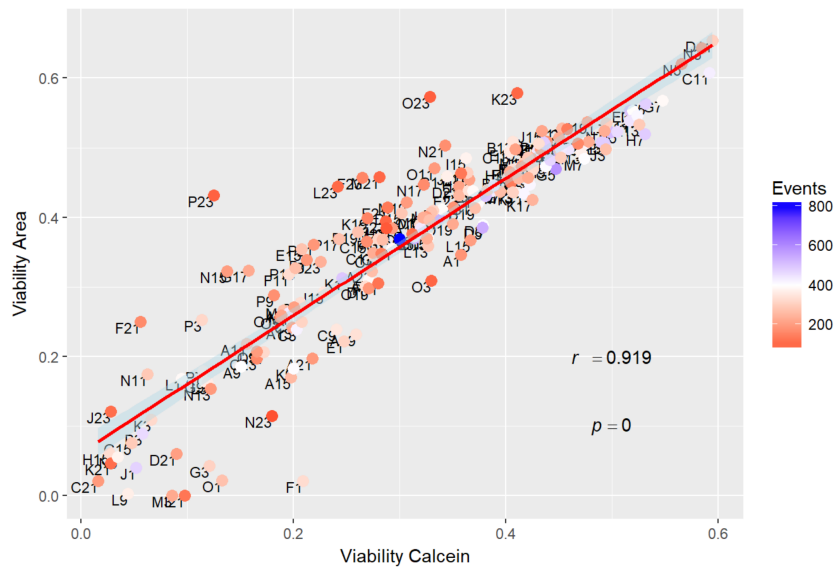


Figure 3.7: **Evaluating nuclear area as readout to detect alive CLL cells.** Pearson correlation between percentages of alive CLL cells in mono-cultures obtained either by using Calcein AM signal (Viability Calcein) or nuclear area determine from Hoechst signal (Viability Area). Points and labels represent well coordinates with different drug conditions. The number of analysed cells (events) per well are colour-coded. The experiment was conducted in a joined effort with Tobias Roider. The analysis and figure was produced by Tobias Roider and used with permission.

mono-cultures of CLL (Dietrich et al., 2018). This study was used as reference to select suitable drug concentrations, which would affect the percentage of alive CLL cells, but not completely kill cancer cells of all patients. However, it was unknown how co-culturing of cells would affect drug response. Therefore, a 15-fold increase in concentration steps was chosen, to ensure that potentially interesting effects are not missed.

### 3.1.6 Co-culture drug sensitivity screen

After successful optimisation of the screening protocol the co-culture drug sensitivity screen was carried out (Fig. 3.8). In preparation of the screen, one batch of HS-5 cells was produced, irradiated and frozen in aliquots of  $2 \times 10^7$  cells, which is sufficient for screening five patient samples. Drug plates were prepared, containing all of the drugs in DMSO, which can be thawed on the screening day, diluted in medium and directly added to the assay plates. For screening ten patient samples one drug plate is needed. For each patient one 384-well assay plate containing all drug conditions in mono- and co-cultures was prepared on the screening days. (Herbst et al., 2020a)

The cohort comprised samples from in total 81 different CLL patients with a median age of 70 years, which represents well the reported median age of CLL patients at diagnosis (Bosch and Dalla-Favera, 2019). Out of all patients 25 % had received treatment prior to sample collection. Out of these, the majority had been treated with chemotherapeutic agents and only three pa-

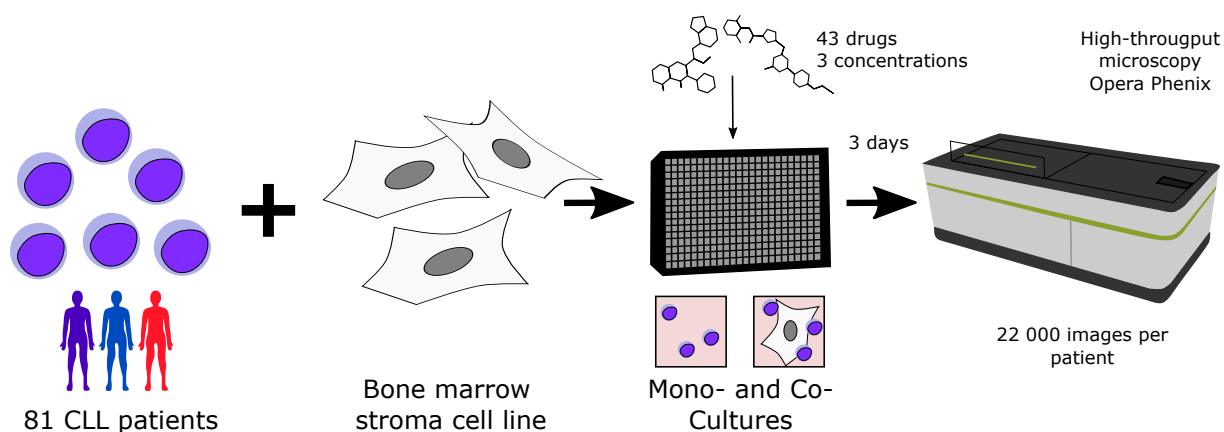


Figure 3.8: **Overview of the co-culture drug sensitivity screen.** CLL cells from 81 patients were co-cultured with the human bone marrow stroma cell line HS-5 in 384 well plates and treated with a panel of 43 drugs in three concentrations. In addition, plates contained the same conditions as CLL mono-cultures to enable direct comparison between the culture conditions. After an incubation time of three days the percentages of alive cells were determined using high-throughput confocal microscopy with an Opera Phenix microscope (Perkin Elmer). (Herbst et al., 2020a)

tients had received targeted therapy with BCR inhibitors. In total, six patients, corresponding to 7% of the cohort, had been in treatment at the time of sample collection, all of them receiving treatment with either of the BCR inhibitors ibrutinib or idelalisib, in two cases in combination with the anti-CD20 antibody rituximab. Patients in treatment at the time of sample collection were excluded for all analyses involving time to next treatment. (Herbst et al., 2020a)

In general, the conduction of the co-culture screen went smoothly and no major problems were encountered. All patients were screened within a time-frame of eight months. No systematic changes of dye intensities or drug potencies were observed over time. An example image of a co-culture is shown in Fig. 3.9. Large stroma cells and small, round CLL cells can clearly be distinguished by size. The blue channel shows the signal from Hoechst staining. In addition, a signal shown in white is depicted. This signal originates from a lysosomal dye which had been additionally included in the screen with the purpose of reading out autophagy. However, this data will not further be mentioned in this thesis. (Herbst et al., 2020a)

### 3.1.6.1 Quality control: Correlation of replicates

For quality control, some patients samples were screened in duplicates. In general, technical replicates correlated well (Pearson correlation), regardless of whether the sample had been repeated on the same screening day, on the same plate in different wells (Fig. 3.10a,  $r = 0.84$ ), on the same screening day, on different plates (Fig. 3.10b,  $r = 0.87$ ) or on different screening days (Fig. 3.10c,  $r = 0.88$ ). (Herbst et al., 2020a)

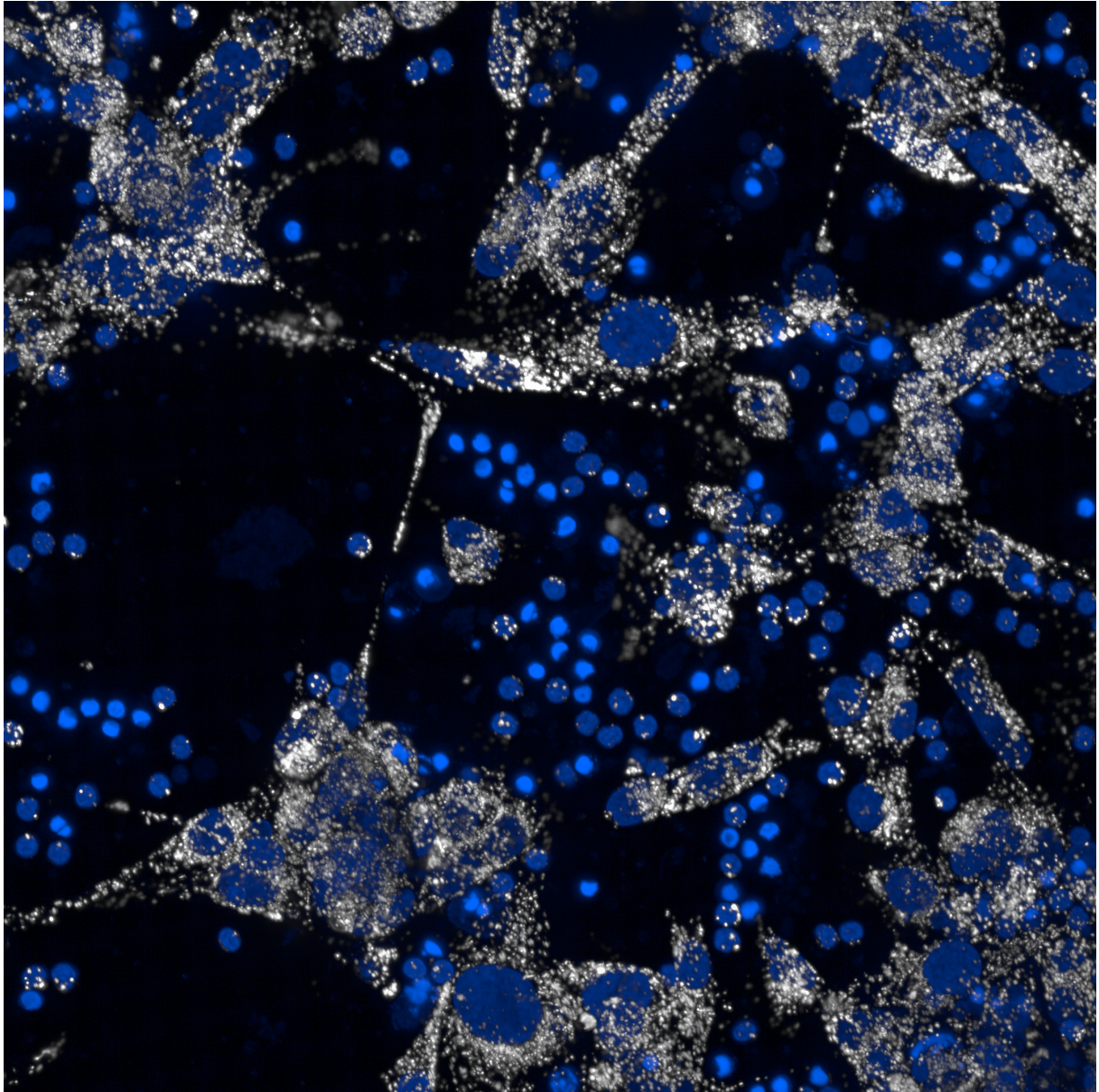


Figure 3.9: **Example image of a co-culture well in the high-throughput drug screen.**  
Blue = Hoechst, white = lysosomal dye NIR. (Herbst et al., 2020a)

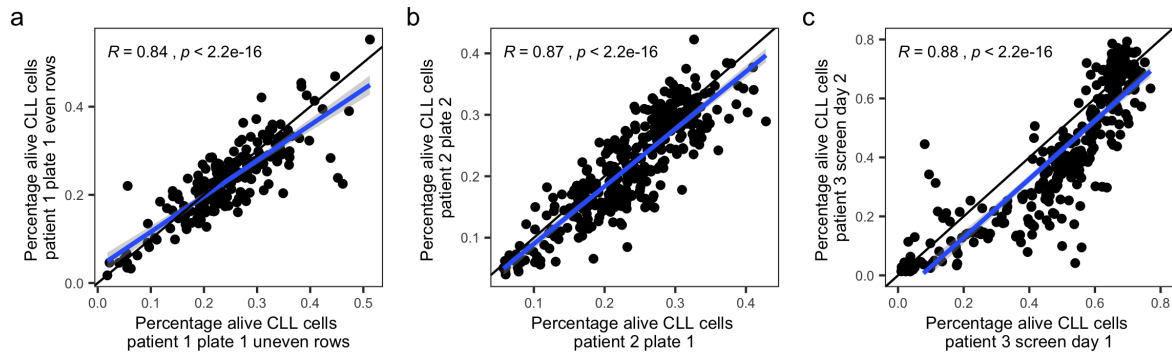


Figure 3.10: **Correlation between replicates in co-culture drug sensitivity screen.** Correlation of the percentages of alive cells between replicates **a**, of different wells of the same patient sample, screened on one day in the same assay plate, **b**, of the same patient sample, screened on the same day, but in different assay plates or **c**, of the same patient sample screened on different days.  $R$  denotes the Pearson correlation coefficient. The blue line is the regression line, the black line is the line with slope = 1 and intercept = 0. Both mono- and co-culture wells were included in the analysis.

### 3.1.6.2 Quality control: Culture plate edge effect

A common problem observed in drug-sensitivity screening is the culture plate edge-effect (He et al., 2018; Mattiazzi Usaj et al., 2016). The effect occurs due to increased evaporation of liquid in wells located on the edge of the culture plates, which can influence cell viability. A negative impact of an edge effect on data analysis and interpretation can largely be avoided by careful experimental planning. If the drug plate layout is kept constant across all samples, similar edge effects act on the same drug conditions across plates, which allows the comparability between patients. Moreover, wells directly located next to each other experience similar external influences, making them comparable. These considerations were taken into account for the design of this screen to ensure interpretability of the results, even in the presence of this bias. Thus, mono- and co-culture wells with the same conditions were for example directly placed next to each other.

Yet, we were interested in how co-culturing affects the occurrence of an edge effect. For this, the percentages of alive cells in only the solvent control wells were plotted per patient in a joined effort with Eva Schitter. The distances of the wells from the edge of the plate were colour-coded (Fig. 3.11). In mono-cultures a clear edge effect was visible. Fewer alive cells in wells located on the edge of the plates were observed than in solvent control wells located in the center of the assay plates. In contrast, no edge effect could be detected in the co-cultures. Here, the percentages of alive cells did not differ between solvent control wells located in the center or edge of the culture plates. CLL cells are known to be vulnerable in *ex-vivo* cultures (Collins et al., 1989). Co-culturing with HS-5 stroma cells seems to stabilise CLL cells *ex-vivo* and, therefore, increases the robustness of the screen. (Herbst et al., 2020a)

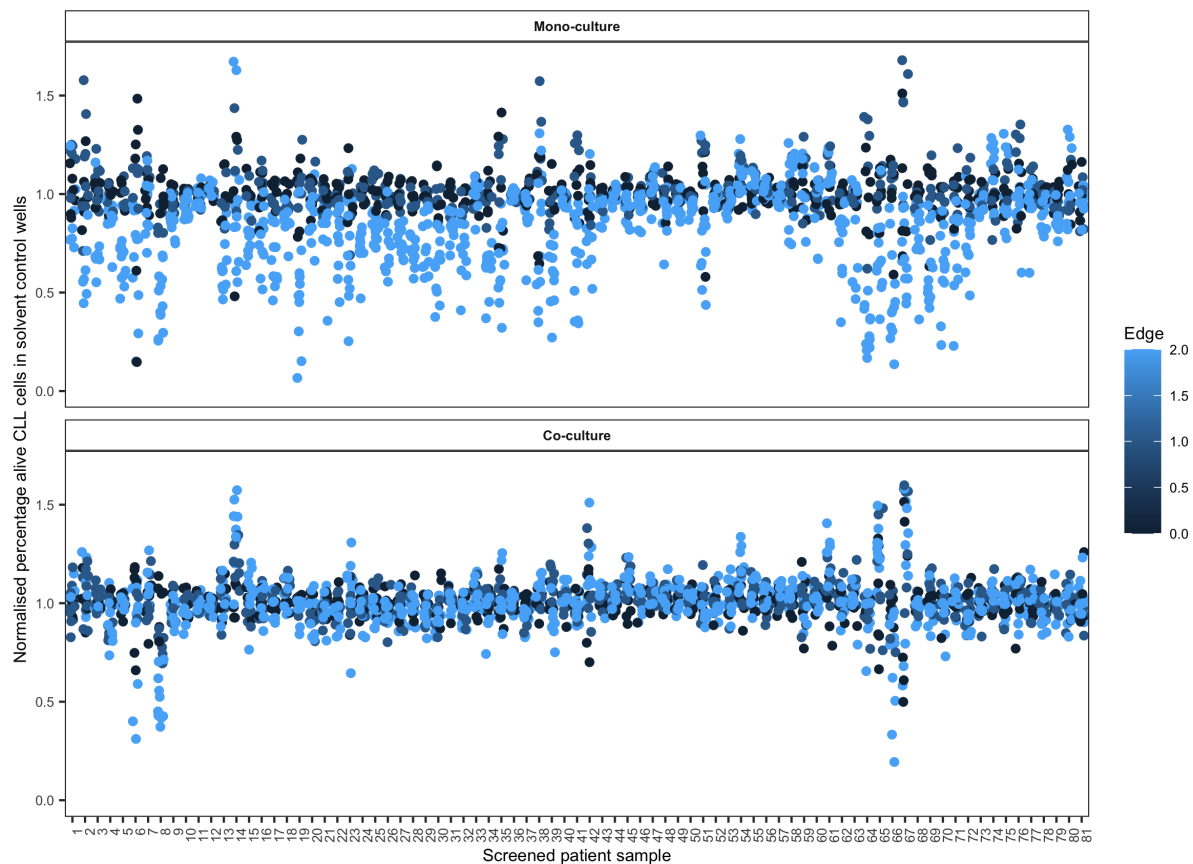


Figure 3.11: **Edge effect in mono- and co-cultures in high-throughput drug screen.**

Percentages of alive cells of solvent control wells for mono- and co-cultures. Percentages of alive cells were normalised to the mean of the solvent control wells of the respective cultures located in the center of the assay plates. The distance of the wells from the edge of the assay plate is colour-coded. 2 = located on edge of culture plate, 1 = located one well away from edge of culture plate, 0 = located in the center of the culture plate. Screened patient samples are ordered according to the date at which the plate was screened.

## 3.2 Proteogenomic characterisation of CLL patient samples

The results described here (section 3.2) have been submitted for publication (Herbst et al., 2020c). The text in the manuscript was originally written by me and has been modified for this thesis.

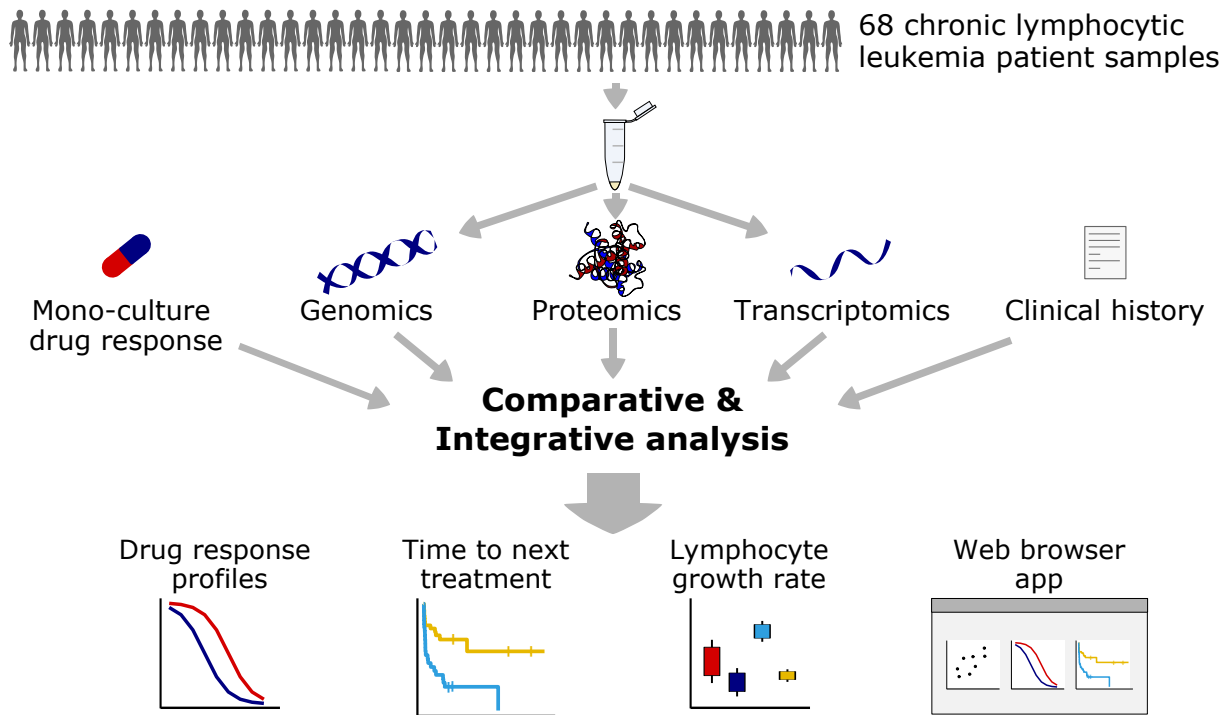


Figure 3.12: Overview proteogenomics to characterise cell-intrinsic factors influencing CLL drug response and outcome. (Herbst et al., 2020c)

### 3.2.1 Acquisition of multi-omics dataset of CLL

#### 3.2.1.1 Study outline

In order to gain insights into cell-intrinsic factors influencing drug response and outcome, 68 of the CLL patient samples were, in addition to the *ex-vivo* drug sensitivity screen, characterised further by proteogenomics (Fig. 3.12). This approach integrates in-depth mass-spectrometry based proteomics with other omics datasets to trace the molecular consequences of genetic alterations. Currently the value of proteogenomics is being demonstrated for a handful of cancer entities by providing insights into the mechanisms of tumour development and progression (Akbari et al., 2014; Archer et al., 2018; Clark et al., 2019; Johansson et al., 2019; Yang et al., 2019; Zhang et al., 2016). Integration of proteomics with other omics datasets could help to understand the heterogeneous clinical course of CLL.

For this, and whenever possible, aliquots of cells matching to the CLL sample analysed in the *ex-vivo* drug sensitivity screen were used. One aliquot per patient was thawed and CD19<sup>+</sup> cancer cells were enriched by magnetic-activated cell sorting. The resulting cell pellet was split

into one part which was used for proteomics and, where possible, one part for RNA sequencing and one part for DNA panel sequencing (Fig. 3.12). This paired approach enabled an unbiased view on different layers of tumour heterogeneity without variations in sample preparation affecting the comparability between datasets. Additionally, information on the presence of clinically relevant copy number changes, patient characteristics, treatment history and time-to-next treatment (TTT) was obtained (Fig. 3.12). (Herbst et al., 2020c)

So far, proteogenomic studies on primary cancer patient samples have focused on the comprehensive measurement of molecular alterations. However, information on how the system reacts to perturbations could establish a direct link between molecular changes and functional consequences. A study showing the value of such an approach in primary cancer cells is currently lacking. Therefore, our proteogenomics data for CLL was integrated with the high-throughput *ex-vivo* drug sensitivity screen described in section 3.1. In the current section (3.2) only drug responses from mono-cultures were considered, while the co-culture drug screening data is presented in section 3.3.

### 3.2.1.2 Proteomic profiling of the cohort

Proteome data from 68 CLL samples was obtained. Measurement of the entire proteome with the help of tandem mass tag (TMT 10-plex) isobaric labelling was performed by our collaborators in the group of Janne Lehtiö at the Karolinska Institute in Stockholm. In total, proteomic analysis identified and quantified 9845 proteins (gene symbol-centric) at 1% FDR based on 168207 unique peptides with an overlap of 7311 proteins quantified across all samples. Median protein sequence coverage was 37.8% with a median of six unique peptides and 10.5 PSM per quantified protein. (Herbst et al., 2020c)

### 3.2.1.3 Transcriptomic profiling of the cohort

In total, matching transcriptome data was obtained for 59 samples with proteomic characterisation. For this, total RNA was extracted from pellets with the RNeasy Mini Kit. Library preparation and sequencing was performed by the EMBL genecore facility. A total of 7199 proteins quantified by mass spectrometry overlapped with the transcriptomics data. (Herbst et al., 2020c)

### 3.2.1.4 Genetic profiling of the cohort

For 67 CLL patient samples mutational information could be measured directly from the samples used for proteomic and transcriptomic profiling. For all other patients for which cells were used in the *ex-vivo* drug sensitivity screen mutational information was kindly provided by Thorsten Zenz, NCT Heidelberg. The IGHV status could be determined for 75 of the 81 CLL patients in the complete cohort. For all patients, information on copy-number aberrations was available from routine testing in the clinic.

In total our cohort consisted of 56% M-CLL and 44% U-CLL patients. In the subset of patients with proteomic profiling the frequencies were 52% and 48% respectively. These fre-

quencies are representative of the frequencies usually observed in CLL patient cohorts (Hamblin et al., 1999). Trisomy 12 was detected in 27 % of all patient samples and 23 % of the patients with available proteomics data, which is slightly more than the expected frequency (Abruzzo et al., 2018). Overall, mutations in the genes of *ATM*, *BIRC3*, *EGR2*, *NOTCH1*, *POT1*, *SF3B1*, *TP53* and *XPO1* and the copy-number aberrations del11q, del13q14, del17p13, gain8q and trisomy 12 were present in at least three patients and were, therefore, considered for further analyses.

### 3.2.2 Interplay between proteomics, transcriptomics and genetic alterations and functional consequences

To connect genotype with molecular phenotype, associations between recurrent genetic alterations of CLL, mRNA expression- and protein abundance were investigated. For this, protein abundance was regressed on recurrent genetic alterations of CLL. Trisomy 12 had the strongest impact on protein abundance (Fig. 3.13a), with 54 proteins being significantly up- and 13 proteins downregulated (adjusted  $p < 0.001$ ;  $|\log_2 \text{fold change}| > 0.5$ ). In addition, IGHV mutational status (19 proteins) and *SF3B1* mutations (29 proteins) were associated with multiple differentially abundant proteins. Among the significantly differential proteins associated with IGHV status was *ZAP70*, which is a known surrogate marker for IGHV status (Crespo et al., 2003), underlining the validity of this approach. Next gene expression profiles between patient samples with and without recurrent genetic alterations of CLL were compared. While trisomy 12 (549 transcripts) and IGHV status (205 transcripts) were also associated with many significant gene expression changes (adjusted  $p < 0.001$ ;  $|\log_2 \text{fold change}| > 1.5$ ), only very few genes were differentially expressed between patient samples with and without *SF3B1* mutations (14 transcripts; Fig. 3.13b). (Herbst et al., 2020c)

Next, an analysis was conducted investigating whether the protein abundance changes associated with trisomy 12 were related to gene dosage effects. Trisomy 12 increased the abundance of proteins located on chromosome 12 (Fig. 3.13c), but 63 % of all differentially abundant proteins were located on other chromosomes. Gene dosage effects translated into altered protein levels for all further important structural aberrations of CLL (del17p, del13q, gain8q and del11q, Fig. S6). Similar trends were also seen on RNA level (Fig. 3.13d and Fig. S7). As shown for other disease entities (Johansson et al., 2019; Yang et al., 2019; Zhang et al., 2016), the data confirms in CLL that gene dosage effects translate into transcriptomic, as well as proteomic changes. (Herbst et al., 2020c)

Although some recurrent genetic alterations of CLL, e.g. trisomy 12 and IGHV, translated into protein abundance as well as RNA expression changes, the overall correlation of protein abundance and gene expression was rather low (Fig. 3.14a; median Spearman's rank correlation  $\rho = 0.24$ ). 42 % of genes and corresponding proteins were positively correlated (FDR  $< 5\%$ ). This degree of correlation was comparable to gene  $\sim$  protein correlations reported for other cancer entities (Johansson et al., 2019; Mun et al., 2019; Yang et al., 2019; Zhang et al., 2016). Differentially abundant proteins associated with trisomy 12 or IGHV status exhibited higher gene  $\sim$  protein correlations than unassociated proteins (Fig. 3.14b; median Spearman's rank

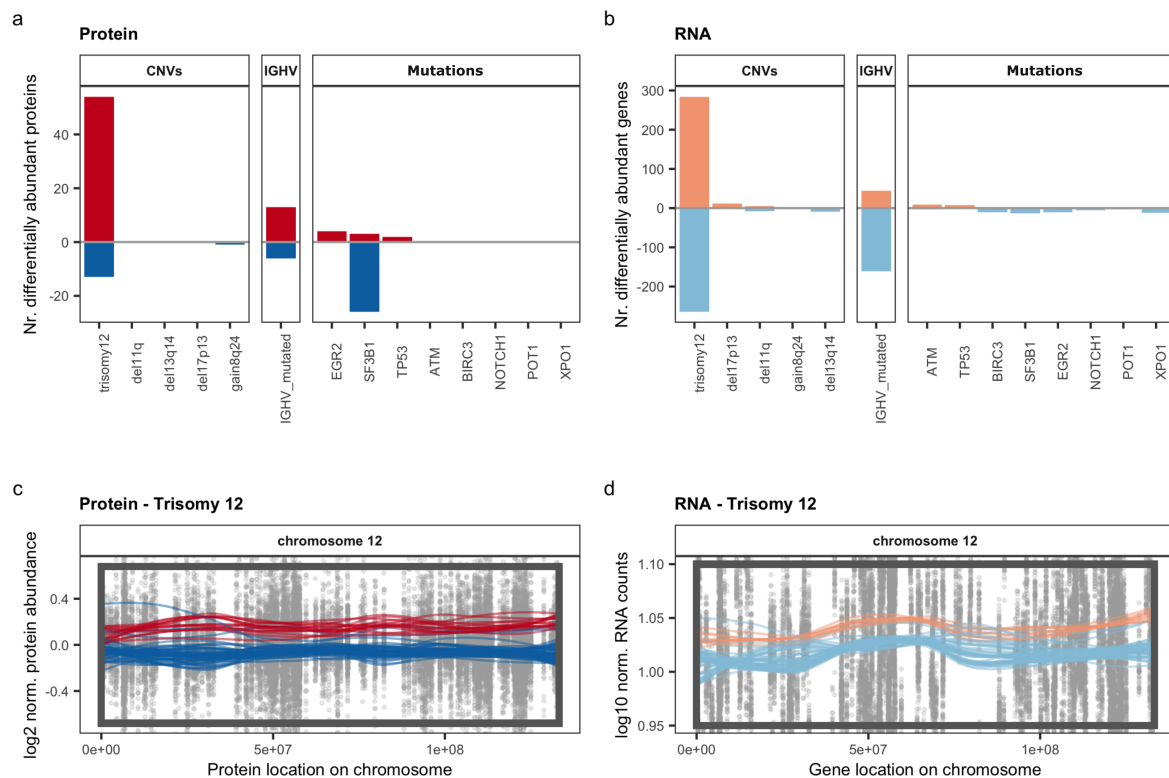


Figure 3.13: **Differential protein and transcript abundances in respect to genetic alterations.** **a**, Number of significantly differentially abundant proteins (adjusted  $p < 0.001$ ;  $|\log_2FC| > 0.5$ ) in relation to recurrent genetic alterations; red/positive numbers = upregulated, blue/negative numbers = downregulated. **b**, Number of significantly differentially expressed genes (adjusted  $p < 0.001$ ;  $|\log_2FC| > 1.5$ ) in relation to recurrent genetic alterations; red/positive numbers = upregulated, blue/negative numbers = downregulated. **c & d**, Levels of proteins and transcripts from chromosome 12 were affected by trisomy 12. Protein abundance (**c**) and gene expression levels (**d**) for chromosome 12 are shown. Points represent individual values for protein/gene - patient pairs. Lines are locally weighted scatterplot smoothed values for individual patients with (red) or without (blue) trisomy 12. The box is the region affected by trisomy 12. CNVs = Copy number variations. (Herbst et al., 2020c)

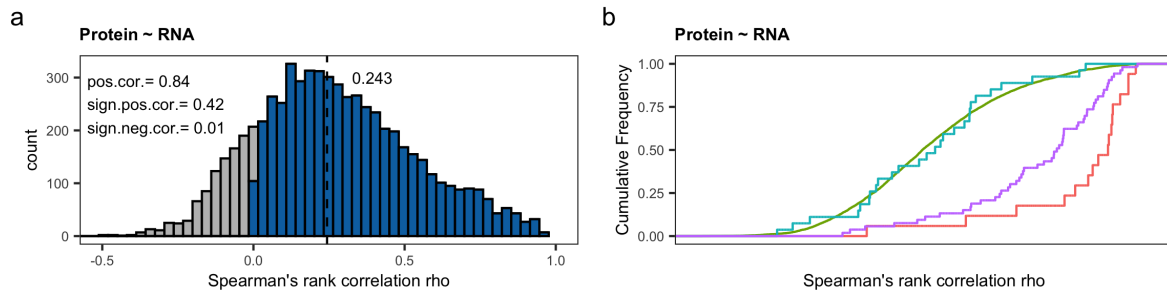


Figure 3.14: **Correlation of RNA and proteins.** **a**, Distribution of Spearman's rank correlations for protein-RNA pairs. pos.cor. = percentage of pairs with  $\rho > 0$ . sign.pos.cor. = percentage of pairs with  $\rho > 0$  and  $\text{FDR} < 5\%$ . sign.neg.cor. = percentage of pairs with  $\rho < 0$  and  $\text{FDR} < 5\%$ . 0.243 is the median  $\rho$ . **b**, Cumulative density distribution of protein-RNA Spearman's rank correlations for the proteins significantly differentially abundant in IGHV mutated (red), trisomy 12 (pink) or *SF3B1* mutated (blue) CLL in comparison to all other proteins without these associations (green). (Herbst et al., 2020c)

correlation  $\rho$  trisomy 12 = 0.69 and IGHV = 0.86). This was not the case for differentially abundant proteins associated with *SF3B1* mutations (Fig. 3.14b; median Spearman's rank correlation  $\rho$  = 0.29). This suggests that for trisomy 12 and IGHV, changes in the proteome are predominantly caused by changes in the transcriptome, while differential protein abundances for *SF3B1* mutations seem to be regulated by post-transcriptional mechanisms. (Herbst et al., 2020c)

Even though *TP53*, *ATM* and *XPO1* mutations were associated with only few differentially abundant proteins, biologically relevant changes for these alterations were detected. p53 for instance, was the most upregulated protein in *TP53* mutated CLL compared to *TP53* wild-type CLL samples (Fig. 3.15a). Even though *TP53* is a tumour suppressor gene, *TP53* mutations do not only lead to a loss of the protective function of p53, but often also support pro-tumour activities of this protein (Dittmer et al., 1993). The observation that p53 is upregulated in *TP53* mutated CLL recapitulates the well established finding that these tumours accumulate high levels of mutant p53, which contributes to mutant p53 gain-of-function properties (Jethwa et al., 2018). In contrast, *TP53* transcripts were significantly downregulated in *TP53* mutated CLL samples (Fig. 3.15b; Wilcoxon signed-rank test  $p = 0.005$ ), suggesting that post-transcriptional mechanisms are responsible for the accumulation of mutant p53, as previously shown (Jethwa et al., 2018). As expected, *TP53* mutated CLL samples responded worse to *ex-vivo* treatment with chemotherapeutic agents or the MDM2 inhibitor nutlin 3a than *TP53* wild-type samples (Fig. 3.15c; Wilcoxon signed-rank test,  $p = 0.003$ , Jethwa et al. (2018)). This example illustrates how the fate and functional consequences of a genetic alteration could be traced across multiple omics layers. Apart from this well studied example of *TP53*, specific and biologically relevant protein abundance changes were identified for *ATM* and *XPO1* mutations. Protein levels of ATM were lower in *ATM* mutated than *ATM* wild-type patient samples, indicating a

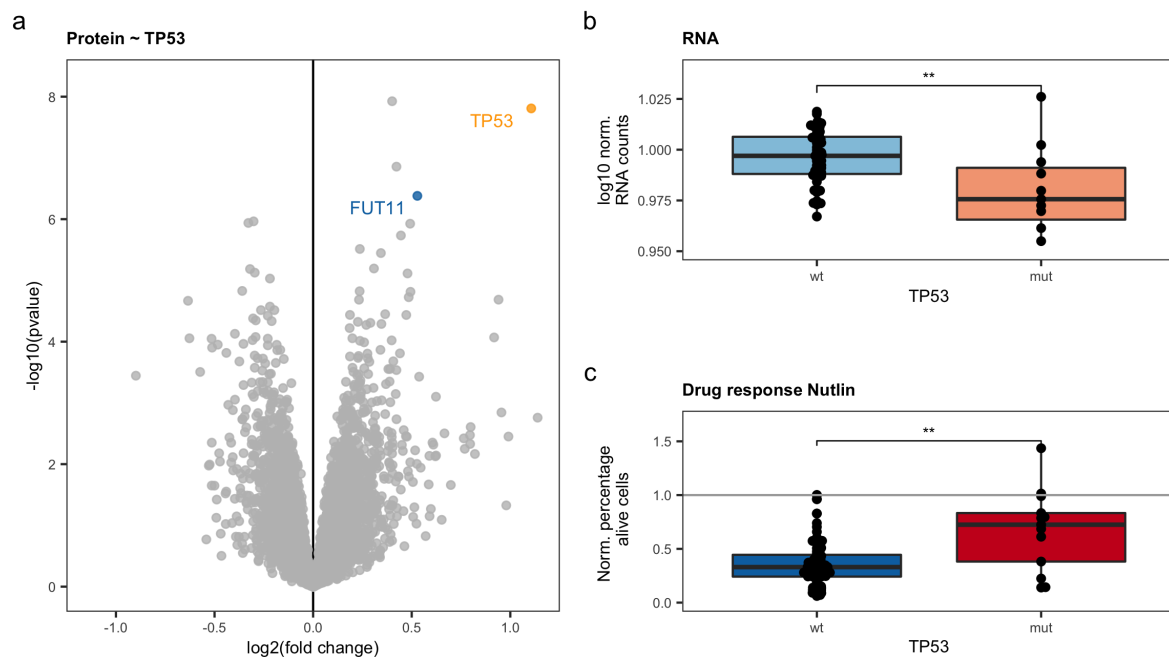


Figure 3.15: **Consequences of *TP53* mutations.** **a**, Volcano plot indicating differentially abundant proteins in *TP53* mutated CLL in comparison to wild type CLL. Blue and yellow indicate significantly differential proteins (adjusted  $p < 0.001$ ;  $|\log_2 \text{fold change}| > 0.5$ ). **b**, *TP53* transcript levels in *TP53* mutated (mut) and wild type (wt) CLL samples; Wilcoxon signed-rank test  $p = 0.005$ . **c**, Percentages, normalised to solvent control, of alive cells of *TP53* mutated (mut) and wild type (wt) CLL samples treated *ex-vivo* with  $9 \mu\text{M}$  nutlin 3a for 3 days. (Herbst et al., 2020c)

loss-of-function phenotype for this tumour suppressor (Fig. S8a). This association was only observed on protein (Wilcoxon signed-rank test,  $p = 0.001$ ), but not on transcript level (Wilcoxon signed-rank test,  $p = 0.17$ , Fig. S8b). Furthermore, *XPO1* protein was downregulated in *XPO1* mutated CLL samples (Wilcoxon signed-rank test,  $p = 0.004$ , Fig. S8c). Again we did not find downregulation of *XPO1* on the transcript level (Wilcoxon signed-rank test,  $p = 0.18$ , Fig. S8d). In line with the downregulation of *XPO1* protein, no increased response of *XPO1* mutated CLL to the *XPO1* inhibitor selinexor was observed (Wilcoxon signed-rank test,  $p > 0.1$ , Fig. S8e). (Herbst et al., 2020c)

Consequently, these results showed that the CLL proteome mirrors many changes which are also present on RNA level, but can in addition uncover biological relationships not detectable from the transcriptome. (Herbst et al., 2020c)

### 3.2.3 High abundance of BCR signalling proteins was associated with better outcome

To investigate the relationship between protein levels and clinical outcome protein abundance was regressed on time to next treatment (TTT). For indolent diseases, like CLL, TTT is fre-

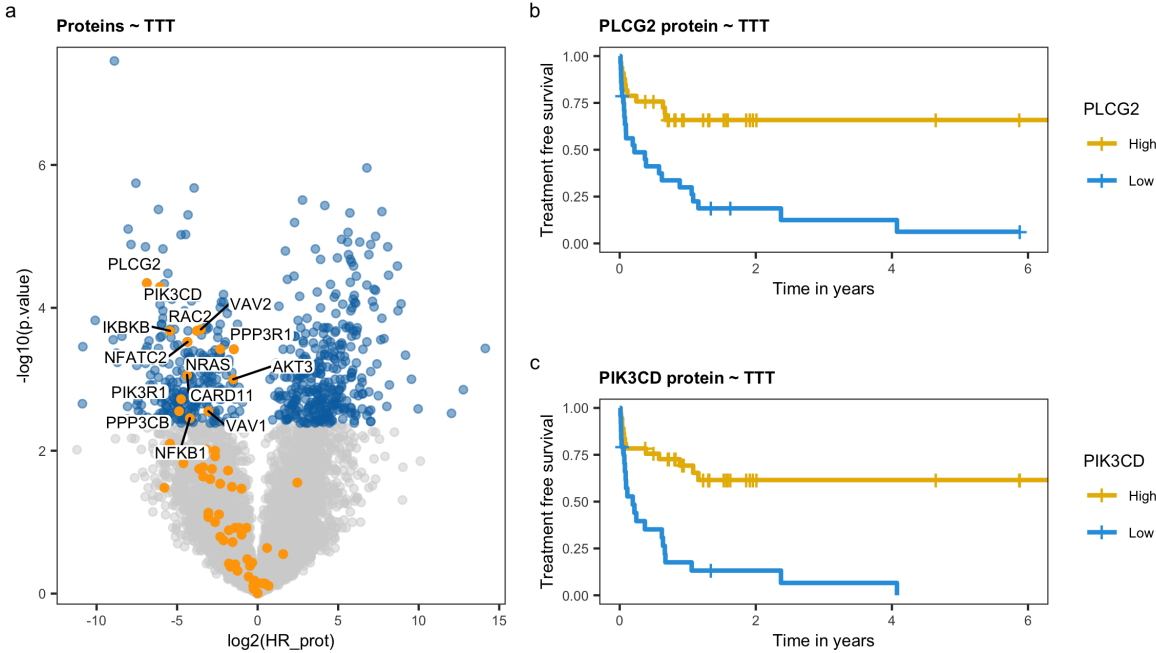


Figure 3.16: **Relation of protein abundance and time to next treatment (TTT).** a, Log2 of Hazard ratios and  $-\log_{10}$  of p-values calculated in Cox regression of protein abundance versus TTT. Proteins significantly associated with TTT (blue; FDR < 5%) and proteins in KEGG BCR signalling pathway (yellow) are color coded. BCR signalling proteins significantly associated with TTT are labelled. b & c, Kaplan-Meier curves for two BCR proteins significantly associated with TTT. (Herbst et al., 2020c)

quently used as measurement for clinical outcome, as this parameter does not require an extensive follow-up time and is not confounded by cancer unrelated deaths in the elderly population of CLL patients. 605 proteins (8.3% of all detected proteins) were found to be significantly ( $FDR < 0.05$ ) associated with TTT (Fig. 3.16a). Proteins which were associated with TTT were significantly enriched for BCR signalling components ( $FDR < 10\%$ ; shown in orange in Fig. 3.16a). In general high levels of proteins involved in this pathway predicted longer TTT (examples shown in Fig. 3.16b and c). However, ZAP70 had a positive hazard ratio, meaning that CLL with high levels of ZAP70 had shorter TTT. This is in accordance with the literature, as ZAP70 is known to be upregulated in U-CLL, which have in general worse outcome than M-CLL patients (Crespo et al., 2003). (Herbst et al., 2020c)

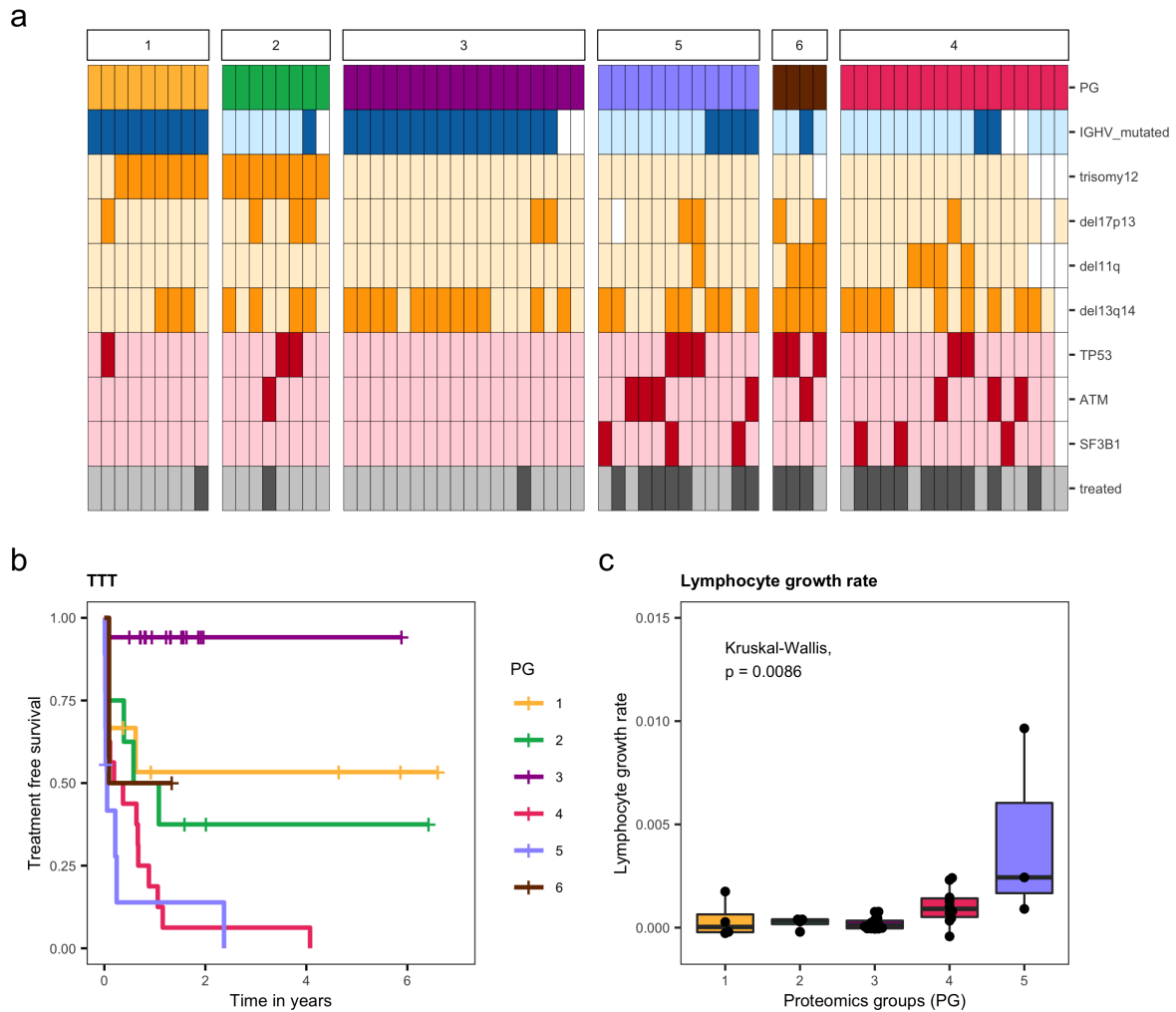
### 3.2.4 Proteomics based stratification of CLL identified six distinct subgroups

To further explore the clinical heterogeneity between CLL patients the existence of proteomic subgroups among CLL patients was assessed by performing consensus clustering on the protein dataset. This computational method evaluates the existence and number of patient subgroups and their robustness. Six proteomics groups (PG) within the cohort were identified (Fig. S9). T-distributed stochastic neighbour embedding (t-SNE) and principal component analysis (PCA) supported the partition into these subgroups (Fig. S10). (Herbst et al., 2020c)

Next, associations between the proteomics groups and genetic alterations were assessed (Fig. 3.17a). PG1-4 (PG1  $n = 9$ , PG2  $n = 8$ , PG3  $n = 18$ , PG4  $n = 17$ ) represented all four possible combinations of trisomy 12 versus IGHV status (Fisher's exact test,  $FDR < 10\%$ ). Of note, two patients in the trisomy 12 enriched subgroup PG1 had not been classified as trisomy 12, however, one of them, nevertheless, harboured a subclonal (11%) trisomy 12 falling below the threshold of 20%, which had been defined as minimum required clone size. For PG6 ( $n = 4$ ) an enrichment of *TP53* mutations was observed (Fisher's exact test,  $FDR < 10\%$ ). PG5 ( $n = 12$ ) contained only trisomy 12 negative patients, but no other association with known recurrent genetic alterations could be detected. (Herbst et al., 2020c)

Additionally, this grouping separated patients with different TTT (Fig. 3.17b; logrank test,  $p < 0.0001$ ). The M-CLL, chromosome 12 wild type group PG3 had the longest TTT, as expected (Bosch and Dalla-Favera, 2019). The group for which no genetic association could be detected (PG5) showed the poorest outcome, highlighting its clinical significance. *In-vivo* lymphocyte growth rates, even though only available for 35 patients, also differed between groups (Kruskal-Wallis test,  $p = 0.009$ ) and were highest for PG5 (Fig. 3.17c). These results indicate a clinical relevance of the identified groups. (Herbst et al., 2020c)

To explore the relationship between the proteomics groups and the transcriptome, consensus clustering was also performed on the RNA data. This identified five subgroups, of which only three contained more than three patients. These transcriptome based subgroups only partially overlapped with the subgroups identified by proteomics profiling (Fig. 3.18). PG1-4 corresponded well to the transcriptomics groups, even though the two trisomy 12 subgroups



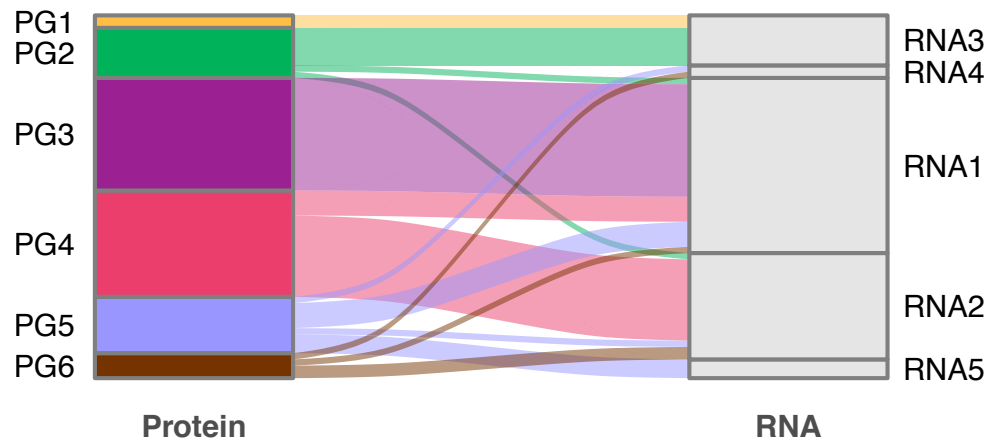


Figure 3.18: **Comparison consensus cluster groups from protein and RNA.** Comparison of patient grouping from consensus clustering on proteome and transcriptome data. PG1-4 were partially supported by transcriptomics, while PG5 and PG6 were only apparent from proteomics. (Herbst et al., 2020c)

PG1 and PG2 were merged into one subgroup in transcriptomics-based clustering. In contrast, PG6 CLL samples were split across multiple transcriptomic-based subgroups. Protein and RNA levels did not correspond well for TP53 (Fig. 3.15a,b) which explains why the *TP53* mutation-enriched subgroup PG6 could not be separated on the transcriptome level. Even though clearly distinguishable from the proteome, also PG5 was not transcriptionally distinct from the other subgroups, as transcriptomic-based clustering split PG5 across multiple groups. Therefore, neither an association of PG5 with genetics nor transcriptomics was found. (Herbst et al., 2020c)

Biological relevance of the groups was further supported by their distinct mono-culture drug response profiles. Interestingly, the U-CLL, trisomy 12 subgroup PG2, showed increased *ex-vivo* sensitivity to the BCR inhibitors duvelisib (PI3Ki), idelalisib (PI3Ki) (Fig. 3.19a), ibrutinib (BTKi) and BAY61-3606 (SYKi) (Fig. S11a,b). As expected, the *TP53* mutation-enriched group PG6 was the group least responsive to chemotherapeutic agents like doxorubicin, cytarabine (Fig. 3.19b) and fludarabine (Fig. S11c). (Herbst et al., 2020c)

Taken together, unsupervised clustering of proteomic profiles classified CLL patients into six biologically and clinically relevant subgroups of which five could be explained by genetic characteristics, while one subgroup (PG5) was only detectable from the proteome. (Herbst et al., 2020c)

### 3.2.5 Deregulated pathways and drug vulnerabilities of newly discovered poor outcome proteomics group 5 (PG5)

The previously unappreciated subgroup PG5 had the shortest TTT, fastest *in-vivo* lymphocyte growth rate and showed no association with known genetic alterations or transcriptomic changes. To identify which proteins drive clustering of PG5, differential protein abundances between PG5 and the other subgroups were calculated. Enrichment analysis identified BCR

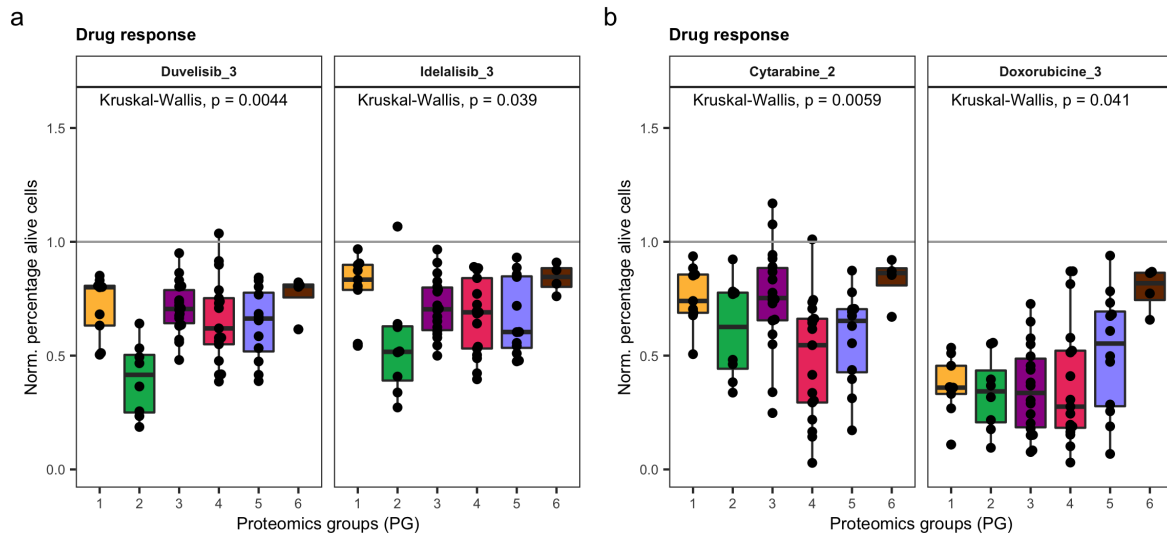


Figure 3.19: **Response of proteomics groups (PGs) to B-cell receptor inhibitors and chemotherapeutics.** **a**, Percentages of alive cells, normalised to solvent control, across PGs treated *ex-vivo* with  $4.5 \mu\text{M}$  duvelisib (Duvelisib\_3) or  $9 \mu\text{M}$  idelalisib (Idelalisib\_3) for 3 days. **b**, Percentages of alive cells, normalised to solvent control, across PGs treated *ex-vivo* with  $1.5 \mu\text{M}$  cytarabine (Cytarabine\_2) or  $0.45 \mu\text{M}$  doxorubicine (Doxorubicine\_3) for 3 days. (Herbst et al., 2020c)

proteins such as BTK, PLCG2 and PIK3CD among the most downregulated proteins in PG5 (Fig. 3.20a, S12). Downregulation of these central BCR signalling components was independent of the IGHV mutation status, which is an important surrogate for BCR activity in CLL. In spite of downregulation of most of the BCR signalling proteins, the two established markers ZAP70 and IGHM were not specifically altered in PG5. These two proteins showed the expected distribution (Crespo et al., 2003) with a significant higher abundance in U-CLL than M-CLL samples (Wilcoxon signed-rank test, both  $p < 0.001$ ). Of note, BCR signalling protein abundances were highest in trisomy 12 patients (Fig. S12). In line with the short TTT of PG5, low abundances of PLCG2 or PIK3CD were also associated with short TTT (Fig. 3.16b,c; Cox regression, FDR  $< 1\%$ ). These results suggest that PG5 is not strongly defined by BCR signaling. (Herbst et al., 2020c)

As BCR signalling is one of the most important pathways in CLL, the question arises which molecular changes are instead driving the aggressiveness of PG5. The subgroup was further characterized by a high abundance of enzymes degrading branched chain amino acids or fatty acids and enzymes of the tricarboxylic acid cycle (Fig. 3.20b), suggesting that this subgroup is driven by metabolic reprogramming. This was further supported by the increased *ex-vivo* sensitivity of PG5 to enasidenib, an inhibitor of the tricarboxylic acid cycle enzyme IDH2, and the two drugs targeting the AKT/mTOR pathway rapamycin and MK2206 (Fig. 3.21). (Herbst et al., 2020c)

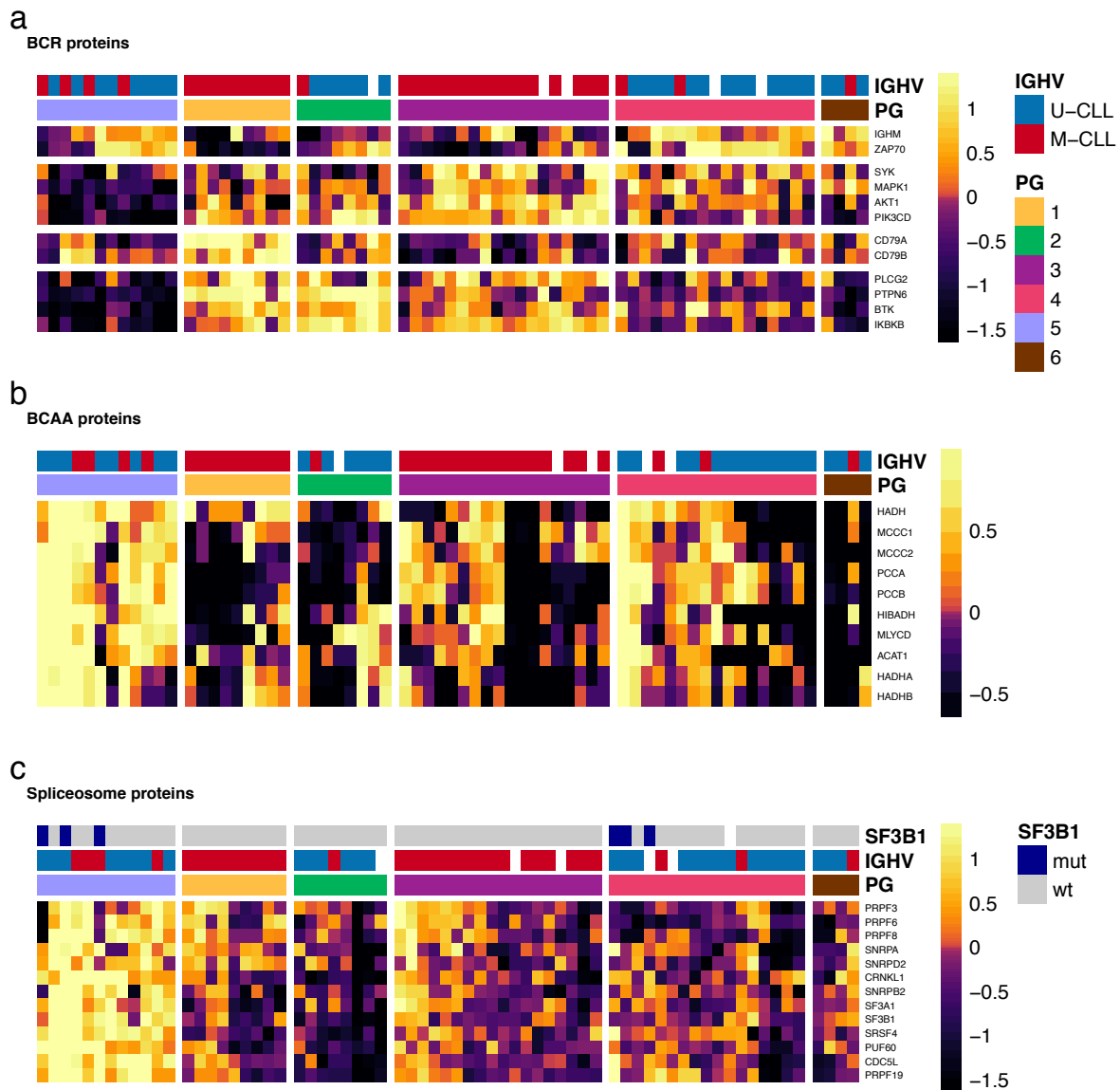


Figure 3.20: **Heatmaps of protein abundances for enriched pathways in proteomics group 5 (PG5).** Heatmaps of log<sub>2</sub> protein abundances for selected BCR proteins (a), proteins involved in the metabolism of branched chain amino acids (BCAA, b) and spliceosome components (c). Patients were grouped according to PG. Proteins were clustered hierarchically. (Herbst et al., 2020c)

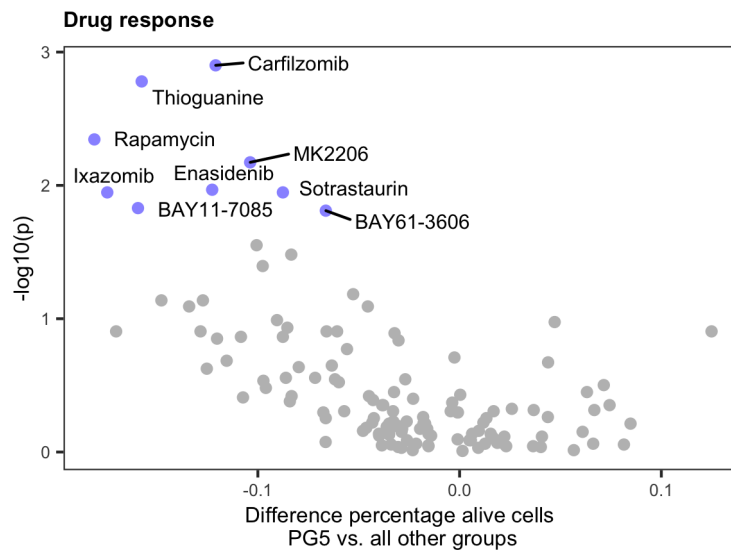


Figure 3.21: **Volcano plot of differential *ex-vivo* drug responses of proteomics group 5 (PG5) in comparison to all other proteomics groups.** Wilcoxon signed-rank test; blue = FDR < 25 %. (Herbst et al., 2020c)

In addition, the spliceosome was identified as the top upregulated pathway in PG5 (Fig. 3.20c). Very low correlation between protein and mRNA levels of components of the spliceosome existed (Fig. 3.21a; median  $\rho = -0.015$ ), which explains why PG5 was not detectable on the transcriptome level. For CLL, altered splicing mechanisms through mutations in the splice-factor *SF3B1* have been well described (Bosch and Dalla-Favera, 2019). However, mutations of *SF3B1* were not enriched in PG5 (Fisher's exact test, BH adjusted  $p = 0.39$ ). Moreover, even though *SF3B1* protein levels did not differ between *SF3B1* mutated and wild type cancers (Fig. 3.21c), they were higher in PG5 than in all other subgroups (Fig. 3.21b). It has recently been reported that the tumourigenic effect of *SF3B1* mutations is mediated by inclusion of a poison-exon in the tumour suppressor *BRD9*, followed by downregulation of *BRD9* protein (Inoue et al., 2019). Mis-splicing (Fig. 3.21d) and downregulation (Fig. 3.21e) of *BRD9* in *SF3B1* mutated cancers could be confirmed, but neither mis-splicing nor downregulation of *BRD9* was detected for PG5 (Fig. 3.21f,g). These analyses suggest an independent mechanism of splicing alteration for PG5 than the one reported for *SF3B1* mutated CLL. (Herbst et al., 2020c)

Additionally, PG5 showed preferential sensitivity to the two proteasomal inhibitors carfilzomib and ixazomib used in the *ex-vivo* sensitivity screen (Fig. 3.21). This is in line with the observation that proteasomal proteins were significantly downregulated in PG5, even though the trend was not as clear as for the other pathways. Carfilzomib and ixazomib are two FDA approved drugs, which could, in addition to metabolic drugs, be further explored as rational treatments for PG5. (Herbst et al., 2020c)

In conclusion, the poor outcome group PG5 was characterized by low BCR abundance,

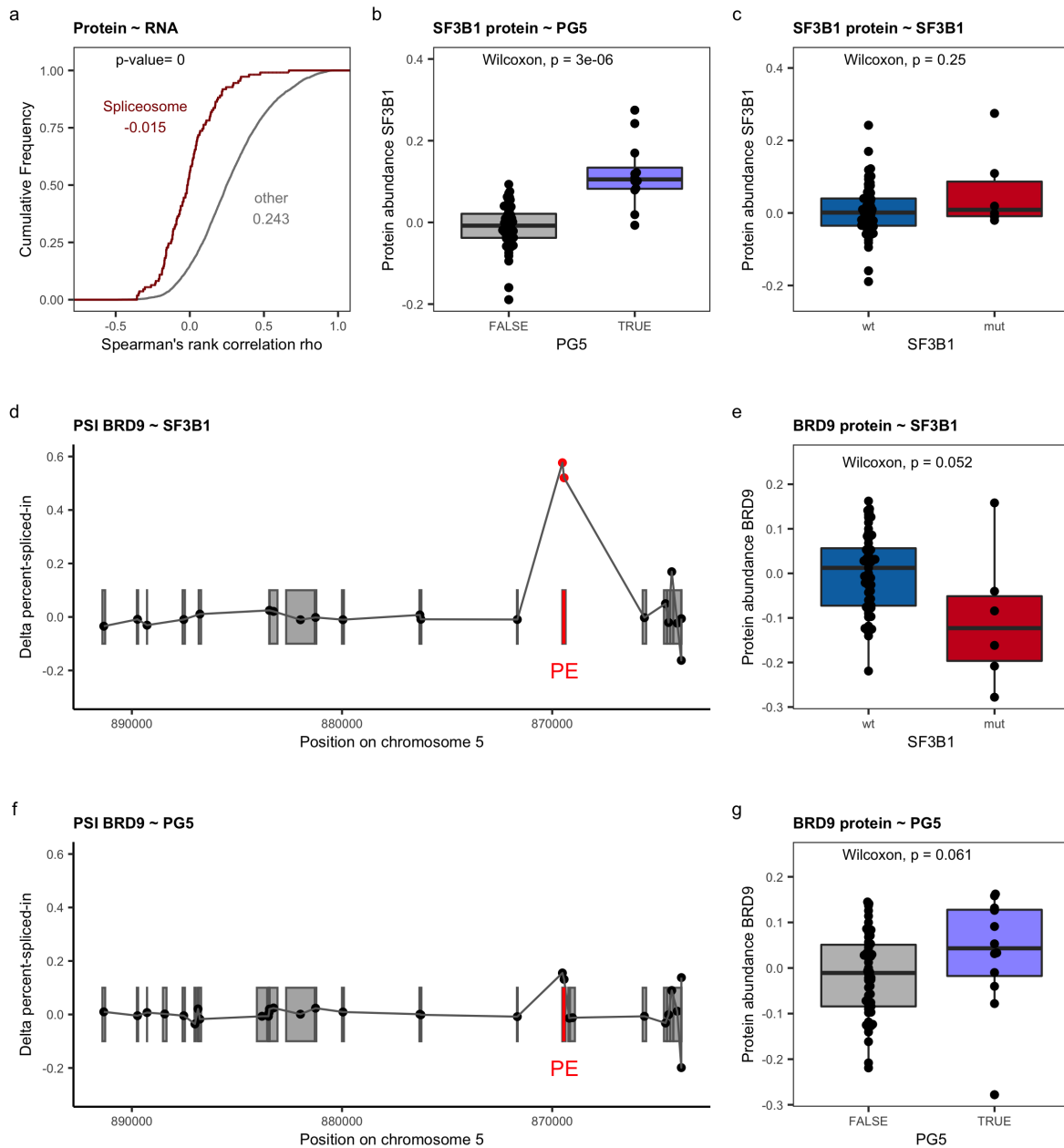
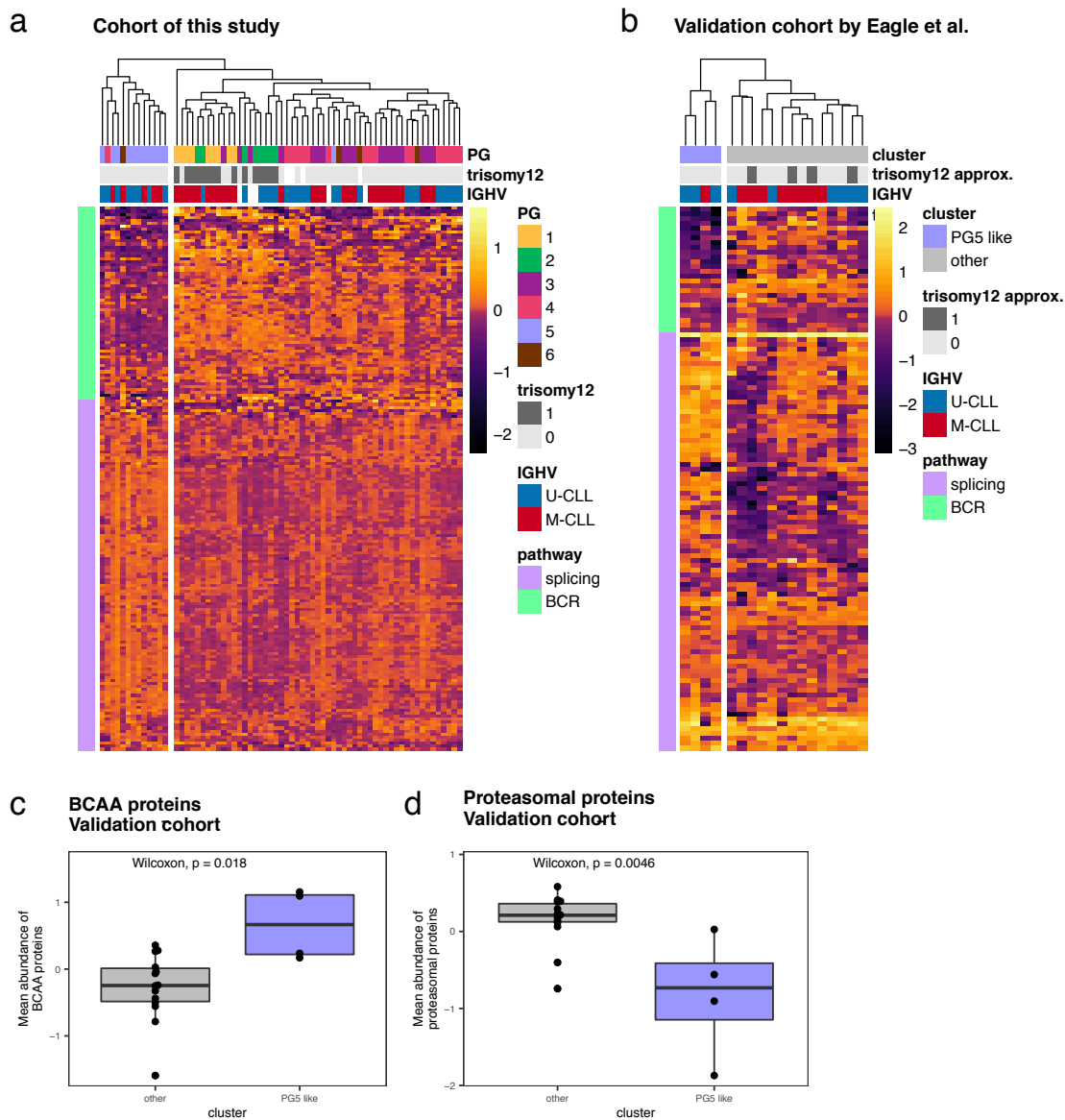


Figure 3.22: **Relationship between splicing and proteomics group 5 (PG5).** **a**, Cumulative density distribution of protein-mRNA Spearman's rank correlations for KEGG components of the spliceosome (red) in comparison to all other proteins (gray). A two-sided Kolmogorov-Smirnov test was used to determine the p-value. **b**, SF3B1 log<sub>2</sub> protein abundances in PG5 (TRUE) vs. all other groups (FALSE). **c**, SF3B1 log<sub>2</sub> protein abundances in *SF3B1* mutated (mut) vs. wild-type (wt) samples. SF3B1 protein levels were independent of *SF3B1* mutations. **d**, *SF3B1* mutated CLL showed an increase in the percent-spliced-in (PSI) value of the poison exon (PE) in BRD9. **e**, BRD9 log<sub>2</sub> protein abundances in *SF3B1* mutated vs. wt CLL. **f**, PG5 did not show an altered PSI value of the poison exon in BRD9. **g**, BRD9 log<sub>2</sub> protein abundances in PG5 (TRUE) vs. all other groups (FALSE). (Herbst et al., 2020c)

metabolic reprogramming, and a preferential sensitivity to metabolic and proteasomal inhibitors. (Herbst et al., 2020c)

### 3.2.6 Validation of the proteomics group 5 (PG5) in an independent cohort

Next, the relevance of PG5 for CLL beyond this patient cohort was investigated. To this end, a proteomic signature describing PG5 was established. BCR proteins were strongly down- and spliceosomal proteins strongly upregulated in PG5. Unsupervised hierarchical clustering of these protein abundances clearly distinguished PG5 from the other subgroups (Fig. 3.23a). To date no other comprehensive analysis of a large cohort of CLL patients exists. However, a proteomic comparison of nine U-CLL vs. nine M-CLL patients from the study of Eagle et al. (2015) is publicly available. The signature of BCR and spliceosomal proteins was used to assess whether a PG5-like subgroup was present in the external cohort by Eagle et al. Indeed, hierarchical clustering on all available BCR and spliceosomal proteins discovered a prominent subgroup with downregulated BCR and upregulated spliceosomal proteins (Fig. 3.23b). The group consisted of four patients, representing 22 % of the validation cohort, which fits well to the representation of PG5 in our cohort (18 %). In accordance with PG5, the subgroup contained U-CLL and M-CLL patients. No information on trisomy 12 is publicly available for the cohort by Eagle et al., however, its presence was estimated by calculating the mean abundance of proteins located on chromosome 12. None of the patients in the PG5-like cluster belonged to the patients with the 20 % highest abundances of proteins on chromosome 12, which is the average occurrence of trisomy 12 described in the literature (Abruzzo et al., 2018). Finally, it was assessed how the other pathways deregulated in PG5 behave in this PG5-like cluster. Indeed, and in line with the observations in PG5, BCAA proteins were found to be up- and proteasomal proteins were found to be downregulated in the PG5-like cluster (Fig. 3.23c,d). These results strongly supports the general existence of PG5 in CLL. (Herbst et al., 2020c)



**Figure 3.23: Validation of proteomics group 5 (PG5) in an independent cohort.** **a**, Unsupervised hierarchical clustering of log<sub>2</sub> protein abundances of BCR and spliceosomal proteins separated PG5 patients from all other proteomics groups. **b**, Unsupervised hierarchical clustering of BCR and spliceosomal proteins on CLL proteomics dataset by Eagle et al. (2015) split off a PG5-like subgroup with size and genetic characteristics similar to PG5. The PG5-like subgroup had **c**, upregulated proteins involved in branched chain amino acid (BCAA) degradation and **d**, downregulated proteasomal proteins, comparable to PG5. trisomy 12 approx. = patients belong to the 20% of samples with the highest abundance of proteins on chromosome 12 which is used as surrogate for trisomy 12. (Herbst et al., 2020c)

### 3.3 Influence of the bone marrow microenvironment on drug response

The results described in this section (3.3) are currently in preparation for publication (Herbst et al., 2020a). The text was written by me for this thesis and will be modified for the publication.

Not only cell-intrinsic, but also cell-extrinsic factors influence tumour progression, survival and the emergences of drug resistances. To investigate the functional consequences of the interplay between leukemia cells and the bone marrow niche, the data from the *ex-vivo* co-culture drug sensitivity screen was analysed. Where appropriate, the comprehensive molecular characterisation of CLL samples described in section 3.2 was used to gain further insights into the interplay between cell-intrinsic and extrinsic factors.

#### 3.3.1 Spontaneous apoptosis of CLL cells in mono-cultures

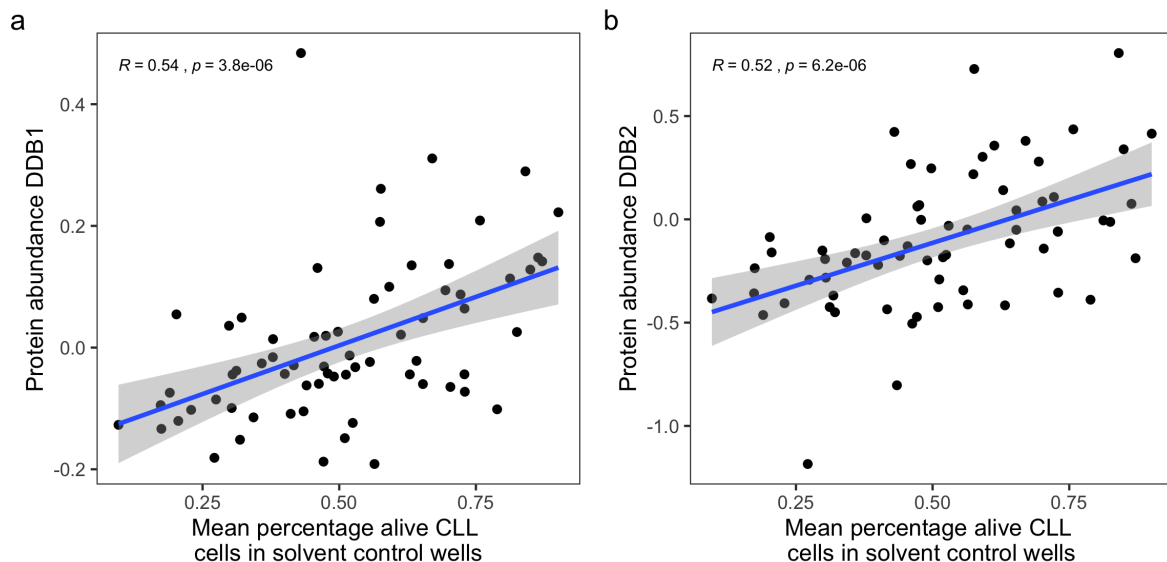


Figure 3.24: **Spontaneous apoptosis correlated with protein expression of DDB1 and DDB2.** Correlation between mono-culture percentages of alive cells in solvent control (DMSO) treated cultures with **a**, DDB1 or **b**, DDB2 protein abundances. Spearman correlation coefficients, p-values and linear fits (blue line) with confidence intervals (grey) are shown. Points represent individual patient samples.

It has been reported that CLL cells cultured *ex-vivo* undergo spontaneous apoptosis due to a lack of signalling input from the microenvironment (Collins et al., 1989). To further understand this behaviour the degree of spontaneous apoptosis was assessed in the comprehensively characterised 81 CLL patient samples. Such an analysis was enabled due to the microscopy-based nature of the drug screen. ATP-based assays read out values which can only be interpreted relative to a control. In contrast, microscopy-based screens are able to measure the percentage of alive cells, which makes the analysis of spontaneous apoptosis possible. The screen confirmed the

occurrence of spontaneous apoptosis in the mono-cultures. Median percentage of alive cells was 51 % after three days of *ex-vivo* culture. Interestingly, the degree of spontaneous apoptosis was very heterogeneous with percentage of alive CLL cells ranging from 10 % to 90 % (Fig. 3.25a). (Herbst et al., 2020a)

To uncover which molecular characteristics define the differences in spontaneous apoptosis, the multi-omics dataset described in section 3.2 was integrated with the data on spontaneous apoptosis. No statistically significant association of the degree of spontaneous apoptosis with any of the measured genetic alterations was detected (two-sided t-test; FDR < 5 %). Moreover, protein abundances were correlated with the degree of spontaneous apoptosis (Spearman correlation). At a FDR of 5 % statistically significant correlations were only detected for two proteins: DNA damage-binding protein 1 (DDB1; Fig. 3.24a;  $\rho = 0.54$ ) and DNA damage-binding protein 2 (DDB2; Fig. 3.24b;  $\rho = 0.52$ ). As DDB1 and DDB2 are involved in DNA damage repair (Lovejoy et al., 2006; Wakasugi et al., 2001), it is likely that high levels of these proteins can prolong the lifespan of CLL cells *ex-vivo* by maintaining genome stability. (Herbst et al., 2020a)

### 3.3.2 Protection of CLL cells from spontaneous apoptosis by bone marrow stroma cells

Co-culturing CLL patient samples with the bone marrow stroma cell line HS-5 decreased spontaneous apoptosis of CLL cells *ex-vivo*. The median percentage of alive CLL cells in co-cultures was 61 % with the percentages of alive CLL cells ranging between 25 % and 82 % (Fig. 3.25a). This was a significant (paired two-sided t-test;  $p < 0.001$ ) increase by 10 %. As the HS-5 cell line represents an artificial system, these results were validated by co-culturing cells from four CLL patients with primary MSCs from three different donors (Fig. 3.25b). Even though the effect sizes varied between different MSCs and were not statistically significant for all tested MSCs (at a significance level of 0.05), in general a trend of the protection of CLL cells from spontaneous apoptosis by MSCs was seen, as previously described (Lagneaux et al., 1998; Panayiotidis et al., 1996). (Herbst et al., 2020a)

However, not all patient samples benefited equally well from the support of stroma cells. Especially U-CLL samples with low percentages of alive cells in the mono-cultures profited from co-culturing with HS-5 cells (Fig. 3.26). Among these, nearly all patient samples with a mono-culture percentage of alive CLL cells of less than  $\sim 60$  % showed an increase in alive CLL cells when co-cultured. Even though among M-CLL patients an increased protective effect for samples with low mono-culture percentages of alive cells was also observed, M-CLL samples were in general less responsive to stroma support. Most of the M-CLL samples with mono-culture percentages of alive cells above  $\sim 40$  % did not profit from co-culturing (Fig. 3.26). For CLL samples for which nearly all cells were still alive after three days in mono-culture, co-culturing was even slightly disadvantageous. However, these effects were marginal and probably due to competition for nutrients in the cell culture medium between stroma and CLL cells. (Herbst et al., 2020a)

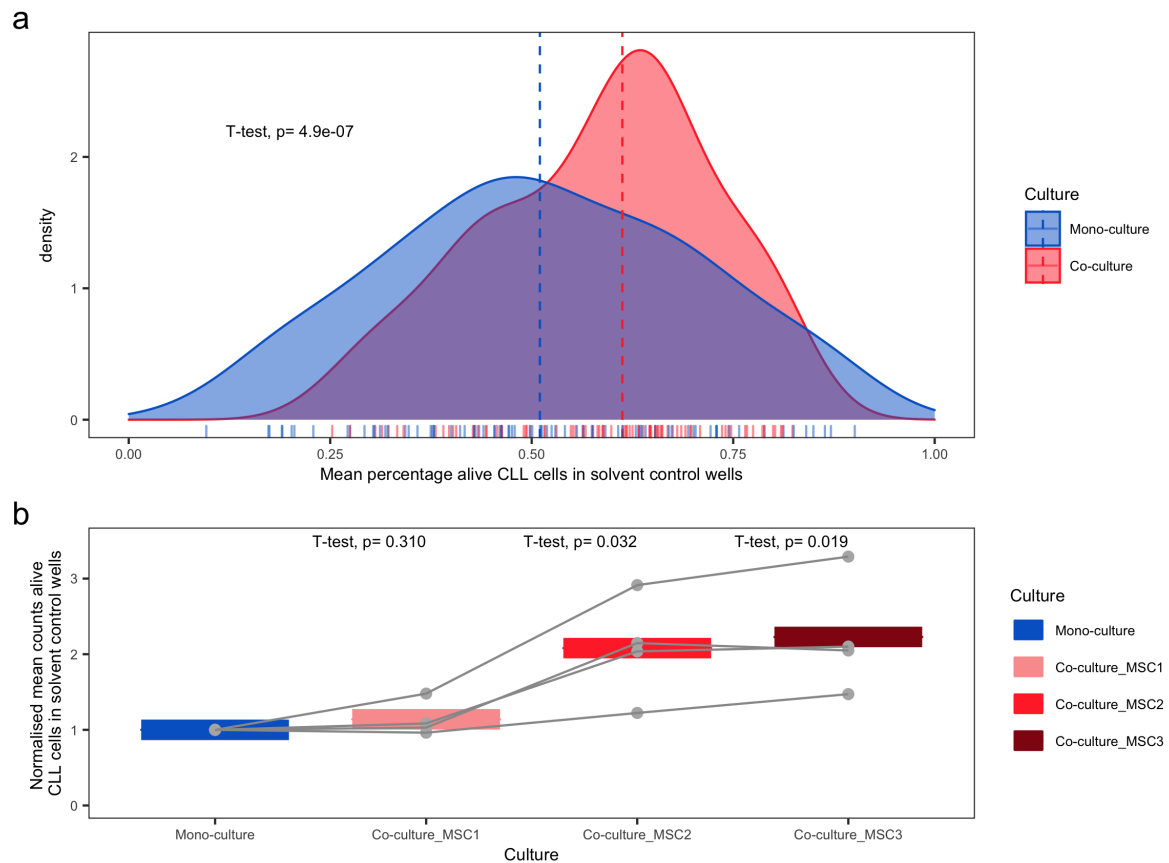


Figure 3.25: **Stroma cells protected CLL from spontaneous apoptosis *ex-vivo*.** **a**, Distribution of the mean percentages of alive CLL cells within the solvent control (DMSO) wells for each patient. Each small line on the bottom represents the measurement of either mono- or co-culture percentages of alive CLL cells of an individual patient. Two-sided paired t-test. **b**, Mean percentages of alive CLL cells treated with solvent control (DMSO), either cultured in mono-culture or co-cultured with MSCs from three different donors (MSC1-3). One-sided t-tests of log of number of alive cells normalised to the mono-cultures.

In conclusion, bone marrow stroma cells in general protect CLL cells from spontaneous apoptosis, even though differences between patient samples existed. Protection was strongest for U-CLL with low mono-culture percentages of alive cells, but for most other CLL sample co-culturing was also not inferior. (Herbst et al., 2020a)

### 3.3.3 Influence of bone marrow stroma cells on drug response by CLL cells

In addition to the unperturbed conditions, the responses of co-cultures to a panel of 43 different drugs were measured. All concentrations in which stroma cells were killed by the drugs were excluded, as these conditions do not represent proper co-cultures. To get a first overview of the data, Spearman drug-drug correlations were calculated. This was done for mono- and co-cultures separately. Unsupervised hierarchical clustering of mono-culture drug-drug correlations

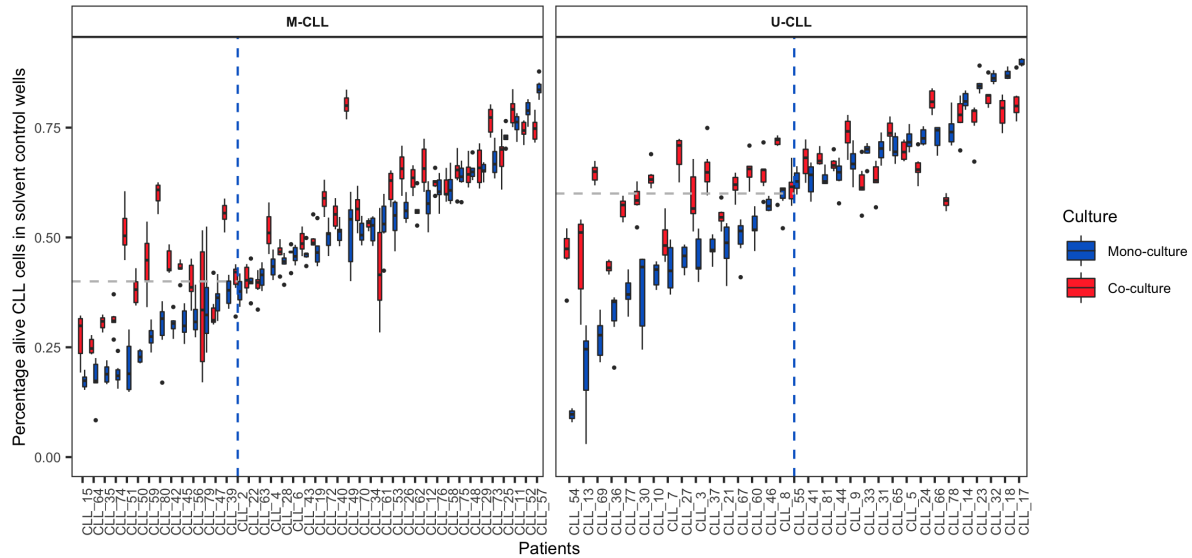


Figure 3.26: **Influence of the degree of spontaneous apoptosis and IGHV status on the protective effect by stroma cells.** Especially U-CLL samples with a high degree of spontaneous apoptosis profited from co-culturing. Percentages of alive cells per patient and culture are shown. Technical replicates of mono- and co-cultures of solvent control wells (DMSO) are represented as box plots. Samples were split into M-CLL and U-CLL and ordered according to mean mono-culture percentages of alive cells. Lines indicate 40% (U-CLL) and 60% (M-CLL).

revealed clusters of drugs with high correlations (Fig. 3.27a). Among these was a cluster containing the BCR signalling inhibitors ibrutinib, dasatinib, duvelisib, idelalisib and PRT062607. Another cluster contained the BET inhibitors I-BET-762 and JQ1. The correspondence between responses to drugs with similar targets proves the validity of the drug-sensitivity assay. To assess whether this still holds true in the context of the microenvironment, hierarchical clustering was also performed on the drug-drug correlations within the co-cultures (Fig. 3.27b). Indeed, and in correspondence to the mono-cultures, one cluster was uncovered containing the BCR signalling inhibitors ibrutinib, duvelisib, idelalisib and PRT062607. Additionally, the high correlation between the BET inhibitors I-BET-762 and JQ1 was still present in the co-cultures. This demonstrates, that the drug sensitivity data produces results which are meaningful and relevant for CLL biology, even in the context of stroma cell co-cultures. (Herbst et al., 2020a)

To further evaluate the suitability of bone-marrow stroma cell co-cultures for assessing drug responses in CLL, known associations between drug response and genetic alterations were analysed. As previously reported (Dietrich et al., 2018), cells from U-CLL patients responded better than M-CLL patients to treatment with ibrutinib in mono-cultures (Fig. 3.28a; Wilcoxon signed-rank test  $p = 5.7 \times 10^{-5}$ ). A similar difference in sensitivities could be observed in the co-cultures (Fig. 3.28b; Wilcoxon signed-rank test  $p = 0.04$ ). Moreover, cells from *TP53* wild type patients responded better than *TP53* mutated patients to treatment with nutlin 3a, as expected (Jethwa et al., 2018). This effect was present in mono- (Fig. 3.28c; Wilcoxon signed-rank test  $p = 0.003$ )

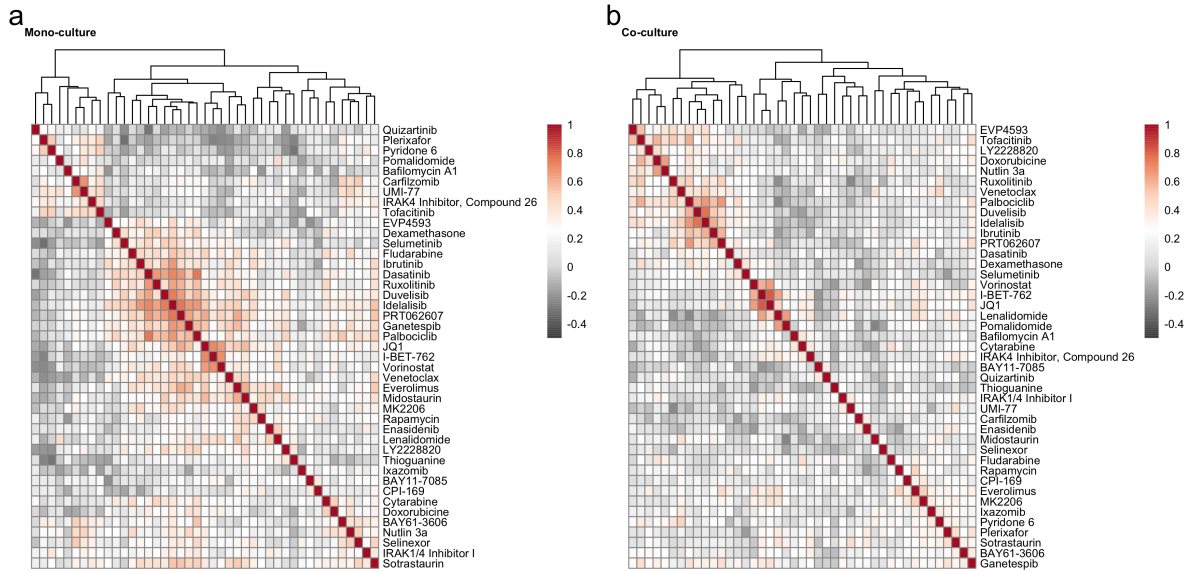


Figure 3.27: **Drug-drug correlations in mono- and co-cultures.** **a**, Hierarchically clustered Spearman drug-drug correlation coefficients within CLL mono-cultures. **b**, Hierarchically clustered Spearman drug-drug correlation coefficients within CLL co-cultures.

as well as in co-cultures (Fig. 3.28d; Wilcoxon signed-rank test  $p = 2.7 \times 10^{-5}$ ). The preservation of known associations between genetics and drug response in co-cultures, together with the results from the drug-drug correlation analysis, shows that the main biological axes of CLL are still preserved in co-cultures. This justifies the use of co-culture models to study *ex-vivo* CLL drug response. (Herbst et al., 2020a)

Protection of CLL cells from spontaneous apoptosis by stroma cells systematically elevated the percentage of alive CLL cells in co-cultures (Fig. 3.25). When assessing the effect of stroma cells on drug response of CLL, this higher baseline percentage of alive CLL cells needs to be taken into account. Otherwise, specific effects on drug response could be confounded by the protection from spontaneous apoptosis. To this end, the following linear model was constructed:  $Percentage\ alive\ CLL\ cells \sim effect_{culture\ model} + effect_{drug} + effect_{culture\ model} : effect_{drug}$ . The last term represents an interaction term, which estimates the effect of stroma cells on drug response independent of their effect on spontaneous apoptosis. Before applying the model, drug concentrations which were toxic to stroma cells were excluded, as these conditions do not represent proper co-cultures. Additionally, drugs which did show neither an effect on mono- nor on co-cultures were excluded. This was done as it cannot be ruled out that the respective concentration was too low to be effective or that the drug had lost its activity due to the experimental setup. Finally, conditions in which the mean percentage of alive CLL cells across patients of both mono- and co-culture were reduced to a level below 15% were excluded, as the respective drug concentration was considered as too toxic to see any variabilities between patient responses. All of the excluded conditions are shown in grey in Fig. 3.29. For all other conditions, a Z-score based on the interaction term was calculated. Fig. 3.29 is a heatmap of the

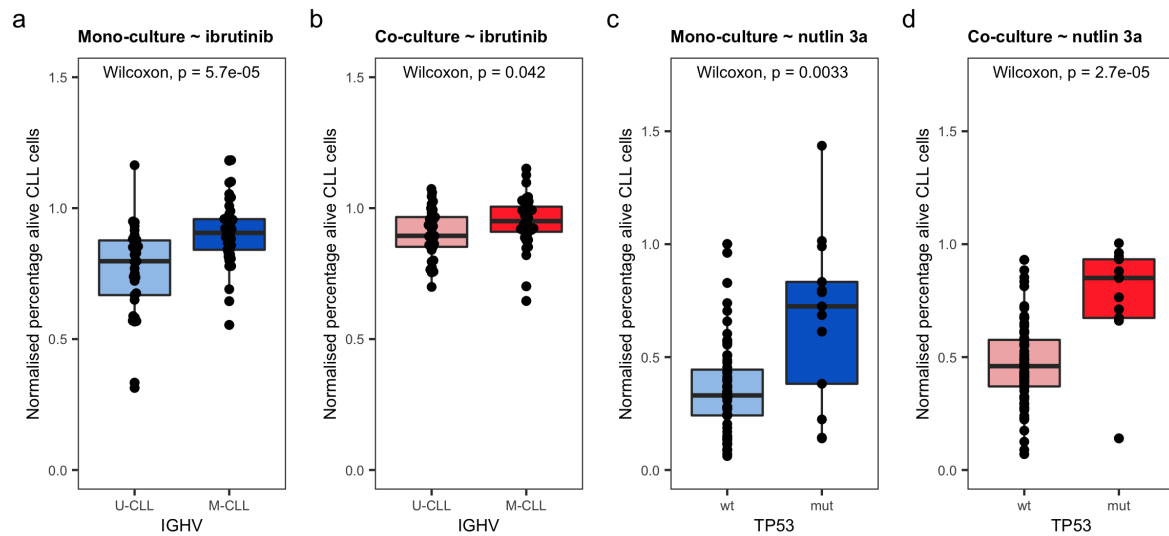


Figure 3.28: **Relationship between *ex-vivo* drug response and genetic factors in mono- and co-cultures.** **a**, Response of U-CLL and M-CLL samples to treatment with 40 nM ibrutinib in CLL mono-cultures. **b**, Response of U-CLL and M-CLL samples to treatment with 40 nM ibrutinib in co-cultures of CLL and HS-5. **c**, Response of *TP53* mutated and wild-type CLL samples to treatment with 9  $\mu$ M nutlin 3a in CLL mono-cultures. **d**, Response of *TP53* mutated and wild-type CLL samples to treatment with 9  $\mu$ M nutlin 3a in co-cultures of CLL and HS-5. Percentages of alive cells were normalised to the mean of the solvent control wells of the respective culture conditions located in the center of the assay plates.

resulting Z-scores of the interaction terms. In addition to the Z-scores, the significance levels were calculated for the presence of an interaction using a two-sided t-test and for the absence of an interaction using the 'two-one-sided t-tests' (TOST) procedure for testing of equivalence (equivalence bounds = 10%). (Herbst et al., 2020a)

This systematic evaluation highlighted multiple drugs with reduced effectiveness in co-cultures. The analysis could confirm, that co-cultures with bone marrow stroma cells protect CLL cells from drug-induced apoptosis by fludarabine (0.6  $\mu$ M:  $Z = 2.45$ , two-sided t-test  $\alpha = 0.05$ ) and doxorubicine (0.45  $\mu$ M:  $Z = 3.59$ , two-sided t-test  $\alpha = 0.05$ ), as reported in the literature (Kurtova et al., 2009; Mraz et al., 2011). Additionally, stroma cells conveyed resistance to treatment with cytarabine (1.5  $\mu$ M:  $Z = 2.58$ , two-sided t-test  $\alpha = 0.05$ ), suggesting that stroma cells protect CLL cells from apoptosis induced by chemotherapeutic agents in general. The effect of stroma cells on fludarabine induced apoptosis was further validated in co-cultures of CLL cells and primary MSCs. In accordance with the results from co-cultures of CLL and HS-5 (Fig. 3.30a), MSCs protected CLL cells from fludarabine induced apoptosis (Fig. 3.30b, anova of  $\log(\text{normalised percentage alive CLL cells})$ ,  $p = 0.02$ ).

Out of all drugs, the response of CLL cells to the FDA approved proteasome inhibitor carfil-

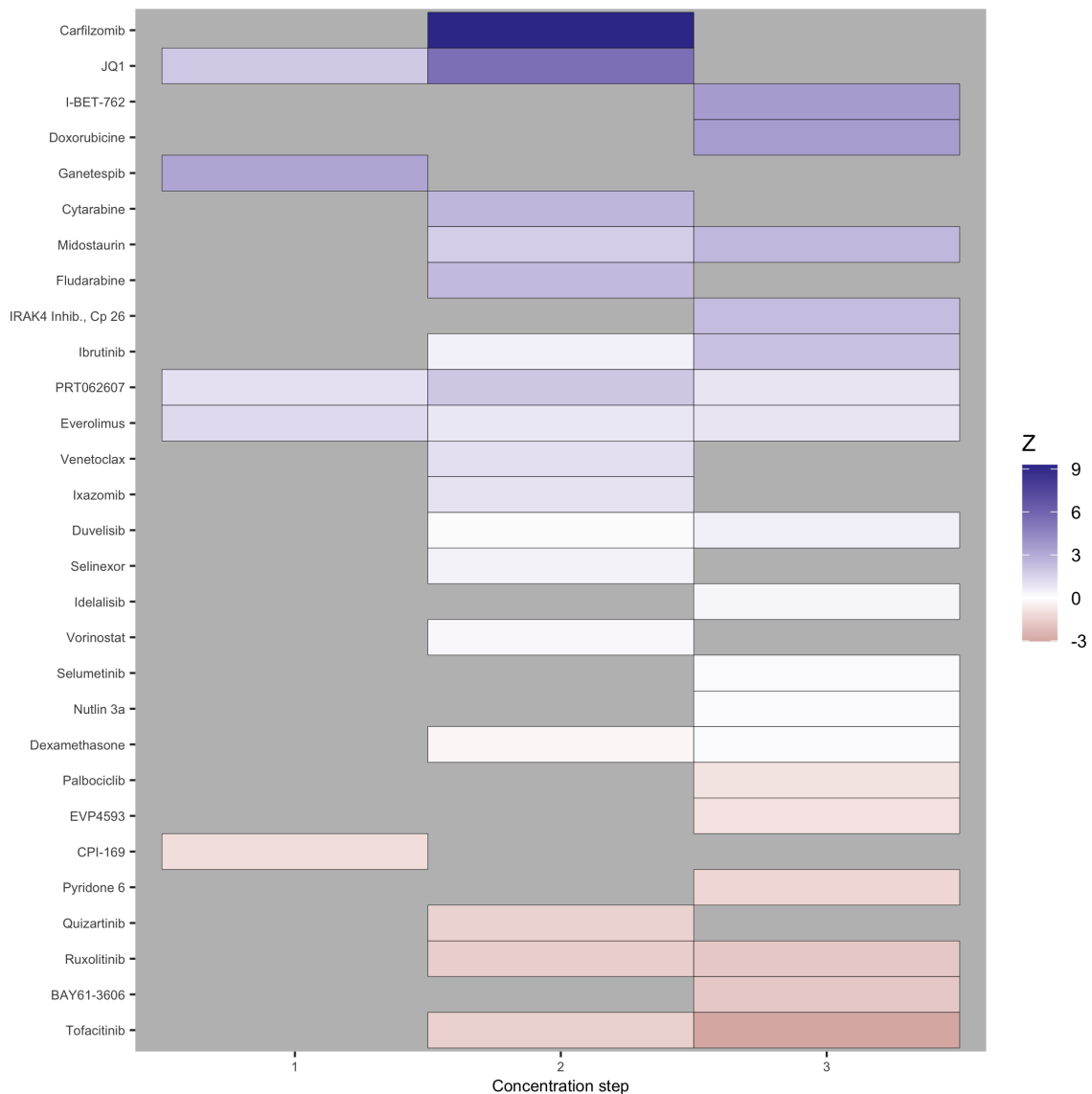
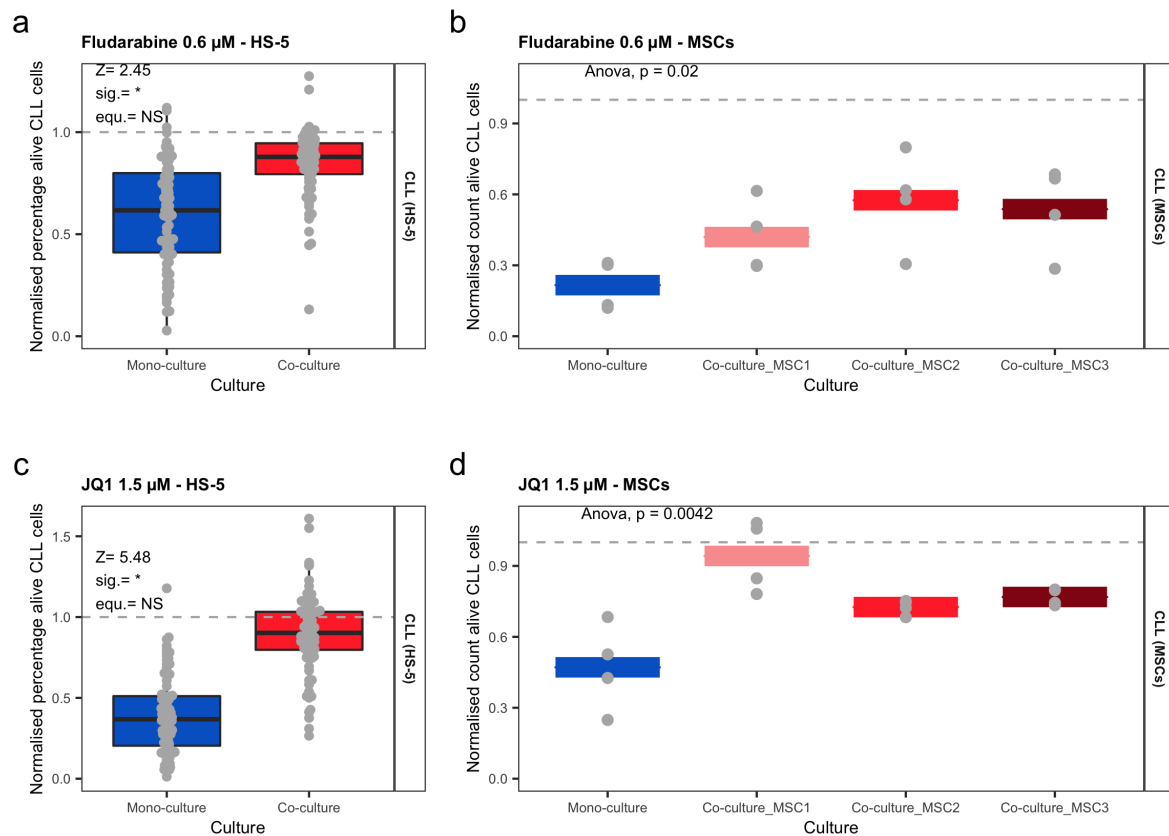


Figure 3.29: **Influence of stroma cells on drug response of CLL.** Z-scores of the interaction term obtained from the linear model  $Percentage\ alive\ CLL\ cells \sim effect_{culture\ model} + effect_{drug} + effect_{culture\ model} : effect_{drug}$ , describing the influence of stroma cells on the effectiveness of a drug against CLL patient samples. Blue (positive Z-score) indicates that the response to the drug was reduced in co-cultures, in comparison to mono-cultures. Red (negative Z-score) indicates that the response to the drug was enhanced in co-cultures, in comparison to mono-cultures. White (Z-score around zero) indicates that the response to the drug was similar in co- and mono-cultures. Conditions which were excluded (see text in section 3.3.3) are shown in grey.



**Figure 3.30: Examples of drugs with decreased effect in co-cultures.** Treatment of CLL cells with 0.6  $\mu\text{M}$  of the chemotherapeutic agent fludarabine was less effective in co-cultures with **a**, HS-5 or **b**, primary MSCs than in mono-cultures of only CLL cells. Treatment of CLL cells with 1.5  $\mu\text{M}$  of the BET inhibitor JQ1 was less effective in co-cultures with **c**, HS-5 or **d**, primary MSCs than in mono-cultures of only CLL cells. Percentages and counts of alive cells were normalised to the mean of the solvent control wells of the respective culture conditions located in the center of the assay plates.

zomib was attenuated the most by stroma cells (15 nM:  $Z = 9.28$ , two-sided t-test  $\alpha = 0.05$ ). At 15 nM CLL cells in co-cultures did not show any decrease of alive CLL cells, while for most of the mono-cultures close to no alive cells remained. For the other proteasome inhibitor ixazomib, however, no significant attenuation of CLL responses was observed (1.5  $\mu\text{M}$ :  $Z = 0.980$ , TOST equivalence test  $\alpha = 0.05$ ). Additionally, response to the two BET inhibitors I-BET-762 (4.5  $\mu\text{M}$ :  $Z = 3.60$ , two-sided t-test  $\alpha = 0.05$ ) and JQ1 (1.5  $\mu\text{M}$ :  $Z = 1.91$ , two-sided t-test  $\alpha = 0.05$ ) was significantly reduced in co-cultures (Fig. 3.30c). Decreased response of CLL cells to JQ1 in the presence of stroma cells could be validated in co-cultures with primary MSCs (Fig. 3.30d, anova of  $\log(\text{normalised percentage alive CLL cells})$ , p-value = 0.004). Thus, the analysis systematically identified drugs for which CLL drug response is reduced by stroma cells. These results are only based on an *ex-vivo* assay, but can nevertheless contribute to the understanding of the emergence of drug resistances from the bone marrow.

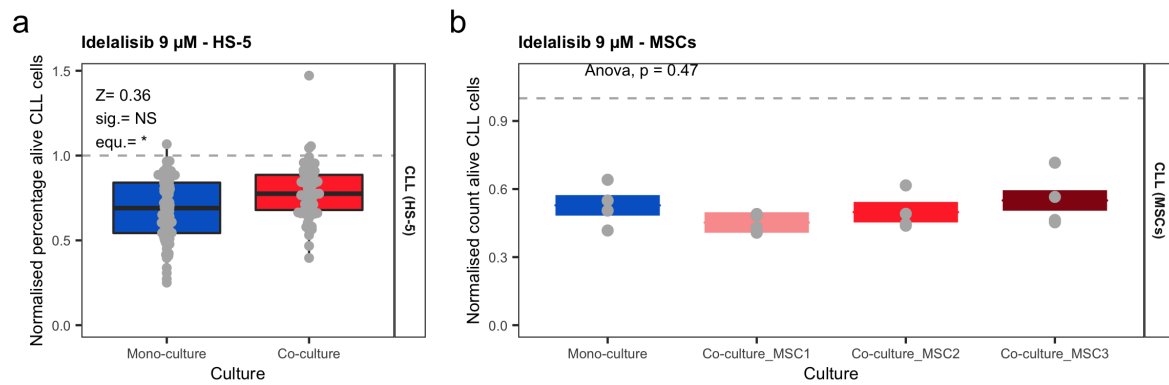


Figure 3.31: **Example of drug with the same effect in co-cultures and mono-cultures.**

Treatment of CLL cells with  $9\ \mu\text{M}$  of the PI3K inhibitor idelalisib was equally effective in co-cultures with **a**, HS-5 or **b**, primary MSCs as in mono-cultures of only CLL cells. Percentages and counts of alive cells were normalised to the mean of the solvent control wells of the respective culture conditions located in the center of the assay plates.

It is important to note, that stroma cells did not change the response to all tested drugs. Many drugs acted similarly on mono- and co-cultures. Among these was the MDM2 inhibitor nutlin 3a ( $9\ \mu\text{M}$ :  $Z = 0.2$ , TOST equivalence test  $\alpha = 0.05$ ). This finding is in accordance with the previous observation that the association of nutlin 3a responses with *TP53* mutations is not changed in co-cultures (Fig. 3.28d). Additionally, sensitivity to the PI3K inhibitors idelalisib ( $9\ \mu\text{M}$ :  $Z = 0.4$ , TOST equivalence test  $\alpha = 0.05$ ) and duvelisib ( $0.3\ \mu\text{M}$ :  $Z = 0.14$ , TOST equivalence test  $\alpha = 0.05$ ;  $4.5\ \mu\text{M}$ :  $Z = 0.57$ , TOST equivalence test  $\alpha = 0.05$ ) was statistically equivalent in mono- and in co-cultures. In accordance with these results obtained in HS-5 cell line co-cultures (Fig. 3.31a), no significant alteration of the response to idelalisib was observed in co-cultures of CLL cells and primary MSCs (Fig. 3.31b, anova of log(normalised percentage alive CLL cells),  $p$ -value = 0.47). For ibrutinib, which like the PI3K inhibitors targets BCR signalling, no clear conclusion could be drawn, as the  $Z$ -values differed considerably between the two analysed concentrations ( $0.5\ \mu\text{M}$ :  $Z = 0.48$ ;  $9\ \mu\text{M}$ :  $Z = 2.17$ ).

Moreover, a statistically equivalent activity of venetoclax, an inhibitor of the anti-apoptotic protein BCL-2, was observed in mono- and co-cultures ( $15\ \text{nM}$ :  $Z = 1.10$ , TOST equivalence test  $\alpha = 0.05$ ). Even though the effect was only on the edge of statistical significance, this finding is highly relevant as venetoclax is frequently used in the clinic and achieves high rates of complete remissions (Roberts et al., 2016; Seymour et al., 2018).

Most importantly, drugs which were more effective in co- than in mono-cultures were detected. Among them was the SYK inhibitor BAY61-3606 ( $9\ \mu\text{M}$ :  $Z = -1.79$ , two-sided t-test  $\alpha = 0.05$ ). Strikingly, all of the three JAK inhibitors used in the drug screen had negative

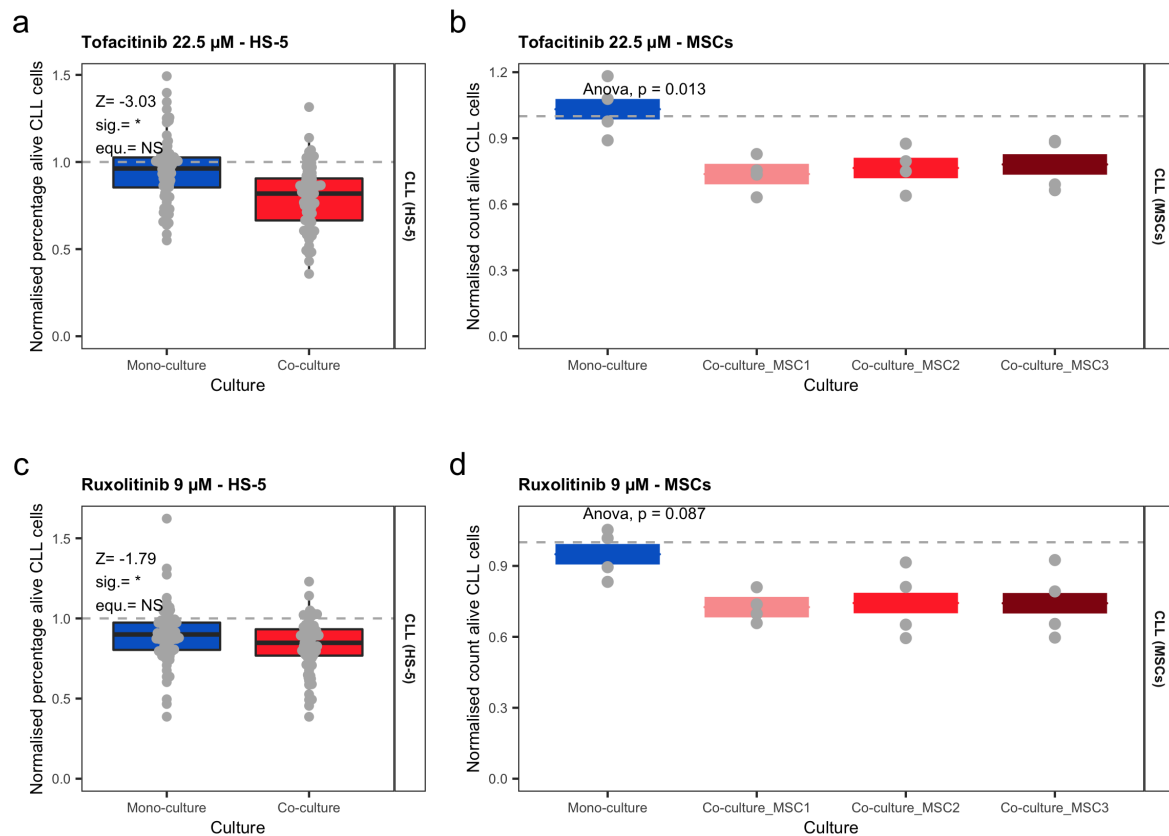


Figure 3.32: **Examples of drugs with increased effect in co-cultures.** Treatment of CLL cells with 22.5  $\mu\text{M}$  of the JAK inhibitor tofacitinib was more effective in co-cultures with **a**, HS-5 or **b**, primary MSCs than in mono-cultures of only CLL cells. Treatment of CLL cells with 9  $\mu\text{M}$  of the JAK inhibitor ruxolitinib was more effective in co-cultures with **c**, HS-5 or **d**, primary MSCs than in mono-cultures of only CLL cells. Percentages and counts of alive cells were normalised to the mean of the solvent control wells of the respective culture conditions located in the center of the assay plates.

Z-scores, indicating increased activity in the co- than in the mono-cultures (tofacitinib 22.5  $\mu\text{M}$ :  $Z = -3.03$ , two-sided t-test  $\alpha = 0.05$ ; tofacitinib 1.5  $\mu\text{M}$ :  $Z = -1.57$ , not significant according to two-sided t-test with  $\alpha = 0.05$ ; ruxolitinib 9  $\mu\text{M}$ :  $Z = -1.79$ , two-sided t-test  $\alpha = 0.05$ ; ruxolitinib 0.6  $\mu\text{M}$ :  $Z = -1.62$ , not significant according to two-sided t-test with  $\alpha = 0.05$ ; pyridone 6 9  $\mu\text{M}$ :  $Z = -1.33$ , not significant according to two-sided t-test with  $\alpha = 0.05$ ). A statistically significant increased sensitivity of co-cultures to the JAK inhibitor tofacitinib was not only observed in the context of the HS-5 cells line (Fig. 3.32a), but could also be confirmed in co-cultures of CLL and primary MSCs (Fig. 3.32b, anova of  $\log(\text{normalised percentage alive CLL cells})$ , p-value = 0.013). In addition, the slight increased response of co-cultures to the JAK inhibitor ruxolitinib (Fig. 3.32c) could be validated in co-cultures with MSCs, even though this was not statistically significant at a significance level of 0.05 (Fig. 3.32d, anova of  $\log(\text{normalised percentage alive CLL cells})$ , p-value = 0.087). The consistently increased re-

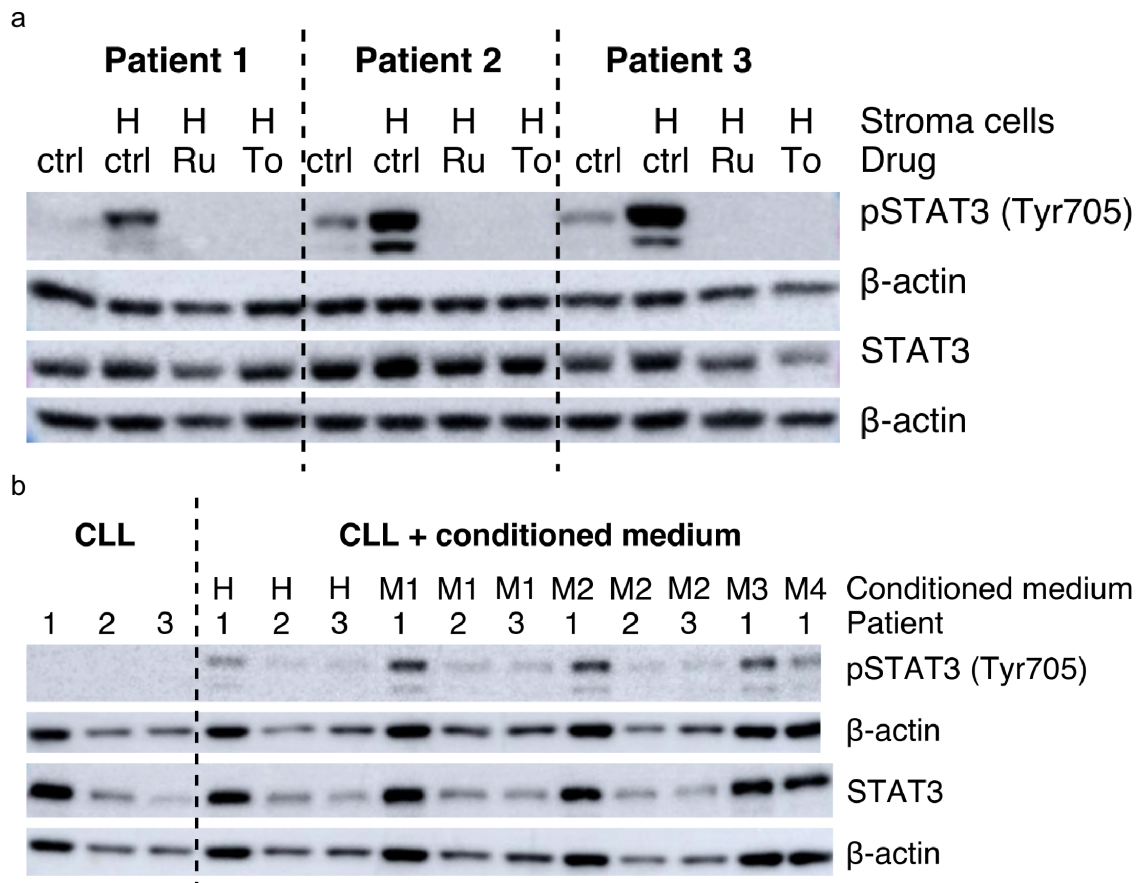


Figure 3.33: **STAT3** was activated by soluble factors secreted by stroma cells. **a**, STAT3 was phosphorylated in CLL cells co-cultured with HS-5 cells. This can be reversed by inhibition with ruxolitinib or tofacitinib. **b**, STAT3 was phosphorylated in CLL cells in the presence of stroma conditioned medium. Ctrl = solvent control (DMSO), Ru = ruxolitinib (10  $\mu$ M), To = tofacitinib (22  $\mu$ M). H = co-cultures with HS-5 cells, M1-4 = co-cultures with MSC cells from four different donors.

sponse of co-cultures across multiple JAK inhibitors suggests a potential value of these inhibitors for overcoming stroma induced drug resistances. (Herbst et al., 2020a)

### 3.3.4 Mechanistic insight into the increased sensitivity of stroma cell co-cultures to JAK inhibitors

To gain further insights into the mechanism through which JAK inhibitors act on co-cultures, the effect of stroma cells on JAK-STAT signalling within CLL was investigated. Co-cultures of CLL cells with HS-5 bone marrow stroma cells increased phosphorylation of STAT3 on residue Tyr705 in CLL cells (Fig. 3.33a). This phosphorylation could be reversed by JAK inhibition with ruxolitinib or tofacitinib. These results indicate that activation of JAK-STAT3 signalling contributes to the increased survival of CLL cells in co-cultures, which can be reversed by JAK inhibition. When looking at non-normalised percentages of alive cells it became apparent that the decrease in alive cells was in most cases of a similar extent as the protection from spontaneous apoptosis. However, in one MSC co-culture percentages of alive CLL cells was even

reduced beyond this level. This shows that JAK inhibition did not only cause the mere reversal of the protection from spontaneous apoptosis by stroma cells but affected CLL viability beyond this. (Herbst et al., 2020a)

Stroma cells interact with CLL cells through direct contact and soluble factors. To disentangle which type of interaction is responsible for STAT3 activation, CLL cells were incubated with conditioned medium from HS-5 stroma cells (Fig. 3.33b). The presence of conditioned medium was enough to increase phosphorylation levels of STAT3 Tyr705. Not only conditioned medium from HS-5 cells, but also from primary MSCs from different donors was able to activate STAT3 (Fig. 3.33b). This shows that this is a general interaction mechanism between CLL and stroma cells and is not only specific for the HS-5 cell line. Thus, JAK-STAT3 mediated protection of CLL cells from apoptosis is at least in part conveyed through soluble factors. (Herbst et al., 2020a)



## 4 Discussion

This thesis presented a comprehensive characterisation of cell-intrinsic and extrinsic factors influencing CLL patient heterogeneity, drug response and outcome. Proteogenomics of a cohort of primary CLL patient samples uncovered associations between genetic, transcriptomic and proteomic changes and functional consequences for drug response and outcome. This also led to the discovery of a new CLL subgroup with short time to next treatment and high proliferative capacity.

Additionally, a high-throughput co-culture drug-sensitivity screen was established to enable the systematic testing of the influence of bone marrow stroma cells on drug response. During the optimisation process extensive phagocytic activity by primary MSCs and the bone marrow stroma cell line NKTert was discovered. If left unconsidered, this phagocytic activity can lead to a systematic bias in co-culture experiments. Using the high-throughput co-culture drug screen, a comprehensive comparison of how bone marrow stroma cells influence drug response of CLL cells was conducted. This analysis identified drugs which have reduced, unaltered and even increased activity in co-cultures. The increased activity of JAK inhibitors in co-cultures was due to an upregulation of STAT3 phosphorylation which could be reversed by JAK inhibition.

### 4.1 Proteogenomic characterisation of CLL

Proteogenomic studies of tumour cells integrate measurements of the cancer proteome with genomic and other cell-intrinsic features. In recent years, this approach has helped to gain insights into the mechanisms of development and progression of many different cancer entities, as proteins are considered the main effectors within the cells. To date, however, an integration of proteogenomic data from primary patient material with functional consequences is lacking. The proteogenomic characterisation described in this thesis is not only the first study analysing the CLL proteome in relation to genomic and transcriptomic features, but also integrates the results with functional consequences assessed by high-throughput *ex-vivo* drug perturbation. (Herbst et al., 2020c)

#### 4.1.1 Effect of mutations on other molecular layers in CLL

Many known associations between genetics, transcriptomics, proteomics, outcome and drug response could be recapitulated by the proteogenomic analysis, which provides confidence that the obtained results are meaningful. In accordance with clinical observations, *TP53* mutated CLL did not respond well to *ex-vivo* treatment with chemotherapeutics (Zenz et al., 2010). Moreover, and as described before, the accumulation of p53 in *TP53* mutated samples was observed, which

underlines the gain-of-function phenotype of these mutations also in CLL (Dittmer et al., 1993; Oren and Rotter, 2010). It is generally believed that *TP53* mutations do not only deactivate the native function of the protein but also convey new functionalities to p53. These include the ability to induce the expression of a different set of genes and, thereby, contribute to increased proliferation and malignancy (Oren and Rotter, 2010). In the presented investigation increased amounts of TP53 were not observed on transcript level. As described in other cancer proteogenomic studies, correlation between protein and RNA levels was poor (Johansson et al., 2019; Mun et al., 2019; Yang et al., 2019; Zhang et al., 2016), further underlining the importance of the assessment of protein abundances to infer functional consequences. In contrast to *TP53*, mutations in the *ATM* gene, another tumour suppressor, downregulated ATM protein levels. This is in line with the literature, as *ATM* mutations have been reported to only cause loss-of-function phenotypes (Navrkalova et al., 2013). The low abundances of ATM protein upon mutation might be explained by an interference of the mutations with protein folding or stability. The examples of *TP53* and *ATM* illustrate how mutations in tumour suppressor genes can have diverse molecular consequences. Moreover, they exemplify how the effect of genetic alterations can be traced across different molecular and functional layers.

In addition to these well described relationships between genetic factors and molecular consequences, new associations were uncovered. Interestingly, *XPO1* mutations caused a significant decrease in XPO1 protein abundances. Again, this was not detectable on transcript level. XPO1 is a nuclear export protein, among others transporting p53 from the nucleus to the cytoplasm, thereby contributing to important aspects of tissue homeostasis. An overreactivity of XPO1 has been reported in many cancers, including some B-cell malignancies (Camus et al., 2017). To overcome the contribution of XPO1 to disease progression, the XPO1 inhibitor selinexor has been approved for the treatment of multiple myeloma (Podar et al., 2020). It is therefore of great interest, whether patients with other B-cell malignancies could also profit from treatment with selinexor. However, the observed downregulation of XPO1 protein in *XPO1* mutated CLL suggests that these mutations have a loss-of-function, rather than a gain-of-function phenotype in CLL. This implicates that *XPO1* mutated CLL would not profit more from XPO1 inhibition with selinexor. The *ex-vivo* drug responses of *XPO1* mutated CLL to selinexor supported this assumption. However, the dataset only contained samples from three *XPO1* mutated CLL, which is too few to draw robust conclusions. Therefore, the results need to be validated in a larger cohort.

Unlike *TP53*, *ATM* and *XPO1* mutations, which had very focused and specific effects, *SF3B1* mutations affected the proteome in a more general way. Many proteins were differentially abundant in *SF3B1* mutated samples in comparison to wild type CLL. Interestingly, the transcriptome was not considerably affected by these mutations. SF3B1 is part of the U2 small nuclear ribonucleoprotein particle, an essential component of the splicing machinery (Wan and Wu, 2013). As splicing occurs at post-transcriptional level, it makes sense that the main effects of *SF3B1* mutations are only reflected in protein and not RNA abundances. Most of the affected proteins were downregulated, which might indicate a reduced production of protein due to re-

tained introns or the inclusion of poison exons. For *SF3B1* mutations such a mechanism has already been described for the protein BRD9 (Inoue et al., 2019). Thus, *SF3B1* mutations led to the inclusion of a poison exon in the gene for BRD9 and consequently downregulation of protein levels. This finding could be confirmed in the dataset at hand.

#### 4.1.2 Interaction between IGHV status and trisomy 12

Apart from *SF3B1* mutations, IGHV status and trisomy 12 were the alterations with the greatest impact on protein abundances. This is not unexpected, as IGHV is one of the most important prognostic markers in CLL (Damle et al., 1999; Hamblin et al., 1999) and trisomy 12 leads to the duplication of the whole chromosome 12. In contrast to *SF3B1* mutations, the presence of these alterations heavily influenced the transcriptome. Accordingly, unsupervised clustering of proteins or transcripts identified four subgroups of patients defined by the presence or absence of trisomy 12 and IGHV mutations. Similarly to this subdivision, two transcriptomic studies of CLL (Ferreira et al., 2014; Orgueira et al., 2019) discovered four groups with distinct transcriptomic signatures in CLL. In addition to the IGHV status, they described transcriptomic patterns driving the subdivision, which they termed C1 and C2. These signatures were predictive for TTT. As neither study measured the presence of trisomy 12, it is likely that the C1-C2 subgroups are in fact a subdivision into patients with and without trisomy 12. Proving this relationship would further validate the subgroups observed in this thesis. One way of how to confirm this assumption would be the assessment of the distribution of trisomy 12 in the studies by Ferreira et al. (2014) and Orgueira et al. (2019). For this, high expression levels of genes on chromosome 12 could be used as surrogate for trisomy 12.

It is known that the IGHV mutation status influences the sensitivity of CLL cells to stimulation of the BCR and response to treatment with BCR inhibitors (Burger and Wiestner, 2018; Dietrich et al., 2018; Lanham et al., 2003). Even though present in 15-20% of CLL cases (Abruzzo et al., 2018; Bosch and Dalla-Favera, 2019), the biology of trisomy 12 is less well understood. The results presented in this thesis improve the current understanding of trisomy 12. The increased response of U-CLL with trisomy 12 to BCR inhibition, recently described by us (Dietrich et al., 2018), could be confirmed in the microscopy-based drug screen. This thesis further provides a functional explanation for this behaviour. The proteomic analysis showed that BCR signalling proteins are upregulated in trisomy 12 CLL samples. This hints to an amplification of BCR signalling by trisomy 12 and provides the functional explanation for the increased susceptibility of trisomy 12 samples to BCR inhibition. Thus, proteogenomic profiling unravelled the interplay between IGHV status and trisomy 12, two crucial genetic markers of CLL, and the effects on gene expression, protein abundances and drug response. (Herbst et al., 2020c)

#### 4.1.3 Identification of a new poor outcome subgroup

Importantly, proteomics defined a previously unknown CLL subgroup with poor outcome and high proliferative capacity, which accounted for 20% of CLL patients. This proteomics group, named PG5, did not include trisomy 12 patients, but was otherwise independent of any frequent genetic or transcriptional alteration. Surprisingly, PG5 was characterised by a strong down-

regulation of BCR signalling proteins. This is in line with the association of low BCR protein levels with short TTT. As BCR signalling is one of the most important pathways in CLL (Bosch and Dalla-Favera, 2019; Hallek, 2017), the question arises, which signals are instead driving the malignancy of PG5. High levels of metabolic enzymes were detected for PG5. A functional consequence of this upregulation was supported by an enhanced response of PG5 to drugs inhibiting this pathway. Yet, more mechanistic insights need to be gained to fully understand the functional relationship. Additionally, components of the spliceosome were strongly increased in PG5, which was independent of *SF3B1* mutations. To prove that the upregulation of splicing factors can impact splicing and potentially also malignancy, an analysis of differential splicing events in PG5 would need to be conducted. (Herbst et al., 2020c)

In general, more clinical and mechanistic studies are required to validate the existence and improve our understanding of PG5. The identification of a PG5-like subgroup in the dataset by Eagle et al. (2015) further confirmed the general existence of such a subgroup in CLL. To detect PG5 patients in new cohorts, a clinical implementation of mass spectrometry based screening is needed, using the BCR and splicing signature defined in this study as a template. This could aid to identify patients at particular risk for aggressive disease and optimize treatment strategies. (Herbst et al., 2020c)

#### 4.1.4 Technical challenges and limitations of the experimental setup of the proteogenomic study

Different molecular layers for in total 68 CLL patient samples were recorded. Even though this represents the largest CLL cohort ever analysed with proteomics, the number of patients is nevertheless limited. Especially the subdivision into groups of patients with specific mutations or into multiple proteomics groups decreased the sample size further. Even though the recovery of known associations between the different molecular layers gives confidence that many of the obtained results are valid, it is crucial to confirm all new findings in larger datasets. Especially the existence and biological characteristics of PG5 should be validated in a larger and preferably prospective study cohort, as this finding might be relevant for patient classification. A first step has been taken into this directions by the finding that PG5 exists in an external, even smaller CLL patient cohort, highlighting the potential of its general existence and motivates the design of further mechanistic and clinical studies examining the subgroup further. (Herbst et al., 2020c)

Before the preparation for omics profiling or drug screening, patient cells, which had been viably frozen, were thawed and allowed to recover in medium. All of the analyses relied on the assumption that the proteome, transcriptome and drug response of these CLL cells still represented the *in-vivo* state despite the freezing and thawing process. Comparisons of drug response profiles of fresh versus frozen material had been conducted in our laboratory in the past and no differences were observed. Thus, a falsification of the drug responses by freezing can be excluded. The preservation of drug response phenotypes in previously frozen samples additionally implicates that at least the pathways determining drug response are not significantly altered by the freezing process. Yet, the possibility that the proteome or transcriptome are, nevertheless,

changed due to the freezing procedure cannot be excluded. For this, a thorough comparison of the proteomes and transcriptomes of fresh and frozen samples would be needed.

The experimental procedure was designed in a way that one batch of cells was prepared for all three omics profiling procedures and was only split later into individual cell pellets for proteomics, transcriptomics and analysis of mutations. Thus, the molecular profile of the cells was captured at exactly the same time point. This enables direct comparison between the different molecular layers. Additionally, this procedure prevents the introduction of batch effects due to preparation of samples at different time points.

Consequently, the experimental setup for the proteogenomic profiling has some limitations which need to be kept in mind or addressed by further experiments. However, in general many precautions had already been taken to ensure a good quality of the multi-omics dataset.

## 4.2 Phagocytosis by bone marrow stroma cells

Bone marrow stroma cells are commonly used in co-culture models to study the interaction between leukemia cells and the bone marrow niche. This thesis described the surprising discovery that some stroma cells extensively phagocytose apoptotic cells, beyond the extent which would have been expected from non-professional phagocytes. Phagocytosis was independent of the origin and malignancy of the apoptotic cells.

### 4.2.1 Potential *in-vivo* function of phagocytosis by stroma cells

The bone marrow stroma cell line NKTert, but not HS-5, extensively phagocytosed apoptotic cells. This behaviour was also seen in primary MSCs, however, differences between MSCs from individual donors existed. These observations highlight, that the cell type 'bone marrow stroma cell' is a very broad category, and the existence and phenotype of potential subclasses still remains to be fully understood. Baryawno et al. (2019) and Baccin et al. (2020) have made first attempts to categorise all cell types of the human and mouse bone marrow based on transcriptomic profiling. They indeed discovered different mesenchymal subtypes using single-cell sequencing. Considering their different behaviours it is very likely that the HS-5 and NKTert cell lines and the MSCs from individual donors were derived from different mesenchymal subpopulations. To correctly identify to which category a specific bone marrow stroma cell belongs, transcriptomic profiles would need to be compared to these studies. For future investigations routinely subtyping of mesenchymal cells into different categories would need to be implemented to produce consistent results for specific stroma subsets.

The results that NKTert and some primary MSCs are able to phagocytose apoptotic cells in great quantities leads to the assumption that this behaviour also occurs *in-vivo*. During maturation in the bone marrow, B-cells undergo a strict selection process which is highly dependent on the interaction with bone marrow stroma cells. As a consequence of this selection process a large amount of B-cells, which did not meet the selection criteria, become apoptotic (Murphy, 2012).

If left uncontrolled the accumulation of apoptotic cells can lead to great damages within the tissue and severe diseases. Therefore, dead cells need to be cleared quickly without the induction of inflammation through the release of the intracellular content of apoptotic cells (Arandjelovic and Ravichandran, 2015). The amount of professional phagocytes in the bone marrow might not be sufficient to deal with the great number of B-cells undergoing apoptosis due to the selection process during maturation. I hypothesise that a specialised subgroup of stroma cells exists, greatly contributing to the clearance of apoptotic cells. As stroma cells are constantly in close contact with developing B-cells (Murphy, 2012), efficient clearance of apoptotic cells would be ensured. Thus, phagocytosis by stroma cells potentially maintains tissue homeostasis, prevents inflammation and, thereby, is essential for sustaining functional hematopoiesis.

#### **4.2.2 Further directions for the investigation of phagocytosis by stroma cells**

Even though an upregulation of lysosomal proteins in NKTert in comparison to HS-5 was observed, no explanation for the differences in phagocytic activity could be found. Stroma cells phagocytosed only apoptotic cells and did not harm alive cells, suggesting selectivity for apoptotic cells. The mechanism underlying this target recognition, however, remains to be elucidated. In general, signals regulating phagocytosis are grouped into two categories: 'eat-me' and 'don't-eat-me' signals. 'Eat-me' signals are displayed by apoptotic cells and trigger their uptake by phagocytes. An example for this is the exposure of phosphatidylserines on the outer surface of the cell membrane. The expression of 'don't-eat-me' signals prevents the uptake of cells through phagocytosis (Arandjelovic and Ravichandran, 2015). Many cancer cells have hijacked this mechanism and have increased expression levels of 'don't-eat-me' signals, thereby evading destruction by the immune system (Chao et al., 2010). Therapies targeting the 'don't-eat-me' CD47 signal on cancer cells are currently in clinical trials and the results look promising (Advani et al., 2018; Chao et al., 2010). Through the masking of CD47, cancer cells are no longer protected from phagocytosis by macrophages which induces the clearance of malignant cells. In an experiment not further described in this thesis I observed that NKTert cells also rapidly take up glass beads coated with phosphatidylcholin or left uncoated. This hints to the importance of a 'don't-eat-me', rather than an 'eat-me' signal in stroma cell phagocytosis. However, my Master student Tina Becirovic could demonstrate that the responsible 'don't-eat-me' signal is not CD47. Thus, it would be highly interesting to uncover which signal is instead driving target cell recognition in stroma cells. The discovery of the relevant signal might even lead to a potential exploitation of the respective mechanism for cancer therapy. Engaging bone marrow stroma cells in cancer cell phagocytosis would be highly interesting as this might lead to the clearance of minimal residual disease from the bone marrow of leukemia patients.

#### **4.2.3 Implication of phagocytosis by stroma cells for co-culture studies**

Phagocytosis of apoptotic cells by stroma cells has direct implications for co-culture studies. The clearance of dead cells from the co-cultures by phagocytosis increases the percentage of alive cells in the cultures. This artificial increase of relative amounts of alive cells can potentially lead to an overestimation of the protective effect by stroma cells. Relative measurement of alive cells is dominating in flow cytometry, which has been the most commonly used assay for

reading out results from co-culture studies. This indicates, that results from co-culture experiments with NKTert or MSCs might have been misinterpreted in the past due to phagocytosis of apoptotic cells. Ding et al. (2018), for example, reported that blocking of lysosomal pathways with chloroquine leads to the presence of more apoptotic CLL cells in NKTert co-cultures. The authors interpreted this finding as a disruption of the protection from apoptosis by NKTert. The results in this thesis, however, suggest that the observed effect is rather due to an inhibition of phagocytosis. (Herbst et al., 2020b)

Great differences between the phagocytic activity of stroma cells existed. For future studies, extensive phagocytosis by the used stroma cells needs to either be excluded by testing the respective cells beforehand or taken into account by using absolute instead of relative measurements. Only such approaches will ensure that the influence of the microenvironment is accurately determined and allow the development of effective treatment strategies to overcome its protection. (Herbst et al., 2020b)

### 4.3 High-throughput co-culture drug sensitivity screen

The bone marrow is a crucial compartment in the development and progression of CLL (Burger and O'Brien, 2018). Bone marrow stroma cells have been shown to protect leukemia cells from spontaneous and drug-induced apoptosis (Kurtova et al., 2009; Lagneaux et al., 1998; Panayiotidis et al., 1996). However, to date a systematic analysis of how stroma cells influence CLL drug response is lacking. This thesis described the establishment of a high-throughput co-culture drug sensitivity screen and its application to systematically evaluate drug responses in co-cultures. In total, responses for 43 drugs in 81 CLL patient samples were measured with the microscopy-based screen. To not confound the results due to phagocytosis by stroma cells, the non-phagocytic cell line HS-5 was used for the screen. For the validation experiments with primary MSCs, absolute counts of alive cells were measured. (Herbst et al., 2020a)

#### 4.3.1 Protection of CLL cells from spontaneous apoptosis by stroma

As described in the literature (Lagneaux et al., 1998; Panayiotidis et al., 1996), protection of CLL cells from spontaneous apoptosis *ex-vivo* could be confirmed. The effect was seen for the cell line HS-5, as well as for primary MSCs. What has not been reported previously is that the effect sizes of the protection were very heterogeneous between patient samples. In general, samples with low percentages of alive cells in mono-cultures profited more from co-culturing. The samples with high rates of spontaneous apoptosis might be especially reliant on external signalling input and, thus, profit more from stroma support. Furthermore, U-CLL patient cells responded better to the supportive effect by bone marrow stroma cells. It is known that U-CLL cells express BCRs which recognise various auto- and foreign antigens, while M-CLL cells have very specialised BCRs which are harder to activate by general stimulation (Burger and Wiestner, 2018; Lanham et al., 2003). The unresponsiveness of M-CLL patient samples to external stimuli might be the reason why they responded less well to stroma support than U-CLL cells. (Herbst et al., 2020a)

### 4.3.2 Effect of stroma cells on drug-induced apoptosis by stroma

This thesis presented a systematic analysis of the effect of stroma cells on drug response of CLL. Importantly, the elevation of the percentage of alive cells by the protection from spontaneous apoptosis was taken into account in the analysis by the usage of a linear model to determine the degree of interaction. So far, it has been neglected in published studies that the systematic increase of the percentage of alive CLL cells through stroma cells can mistakenly be interpreted as protection from drug-induced apoptosis. The established linear model solves this problem. (Herbst et al., 2020a)

In accordance with the literature (Kurtova et al., 2009; Mraz et al., 2011; Zhang et al., 2012), stroma cells protected CLL from fludarabine and doxorubicine induced apoptosis. Additionally, CLL response to cytarabine was reduced in co-cultures. This finding further confirms that the drug class of chemotherapeutics is in general not very active in the context of the bone marrow microenvironment. The largest difference between culture conditions was observed for the drug carfilzomib. No response at all was seen to this proteasome inhibitor in CLL cells co-cultured with HS-5. Stroma-mediated protection of CLL from carfilzomib-induced apoptosis had already been mentioned by Gupta et al. (2013). Whether this is a general behaviour of proteasome inhibitors needs to be investigated further, as in my hands the other proteasome inhibitor ixazomib did not exhibit a reduced efficacy in co-cultures. Besides the confirmation of these known associations, the screen uncovered a new drug class with altered action in bone marrow stroma cell co-cultures. Thus, the BET inhibitors JQ1 and I-BET-762 were not as active in co-cultures as in CLL mono-cultures. So far, BET inhibitors are not clinically approved, but are in clinical trial. The usage of BET inhibitors as single agents is, however, limited by the lack of long term responses and the development of resistances. Resistances have so far not been associated with the occurrence of mutations (Alqahtani et al., 2019). Thus, the protective effect by the bone marrow niche might be a plausible explanation for the emergence of these resistances. (Herbst et al., 2020a)

For many drugs used in the conventional CLL treatment regimens, less efficacy in the context of the bone marrow has been shown (Gupta et al., 2013; Kay et al., 2007; Kurtova et al., 2009; Panayiotidis et al., 1996). Therefore, it is important to realise that not all drugs are affected by the presence of bone marrow stroma cells. The response to PI3K inhibitors, for example, was statistically equivalent in mono- and co-cultures. For the other clinically used BCR inhibitor ibrutinib the results were inconclusive. Stroma cells were protective in one of the used concentrations, while responses were equivalent in another concentration. In the clinic response to ibrutinib treatment is rarely complete (Byrd et al., 2013), suggesting that at least some degree of protection by the bone marrow exists, as previously described (Cheng et al., 2014; Guo et al., 2017). In contrast to the target of ibrutinib BTK, PI3K has been proposed to be a major player in tonic BCR signalling (Kraus et al., 2004; Lam et al., 1997; Srinivasan et al., 2009), which is thought to be independent of antigen signalling (Kraus et al., 2004; Shaffer and Schlessel, 1997). The slightly different roles in BCR signalling of BTK and PI3K might, thus, explain the different effects of stroma cells on drug response. As PI3K inhibitors seem to work independently of

the leukemic niche, it might be justified to evaluate whether PI3K inhibitors would be better suited to prevent protection from the bone marrow, minimal residual disease and the emergence of resistances. However, this would need to be carefully evaluated, as toxicities are more frequently observed with the PI3K inhibitor idelalisib (Burger and O'Brien, 2018) and resistances of circulating CLL cells to ibrutinib occur rarely (Woyach and Johnson, 2015). (Herbst et al., 2020a)

Another inhibitor not affected by the presence of bone marrow stroma cells was venetoclax. The equivalent action of this drug on cells in suspension and cells cultured in conditions mimicking the bone marrow might explain the higher rate of complete remissions and less minimal residual disease in the bone marrow, which can be achieved by venetoclax treatment in the clinic (Roberts et al., 2016; Seymour et al., 2018). (Herbst et al., 2020a)

Most interestingly, some drugs were more active in co-cultures of CLL and stroma cells than in CLL mono-cultures. Especially JAK inhibitors had increased efficacy on CLL in the presence of stroma cells. JAK/STAT signalling is known to be an important pathway for transmitting the signals received from soluble factors, like interleukins (Murray, 2007). The result that soluble factors are enough to trigger the phosphorylation of STAT3 on residue Tyr705 is in accordance with this. It has been reported that phosphorylation of STAT3 on residue Tyr705 is increased in CLL cells co-cultured with bone marrow stroma cells (Severin et al., 2019), which could be confirmed. This phosphorylation could be reversed by inhibition with different JAK inhibitors. The results motivate the use of drugs like the FDA approved inhibitor ruxolitinib to overcome the influence of the bone marrow. Especially combination therapies with drugs exhibiting good activities in the blood might be of high interest. First clinical studies are moving into this direction (Spaner et al., 2019, 2016). (Herbst et al., 2020a)

The findings highlighted above emphasise that high-throughput co-culture drug screens can be useful to motivate further investigations evaluating how to overcome the protection from the microenvironment. Moreover, it could be used to assess the activity of newly developed drug candidates in the bone marrow.

### 4.3.3 Mono- versus co-culture high-throughput drug screens

High-throughput drug sensitivity screens enable the assessment of drug responses of primary cancer cells *ex-vivo*. Yet, all results obtained from these studies should be validated using *in-vivo* models or through the analysis of clinical data, as all model systems have limitations, do not reflect all of the possible interactions within an organism and rely on assumptions. However, it is generally said, that even though all models are wrong, some of them prove to be useful. The question arises whether mono- or co-culture models are more useful for studying cancer cell drug responses in high-throughput. This question cannot be easily answered, as both models have advantages and disadvantages. Mono-cultures are easier to handle and analyse than co-cultures. However, the influence of the bone marrow is completely neglected in mono-cultures, even though the important role of the microenvironment in CLL has become increasingly clear

in recent years and could be further supported in this thesis. Additionally, co-culturing led to a reduction of spontaneous apoptosis for a large set of samples which stabilises the assay and potentially increases its robustness. This makes co-cultures an attractive model for high-throughput screens. The current study demonstrated that CLL disease pathology was still reflected in co-cultures, further encouraging the usage of co-culture models to understand CLL biology. Yet, studies need to carefully evaluate whether they wish to inquire the action of drugs in the niche of the bone marrow or the blood. Depending on this, either mono- or co-cultures should be chosen, as stroma cells do alter the response of CLL cells to some drug classes. Thus, effect sizes for chemotherapeutics are small in stroma co-cultures, even though these compounds are often very active in the blood of patients. Finally, it can be said, that if a co-culture system is chosen, the setup presented in the current study is highly attractive, as it can evaluate responses to many different drugs and concentrations in parallel. The system proved to be very valuable as many known results obtained in low-throughput studies could be recapitulated with this platform. Additionally, it allowed the discovery of new associations and will altogether be very informative for future investigation incorporating more uncharacterised drugs.

## 5 Conclusion

This thesis presented a comprehensive characterisation of cell-intrinsic and extrinsic factors in CLL influencing drug response and outcome (Fig. 5.1).

One aim was to comprehensively explore the cell-intrinsic factors determining the heterogeneity between patients. This was successfully achieved by conducting the first proteogenomic study of a large CLL patient cohort, comprising 81 primary samples. It allowed the description

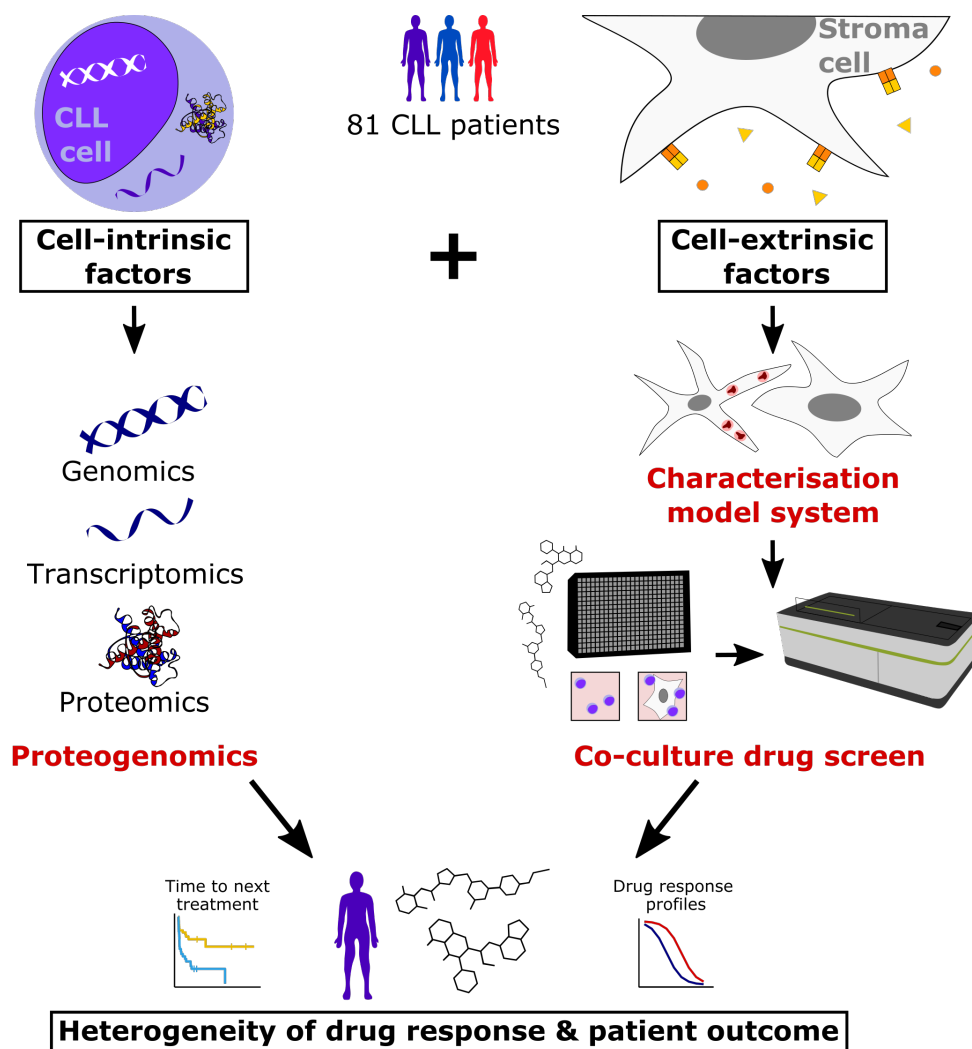


Figure 5.1: **Overview of the work in this thesis.** The effect of cell-intrinsic and extrinsic factors on drug response and patient outcome in CLL was thoroughly explored by conducting proteogenomics of a large CLL patient cohort, characterisation of a model for co-culture drug screening and the usage of this system to explore the impact of stroma cells on drug response.

of the relationships between genetic, transcriptomic and proteomic changes and consequences for drug response and clinical outcome. Importantly, a new patient subgroup with poor outcome, deregulated levels of B-cell receptor signalling, spliceosomal and metabolic proteins and distinct drug vulnerabilities was uncovered.

Additionally, this thesis aimed to examine the role of cell-extrinsic factors in drug sensitivity and resistance. As no appropriate model system for high-throughput drug screening in co-cultures existed, a suitable system needed to be established. Thorough characterisation of different models revealed extensive phagocytic activity by some bone marrow stroma cells. This behaviour can lead to a systematic bias in co-culture studies if left unconsidered.

With the successful establishment of a suitable co-culture model, a systematic co-culture drug sensitivity screen, comprising 43 different compounds, could be conducted. A systematic analysis of the influence of stroma cells on drug sensitivity profiles provided insights into how stroma cells modify drug responses of CLL cells. Bone marrow stroma cells, for example, conveyed protection from apoptosis induced by chemotherapeutics or BET inhibitors. For other drug classes, like PI3K inhibitors or the BCL-2 inhibitor venetoclax, responses were unaltered in co-cultures with stroma cells. Most importantly, drugs with higher activity in the context of the bone marrow microenvironment were discovered e.g. JAK inhibitors.

In conclusion, this thesis provides not only a thorough assessment of the suitability of co-cultures for high-throughput drug screening, but also highlights future directions for better CLL patient classification and for overcoming the protection by the bone marrow microenvironment.

## Bibliography

- 1000 Genomes Project Consortium, Auton, A., Brooks, L. D., Durbin, R. M., Garrison, E. P., Kang, H. M., Korbel, J. O., Marchini, J. L., McCarthy, S., McVean, G. A. and Abecasis, G. R. (2015). A global reference for human genetic variation. *Nature* *526*, 68–74.
- Abruzzo, L. V., Herling, C. D., Calin, G. A., Oakes, C., Barron, L. L., Banks, H. E., Katju, V., Keating, M. J. and Coombes, K. R. (2018). Trisomy 12 chronic lymphocytic leukemia expresses a unique set of activated and targetable pathways. *Haematologica* *103*, 2069–2078.
- Advani, R., Flinn, I., Popplewell, L., Forero, A., Bartlett, N. L., Ghosh, N., Kline, J., Roschewski, M., LaCasce, A., Collins, G. P., Tran, T., Lynn, J., Chen, J. Y., Volkmer, J.-P., Agoram, B., Huang, J., Majeti, R., Weissman, I. L., Takimoto, C. H., Chao, M. P. and Smith, S. M. (2018). CD47 Blockade by Hu5F9-G4 and Rituximab in Non-Hodgkin’s Lymphoma. *The New England Journal of Medicine* *379*, 1711–1721.
- Akbani, R., Ng, P. K. S., Werner, H. M. J., Shahmoradgoli, M., Zhang, F., Ju, Z., Liu, W., Yang, J.-Y., Yoshihara, K., Li, J., Ling, S., Seviour, E. G., Ram, P. T., Minna, J. D., Diao, L., Tong, P., Heymach, J. V., Hill, S. M., Dondelinger, F., Städler, N., Byers, L. A., Meric-Bernstam, F., Weinstein, J. N., Broom, B. M., Verhaak, R. G. W., Liang, H., Mukherjee, S., Lu, Y. and Mills, G. B. (2014). A pan-cancer proteomic perspective on The Cancer Genome Atlas. *Nature Communications* *5*, 3887.
- Alanazi, B., Munje, C. R., Rastogi, N., Williamson, A. J. K., Taylor, S., Hole, P. S., Hodges, M., Doyle, M., Baker, S., Gilkes, A. F., Knapper, S., Pierce, A., Whetton, A. D., Darley, R. L. and Tonks, A. (2020). Integrated nuclear proteomics and transcriptomics identifies S100A4 as a therapeutic target in acute myeloid leukemia. *Leukemia* *34*, 427–440.
- Alberts, B., Johnson, A., Lewis, R., Raff, M., Roberts, K. and Walter, P. (2008). *Molecular Biology of the Cell*. 5 edition, Garland Science.
- Alqahtani, A., Choucair, K., Ashraf, M., Hammouda, D. M., Alloghbi, A., Khan, T., Senzer, N. and Nemunaitis, J. (2019). Bromodomain and extra-terminal motif inhibitors: a review of preclinical and clinical advances in cancer therapy. *Future Science OA* *5*, FSO372.
- Anders, S., Pyl, P. T. and Huber, W. (2015). HTSeq—a Python framework to work with high-throughput sequencing data. *Bioinformatics (Oxford, England)* *31*, 166–9.
- Arandjelovic, S. and Ravichandran, K. S. (2015). Phagocytosis of apoptotic cells in homeostasis. *Nature Immunology* *16*, 907–917.
- Archer, T. C., Ehrenberger, T., Mundt, F., Gold, M. P., Krug, K., Mah, C. K., Mahoney, E. L., Daniel, C. J., LeNail, A., Ramamoorthy, D., Mertins, P., Mani, D. R., Zhang, H.,

- Gillette, M. A., Clauser, K., Noble, M., Tang, L. C., Pierre-François, J., Silterra, J., Jensen, J., Tamayo, P., Korshunov, A., Pfister, S. M., Kool, M., Northcott, P. A., Sears, R. C., Lipton, J. O., Carr, S. A., Mesirov, J. P., Pomeroy, S. L. and Fraenkel, E. (2018). Proteomics, Post-translational Modifications, and Integrative Analyses Reveal Molecular Heterogeneity within Medulloblastoma Subgroups. *Cancer Cell* *34*, 396–410.e8.
- Austen, B., Powell, J. E., Alvi, A., Edwards, I., Hooper, L., Starczynski, J., Taylor, A. M. R., Fegan, C., Moss, P. and Stankovic, T. (2005). Mutations in the ATM gene lead to impaired overall and treatment-free survival that is independent of IGVH mutation status in patients with B-CLL. *Blood* *106*, 3175–82.
- Baccin, C., Al-Sabah, J., Velten, L., Helbling, P. M., Grünschläger, F., Hernández-Malmierca, P., Nombela-Arrieta, C., Steinmetz, L. M., Trumpp, A. and Haas, S. (2020). Combined single-cell and spatial transcriptomics reveal the molecular, cellular and spatial bone marrow niche organization. *Nature Cell Biology* *22*, 38–48.
- Bakker, E., Qattan, M., Mutti, L., Demonacos, C. and Krstic-Demonacos, M. (2016). The role of microenvironment and immunity in drug response in leukemia. *Biochimica et Biophysica Acta* *1863*, 414–426.
- Balakrishnan, K., Burger, J. A., Wierda, W. G. and Gandhi, V. (2009). AT-101 induces apoptosis in CLL B cells and overcomes stromal cell-mediated Mcl-1 induction and drug resistance. *Blood* *113*, 149–53.
- Balakrishnan, K., Peluso, M., Fu, M., Rosin, N. Y., Burger, J. A., Wierda, W. G., Keating, M. J., Faia, K., O'Brien, S., Kutok, J. L. and Gandhi, V. (2015). The phosphoinositide-3-kinase (PI3K)-delta and gamma inhibitor, IPI-145 (Duvelisib), overcomes signals from the PI3K/AKT/S6 pathway and promotes apoptosis in CLL. *Leukemia* *29*, 1811–22.
- Barretina, J., Caponigro, G., Stransky, N., Venkatesan, K., Margolin, A. A., Kim, S., Wilson, C. J., Lehár, J., Kryukov, G. V., Sonkin, D., Reddy, A., Liu, M., Murray, L., Berger, M. F., Monahan, J. E., Morais, P., Meltzer, J., Korejwa, A., Jané-Valbuena, J., Mapa, F. A., Thibault, J., Bric-Furlong, E., Raman, P., Shipway, A., Engels, I. H., Cheng, J., Yu, G. K., Yu, J., Aspesi, P., de Silva, M., Jagtap, K., Jones, M. D., Wang, L., Hatton, C., Palesscandolo, E., Gupta, S., Mahan, S., Sougnez, C., Onofrio, R. C., Liefeld, T., MacConaill, L., Winckler, W., Reich, M., Li, N., Mesirov, J. P., Gabriel, S. B., Getz, G., Ardlie, K., Chan, V., Myer, V. E., Weber, B. L., Porter, J., Warmuth, M., Finan, P., Harris, J. L., Meyerson, M., Golub, T. R., Morrissey, M. P., Sellers, W. R., Schlegel, R. and Garraway, L. A. (2012). The Cancer Cell Line Encyclopedia enables predictive modelling of anticancer drug sensitivity. *Nature* *483*, 603–7.
- Baryawno, N., Przybylski, D., Kowalczyk, M. S., Kfoury, Y., Severe, N., Gustafsson, K., Kokkaliaris, K. D., Mercier, F., Tabaka, M., Hofree, M., Dionne, D., Papazian, A., Lee, D., Ashenberg, O., Subramanian, A., Vaishnav, E. D., Rozenblatt-Rosen, O., Regev, A. and Scadden, D. T. (2019). A Cellular Taxonomy of the Bone Marrow Stroma in Homeostasis and Leukemia. *Cell* *177*, 1915–1932.e16.

- Basu, A., Bodycombe, N. E., Cheah, J. H., Price, E. V., Liu, K., Schaefer, G. I., Ebright, R. Y., Stewart, M. L., Ito, D., Wang, S., Bracha, A. L., Liefeld, T., Wawer, M., Gilbert, J. C., Wilson, A. J., Stransky, N., Kryukov, G. V., Dancik, V., Barretina, J., Garraway, L. A., Hon, C. S.-Y., Munoz, B., Bittker, J. A., Stockwell, B. R., Khabele, D., Stern, A. M., Clemons, P. A., Shamji, A. F. and Schreiber, S. L. (2013). An interactive resource to identify cancer genetic and lineage dependencies targeted by small molecules. *Cell* *154*, 1151–1161.
- Berthold, M. R., Cebron, N., Dill, F., Gabriel, T. R., Kötter, T., Meinl, T., Ohl, P., Thiel, K. and Wiswedel, B. (2009). KNIME - the Konstanz information miner. *ACM SIGKDD Explorations Newsletter* *11*, 26–31.
- Boelens, J., Lust, S., Vanhoecke, B. and Offner, F. (2009). Chronic lymphocytic leukaemia. *Anticancer Research* *29*, 605–15.
- Bosch, F. and Dalla-Favera, R. (2019). Chronic lymphocytic leukaemia: from genetics to treatment. *Nature Reviews Clinical Oncology* *16*, 684–701.
- Branca, R. M. M., Orre, L. M., Johansson, H. J., Granholm, V., Huss, M., Pérez-Bercoff, Å., Forshed, J., Käll, L. and Lehtiö, J. (2014). HiRIEF LC-MS enables deep proteome coverage and unbiased proteogenomics. *Nature Methods* *11*, 59–62.
- Brown, J. R., Byrd, J. C., Coutre, S. E., Benson, D. M., Flinn, I. W., Wagner-Johnston, N. D., Spurgeon, S. E., Kahl, B. S., Bello, C., Webb, H. K., Johnson, D. M., Peterman, S., Li, D., Jahn, T. M., Lannutti, B. J., Ulrich, R. G., Yu, A. S., Miller, L. L. and Furman, R. R. (2014). Idelalisib, an inhibitor of phosphatidylinositol 3-kinase p110 $\delta$ , for relapsed/refractory chronic lymphocytic leukemia. *Blood* *123*, 3390–7.
- Burger, J. A. and O’Brien, S. (2018). Evolution of CLL treatment — from chemoimmunotherapy to targeted and individualized therapy. *Nature Reviews Clinical Oncology* *15*, 510–527.
- Burger, J. A., Quiroga, M. P., Hartmann, E., Bürkle, A., Wierda, W. G., Keating, M. J. and Rosenwald, A. (2009). High-level expression of the T-cell chemokines CCL3 and CCL4 by chronic lymphocytic leukemia B cells in nurselike cell cocultures and after BCR stimulation. *Blood* *113*, 3050–8.
- Burger, J. A., Tsukada, N., Burger, M., Zvaifler, N. J., Dell’Aquila, M. and Kipps, T. J. (2000). Blood-derived nurse-like cells protect chronic lymphocytic leukemia B cells from spontaneous apoptosis through stromal cell-derived factor-1. *Blood* *96*, 2655–63.
- Burger, J. A. and Wiestner, A. (2018). Targeting B cell receptor signalling in cancer: Preclinical and clinical advances. *Nature Reviews Cancer* *18*, 148–167.
- Burns, A., Alsolami, R., Becq, J., Stamatopoulos, B., Timbs, A., Bruce, D., Robbe, P., Vavoulis, D., Clifford, R., Cabes, M., Dreau, H., Taylor, J., Knight, S. J. L., Mansson, R., Bentley, D., Beekman, R., Martín-Subero, J. I., Campo, E., Houlston, R. S., Ridout, K. E. and Schuh, A. (2018). Whole-genome sequencing of chronic lymphocytic leukaemia reveals distinct differences in the mutational landscape between IgHVmut and IgHVunmut subgroups. *Leukemia* *32*, 332–342.

- Byrd, J. C., Furman, R. R., Coutre, S. E., Flinn, I. W., Burger, J. A., Blum, K. A., Grant, B., Sharman, J. P., Coleman, M., Wierda, W. G., Jones, J. A., Zhao, W., Heerema, N. A., Johnson, A. J., Sukbuntherng, J., Chang, B. Y., Clow, F., Hedrick, E., Buggy, J. J., James, D. F. and O'Brien, S. (2013). Targeting BTK with ibrutinib in relapsed chronic lymphocytic leukemia. *The New England Journal of Medicine* *369*, 32–42.
- Camus, V., Miloudi, H., Taly, A., Sola, B. and Jardin, F. (2017). XPO1 in B cell hematological malignancies: from recurrent somatic mutations to targeted therapy. *Journal of Hematology and Oncology* *10*, 1–13.
- Chambers, M. C., Maclean, B., Burke, R., Amodei, D., Ruderman, D. L., Neumann, S., Gatto, L., Fischer, B., Pratt, B., Egertson, J., Hoff, K., Kessner, D., Tasman, N., Shulman, N., Frewen, B., Baker, T. A., Brusniak, M.-Y., Paulse, C., Creasy, D., Flashner, L., Kani, K., Moulding, C., Seymour, S. L., Nuwaysir, L. M., Lefebvre, B., Kuhlmann, F., Roark, J., Rainer, P., Detlev, S., Hemenway, T., Huhmer, A., Langridge, J., Connolly, B., Chadick, T., Holly, K., Eckels, J., Deutsch, E. W., Moritz, R. L., Katz, J. E., Agus, D. B., MacCoss, M., Tabb, D. L. and Mallick, P. (2012). A cross-platform toolkit for mass spectrometry and proteomics. *Nature Biotechnology* *30*, 918–920.
- Chao, M. P., Alizadeh, A. A., Tang, C., Myklebust, J. H., Varghese, B., Gill, S., Jan, M., Cha, A. C., Chan, C. K., Tan, B. T., Park, C. Y., Zhao, F., Kohrt, H. E., Malumbres, R., Briones, J., Gascoyne, R. D., Lossos, I. S., Levy, R., Weissman, I. L. and Majeti, R. (2010). Anti-CD47 Antibody Synergizes with Rituximab to Promote Phagocytosis and Eradicate Non-Hodgkin Lymphoma. *Cell* *142*, 699–713.
- Cheng, S., Ma, J., Guo, A., Lu, P., Leonard, J. P., Coleman, M., Liu, M., Buggy, J. J., Furman, R. R. and Wang, Y. L. (2014). BTK inhibition targets in vivo CLL proliferation through its effects on B-cell receptor signaling activity. *Leukemia* *28*, 649–57.
- Clark, D. J., Dhanasekaran, S. M., Petralia, F., Pan, J., Song, X., Hu, Y., da Veiga Leprevost, F., Reva, B., Lih, T.-S. M., Chang, H.-Y., Ma, W., Huang, C., Ricketts, C. J., Chen, L., Krek, A., Li, Y., Rykunov, D., Li, Q. K., Chen, L. S., Ozbek, U., Vasaikar, S., Wu, Y., Yoo, S., Chowdhury, S., Wyczalkowski, M. A., Ji, J., Schnaubelt, M., Kong, A., Sethuraman, S., Avtonomov, D. M., Ao, M., Colaprico, A., Cao, S., Cho, K.-C., Kalayci, S., Ma, S., Liu, W., Ruggles, K., Calinawan, A., Gümüş, Z. H., Geiszler, D., Kawaler, E., Teo, G. C., Wen, B., Zhang, Y., Keegan, S., Li, K., Chen, F., Edwards, N., Pierorazio, P. M., Chen, X. S., Pavlovich, C. P., Hakimi, A. A., Brominski, G., Hsieh, J. J., Antczak, A., Omelchenko, T., Lubinski, J., Wiznerowicz, M., Linehan, W. M., Kinsinger, C. R., Thiagarajan, M., Boja, E. S., Mesri, M., Hiltke, T., Robles, A. I., Rodriguez, H., Qian, J., Fenyö, D., Zhang, B., Ding, L., Schadt, E., Chinnaiyan, A. M., Zhang, Z., Omenn, G. S., Cieslik, M., Chan, D. W., Nesvizhskii, A. I., Wang, P., Zhang, H. and Clinical Proteomic Tumor Analysis Consortium (2019). Integrated Proteogenomic Characterization of Clear Cell Renal Cell Carcinoma. *Cell* *179*, 964–983.e31.
- Collins, R. J., Verschuer, L. A., Harmon, B. V., Prentice, R. L., Pope, J. H. and Kerr, J. F.

- (1989). Spontaneous programmed death (apoptosis) of B-chronic lymphocytic leukaemia cells following their culture in vitro. *British Journal of Haematology* *71*, 343–50.
- Crassini, K., Shen, Y., Mulligan, S. and Giles Best, O. (2017). Modeling the chronic lymphocytic leukemia microenvironment in vitro. *Leukemia and Lymphoma* *58*, 266–279.
- Crespo, M., Bosch, F., Villamor, N., Bellosillo, B., Colomer, D., Rozman, M., Marcé, S., López-Guillermo, A., Campo, E. and Montserrat, E. (2003). ZAP-70 expression as a surrogate for immunoglobulin-variable-region mutations in chronic lymphocytic leukemia. *The New England Journal of Medicine* *348*, 1764–75.
- Damle, R. N., Wasil, T., Fais, F., Ghiotto, F., Valetto, A., Allen, S. L., Buchbinder, A., Budman, D., Dittmar, K., Kolitz, J., Lichtman, S. M., Schulman, P., Vinciguerra, V. P., Rai, K. R., Ferrarini, M. and Chiorazzi, N. (1999). Ig V gene mutation status and CD38 expression as novel prognostic indicators in chronic lymphocytic leukemia. *Blood* *94*, 1840–7.
- De Silva, N. S. and Klein, U. (2015). Dynamics of B cells in germinal centres. *Nature Reviews Immunology* *15*, 137–48.
- Dietrich, S., Oleś, M., Lu, J., Sellner, L., Anders, S., Velten, B., Wu, B., Hüllein, J., da Silva Liberio, M., Walther, T., Wagner, L., Rabe, S., Ghidelli-Disse, S., Bantscheff, M., Oleś, A. K., Slabicki, M., Mock, A., Oakes, C. C., Wang, S., Oppermann, S., Lukas, M., Kim, V., Sill, M., Benner, A., Jauch, A., Sutton, L. A., Young, E., Rosenquist, R., Liu, X., Jethwa, A., Lee, K. S., Lewis, J., Putzker, K., Lutz, C., Rossi, D., Mokhir, A., Oellerich, T., Zirlik, K., Herling, M., Nguyen-Khac, F., Plass, C., Andersson, E., Mustjoki, S., von Kalle, C., Ho, A. D., Hensel, M., Dürig, J., Ringshausen, I., Zapatka, M., Huber, W. and Zenz, T. (2018). Drug-perturbation-based stratification of blood cancer. *The Journal of Clinical Investigation* *128*, 427–445.
- Ding, L., Zhang, W., Yang, L., Pelicano, H., Zhou, K., Yin, R., Huang, R. and Zeng, J. (2018). Targeting the autophagy in bone marrow stromal cells overcomes resistance to vorinostat in chronic lymphocytic leukemia. *OncoTargets and Therapy* *11*, 5151–5170.
- Dittmer, D., Pati, S., Zambetti, G., Chu, S., Teresky, A. K., Moore, M., Finlay, C. and Levine, A. J. (1993). Gain of function mutations in p53. *Nature Genetics* *4*, 42–46.
- Dobin, A., Davis, C. a., Schlesinger, F., Drenkow, J., Zaleski, C., Jha, S., Batut, P., Chaisson, M. and Gingeras, T. R. (2013). STAR: ultrafast universal RNA-seq aligner. *Bioinformatics (Oxford, England)* *29*, 15–21.
- Döhner, H., Fischer, K., Bentz, M., Hansen, K., Benner, A., Cabot, G., Diehl, D., Schlenk, R., Coy, J. and Stilgenbauer, S. (1995). p53 gene deletion predicts for poor survival and non-response to therapy with purine analogs in chronic B-cell leukemias. *Blood* *85*, 1580–9.
- Döhner, H., Stilgenbauer, S., Benner, A., Leupolt, E., Kröber, A., Bullinger, L., Döhner, K., Bentz, M. and Lichter, P. (2000). Genomic aberrations and survival in chronic lymphocytic leukemia. *The New England Journal of Medicine* *343*, 1910–6.

- Dong, F., Yang, Q., Wu, Z., Hu, X., Shi, D., Feng, M., Li, J., Zhu, L., Jiang, S. and Bao, Z. (2019). Identification of survival-related predictors in hepatocellular carcinoma through integrated genomic, transcriptomic, and proteomic analyses. *Biomedicine and Pharmacotherapy* *114*, 108856.
- Eagle, G. L., Zhuang, J., Jenkins, R. E., Till, K. J., Jithesh, P. V., Lin, K., Johnson, G. G., Oates, M., Park, K., Kitteringham, N. R. and Pettitt, A. R. (2015). Total proteome analysis identifies migration defects as a major pathogenetic factor in immunoglobulin heavy chain variable region (IGHV)-unmutated chronic lymphocytic leukemia. *Molecular & Cellular Proteomics : MCP* *14*, 933–45.
- Fabbri, G. and Dalla-Favera, R. (2016). The molecular pathogenesis of chronic lymphocytic leukaemia. *Nature Reviews Cancer* *16*, 145–162.
- Fegan, C., Robinson, H., Thompson, P., Whittaker, J. A. and White, D. (1995). Karyotypic evolution in CLL: identification of a new sub-group of patients with deletions of 11q and advanced or progressive disease. *Leukemia* *9*, 2003–8.
- Ferreira, P. G., Jares, P., Rico, D., Gómez-López, G., Martínez-Trillos, A., Villamor, N., Ecker, S., González-Pérez, A., Knowles, D. G., Monlong, J., Johnson, R., Quesada, V., Djebali, S., Papasaikas, P., López-Guerra, M., Colomer, D., Royo, C., Cazorla, M., Pinyol, M., Clot, G., Aymerich, M., Rozman, M., Kulis, M., Tamborero, D., Gouin, A., Blanc, J., Gut, M., Gut, I., Puente, X. S., Pisano, D. G., Martin-Subero, J. I., López-Bigas, N., López-Guillermo, A., Valencia, A., López-Otín, C., Campo, E. and Guigó, R. (2014). Transcriptome characterization by RNA sequencing identifies a major molecular and clinical subdivision in chronic lymphocytic leukemia. *Genome Research* *24*, 212–26.
- Fiorcari, S., Brown, W. S., McIntyre, B. W., Estrov, Z., Maffei, R., O'Brien, S., Sivina, M., Hoellenriegel, J., Wierda, W. G., Keating, M. J., Ding, W., Kay, N. E., Lannutti, B. J., Marasca, R. and Burger, J. A. (2013). The PI3-kinase delta inhibitor idelalisib (GS-1101) targets integrin-mediated adhesion of chronic lymphocytic leukemia (CLL) cell to endothelial and marrow stromal cells. *PLoS ONE* *8*, 1–13.
- Friedman, A. a., Letai, A., Fisher, D. E. and Flaherty, K. T. (2015). Precision medicine for cancer with next-generation functional diagnostics. *Nature Reviews Cancer* *15*, 747–756.
- Furman, R. R., Sharman, J. P., Coutre, S. E., Cheson, B. D., Pagel, J. M., Hillmen, P., Barrientos, J. C., Zelenetz, A. D., Kipps, T. J., Flinn, I., Ghia, P., Eradat, H., Ervin, T., Lamanna, N., Coiffier, B., Pettitt, A. R., Ma, S., Stilgenbauer, S., Cramer, P., Aiello, M., Johnson, D. M., Miller, L. L., Li, D., Jahn, T. M., Dansey, R. D., Hallek, M. and O'Brien, S. M. (2014). Idelalisib and rituximab in relapsed chronic lymphocytic leukemia. *The New England Journal of Medicine* *370*, 997–1007.
- Gaidano, G. and Rossi, D. (2017). The mutational landscape of chronic lymphocytic leukemia and its impact on prognosis and treatment. *Hematology* *2017*, 329–337.

- Garnett, M. J., Edelman, E. J., Heidorn, S. J., Greenman, C. D., Dastur, A., Lau, K. W., Greninger, P., Thompson, I. R., Luo, X., Soares, J., Liu, Q., Iorio, F., Surdez, D., Chen, L., Milano, R. J., Bignell, G. R., Tam, A. T., Davies, H., Stevenson, J. A., Barthorpe, S., Lutz, S. R., Kogera, F., Lawrence, K., McLaren-Douglas, A., Mitropoulos, X., Mironenko, T., Thi, H., Richardson, L., Zhou, W., Jewitt, F., Zhang, T., O'Brien, P., Boisvert, J. L., Price, S., Hur, W., Yang, W., Deng, X., Butler, A., Choi, H. G., Chang, J. W., Baselga, J., Stamenkovic, I., Engelman, J. A., Sharma, S. V., Delattre, O., Saez-Rodriguez, J., Gray, N. S., Settleman, J., Futreal, P. A., Haber, D. A., Stratton, M. R., Ramaswamy, S., McDermott, U. and Benes, C. H. (2012). Systematic identification of genomic markers of drug sensitivity in cancer cells. *Nature* *483*, 570–5.
- Gohil, S. H. and Wu, C. J. (2019). Dissecting CLL through high-dimensional single-cell technologies. *Blood* *133*, 1446–1456.
- Goodspeed, A., Heiser, L. M., Gray, J. W. and Costello, J. C. (2016). Tumor-Derived Cell Lines as Molecular Models of Cancer Pharmacogenomics. *Molecular Cancer Research : MCR* *14*, 3–13.
- Guo, A., Lu, P., Coffey, G., Conley, P., Pandey, A. and Wang, Y. L. (2017). Dual SYK/JAK inhibition overcomes ibrutinib resistance in chronic lymphocytic leukemia: Cerdulatinib, but not ibrutinib, induces apoptosis of tumor cells protected by the microenvironment. *Oncotarget* *8*, 12953–12967.
- Gupta, S. V., Hertlein, E., Lu, Y., Sass, E. J., Lapalombella, R., Chen, T. L., Davis, M. E., Woyach, J. A., Lehman, A., Jarjoura, D., Byrd, J. C. and Lucas, D. M. (2013). The Proteasome Inhibitor Carfilzomib Functions Independently of p53 to Induce Cytotoxicity and an Atypical NF- B Response in Chronic Lymphocytic Leukemia Cells. *Clinical Cancer Research* *19*, 2406–2419.
- Hallek, M. (2017). Chronic lymphocytic leukemia: 2017 update on diagnosis, risk stratification, and treatment. *American Journal of Hematology* *92*, 946–965.
- Hamblin, T. J., Davis, Z., Gardiner, A., Oscier, D. G. and Stevenson, F. K. (1999). Unmutated Ig V(H) genes are associated with a more aggressive form of chronic lymphocytic leukemia. *Blood* *94*, 1848–54.
- Harrell Jr, F. E., with contributions from Charles Dupont and many others. (2020). Hmisc: Harrell Miscellaneous. R package version 4.3-1.
- He, L., Kuleskiy, E., Saarela, J., Turunen, L., Wennerberg, K., Aittokallio, T. and Tang, J. (2018). Methods for High-throughput Drug Combination Screening and Synergy Scoring. *Methods in Molecular Biology (Clifton, N.J.)* *1711*, 351–398.
- Herbst, S. A., Kim, V., Schitter, E., Roider, T., Bruch, P., Kolb, C., Knoll, M., Lu, J., Hüllelin, J., von Kalle, C., Lutz, C., Dreger, P., Müller-Tidow, C., Zenz, T., Huber, W. and Dietrich, S. (2020a). The Influence of the Bone Marrow Niche on Drug Response Phenotypes of Blood Cancers. *Manuscript in preparation*.

- Herbst, S. A., Stolarczyk, M., Becirovic, T., Liu, Y., Kolb, C., Herling, M., Müller-Tidow, C. and Dietrich, S. (2020b). Bone marrow stroma cells massively phagocytose apoptotic cells which leads to misinterpretation of co-culture experiments. *Manuscript submitted for publication*.
- Herbst, S. A., Vesterlund, M., Jafari, R., Siavelis, I., Stahl, M., Schitter, E., Iskar, M., Liebers, N., Roider, T., Bruch, P.-M., Lu, J., Richter, S., Knoll, M., Kolb, C., Lenze, A., Cao, X., Scheinost, S., Ganzinger, M., Kriegsmann, K., Kriegsmann, M., Müller-Tidow, C., Dreger, P., Anders, S., Zapatka, M., Stilgenbauer, S., Zenz, T., Huber, W., Tausch, E., Lehtiö, J. and Dietrich, S. (2020c). Proteogenomic subtyping of chronic lymphocytic leukemia identifies a poor outcome population with a distinct drug response profile. *Manuscript submitted for publication*.
- Herishanu, Y., Pérez-Galán, P., Liu, D., Biancotto, A., Pittaluga, S., Vire, B., Gibellini, F., Njuguna, N., Lee, E., Stennett, L., Raghavachari, N., Liu, P., McCoy, J. P., Raffeld, M., Stetler-Stevenson, M., Yuan, C., Sherry, R., Arthur, D. C., Maric, I., White, T., Marti, G. E., Munson, P., Wilson, W. H. and Wiestner, A. (2011). The lymph node microenvironment promotes B-cell receptor signaling, NF-kappaB activation, and tumor proliferation in chronic lymphocytic leukemia. *Blood* *117*, 563–74.
- Herndon, T. M., Chen, S.-S., Saba, N. S., Valdez, J., Emson, C., Gatmaitan, M., Tian, X., Hughes, T. E., Sun, C., Arthur, D. C., Stetler-Stevenson, M., Yuan, C. M., Niemann, C. U., Marti, G. E., Aue, G., Soto, S., Farooqui, M. Z. H., Herman, S. E. M., Chiorazzi, N. and Wiestner, A. (2017). Direct in vivo evidence for increased proliferation of CLL cells in lymph nodes compared to bone marrow and peripheral blood. *Leukemia* *31*, 1340–1347.
- Hothorn, T. (2017). *maxstat: Maximally Selected Rank Statistics*. R package version 0.7-25.
- Hughes, C. S., Foehr, S., Garfield, D. A., Furlong, E. E., Steinmetz, L. M. and Krijgsveld, J. (2014). Ultrasensitive proteome analysis using paramagnetic bead technology. *Molecular Systems Biology* *10*, 757.
- Inoue, D., Chew, G.-l., Liu, B., Michel, B. C., Pangallo, J., D’Avino, A. R., Hitchman, T., North, K., Lee, S. C.-w., Bitner, L., Block, A., Moore, A. R., Yoshimi, A., Escobar-Hoyos, L., Cho, H., Penson, A., Lu, S. X., Taylor, J., Chen, Y., Kadoch, C., Abdel-Wahab, O. and Bradley, R. K. (2019). Spliceosomal disruption of the non-canonical BAF complex in cancer. *Nature* *574*, 432–436.
- Iorio, F., Knijnenburg, T. A., Vis, D. J., Bignell, G. R., Menden, M. P., Schubert, M., Aben, N., Gonçalves, E., Barthorpe, S., Lightfoot, H., Cokelaer, T., Greninger, P., van Dyk, E., Chang, H., de Silva, H., Heyn, H., Deng, X., Egan, R. K., Liu, Q., Mironenko, T., Mitropoulos, X., Richardson, L., Wang, J., Zhang, T., Moran, S., Sayols, S., Soleimani, M., Tamborero, D., Lopez-Bigas, N., Ross-Macdonald, P., Esteller, M., Gray, N. S., Haber, D. A., Stratton, M. R., Benes, C. H., Wessels, L. F. A., Saez-Rodriguez, J., McDermott, U. and Garnett, M. J. (2016). A Landscape of Pharmacogenomic Interactions in Cancer. *Cell* *166*, 740–754.
- Jethwa, A., Słabicki, M., Hüllelein, J., Jentzsch, M., Dalal, V., Rabe, S., Wagner, L., Walther, T., Klapper, W., Bohnenberger, H., Rettel, M., Lu, J., Smits, A. H., Stein, F., Savitski, M. M.,

- Huber, W., Aylon, Y., Oren, M. and Zenz, T. (2018). TRRAP is essential for regulating the accumulation of mutant and wild-type p53 in lymphoma. *Blood* *131*, blood-2017-09-806679.
- Johansson, H. J., Socciarelli, F., Vacanti, N. M., Haugen, M. H., Zhu, Y., Siavelis, I., Fernandez-Woodbridge, A., Aure, M. R., Sennblad, B., Vesterlund, M., Branca, R. M., Orre, L. M., Huss, M., Fredlund, E., Beraki, E., Garred, Ø., Boekel, J., Sauer, T., Zhao, W., Nord, S., Högländer, E. K., Jans, D. C., Brismar, H., Haukaas, T. H., Bathen, T. F., Schlichting, E., Naume, B., Consortia Oslo Breast Cancer Research Consortium (OSBREAC), Luders, T., Borgen, E., Kristensen, V. N., Russnes, H. G., Lingjærde, O. C., Mills, G. B., Sahlberg, K. K., Børresen-Dale, A.-L. and Lehtiö, J. (2019). Breast cancer quantitative proteome and proteogenomic landscape. *Nature Communications* *10*, 1600.
- Johnson, I. (2010). *Molecular Probes Handbook: A Guide to Fluorescent Probes and Labeling Technologies*. Life Technologies Corporation.
- Johnston, H. E., Carter, M. J., Larrayoz, M., Clarke, J., Garbis, S. D., Oscier, D., Strefford, J. C., Steele, A. J., Walewska, R. and Cragg, M. S. (2018). Proteomics Profiling of CLL Versus Healthy B-cells Identifies Putative Therapeutic Targets and a Subtype-independent Signature of Spliceosome Dysregulation. *Molecular & Cellular Proteomics : MCP* *17*, 776–791.
- Kanehisa, M., Sato, Y., Furumichi, M., Morishima, K. and Tanabe, M. (2019). New approach for understanding genome variations in KEGG. *Nucleic Acids Research* *47*, D590–D595.
- Kassambara, A., Kosinski, M. and Biecek, P. (2019). survminer: Drawing Survival Curves using 'ggplot2'. R package version 0.4.6.
- Kawano, Y., Kobune, M., Yamaguchi, M., Nakamura, K., Ito, Y., Sasaki, K., Takahashi, S., Nakamura, T., Chiba, H., Sato, T., Matsunaga, T., Azuma, H., Ikebuchi, K., Ikeda, H., Kato, J., Niitsu, Y. and Hamada, H. (2003). Ex vivo expansion of human umbilical cord hematopoietic progenitor cells using a coculture system with human telomerase catalytic subunit (hTERT)-transfected human stromal cells. *Blood* *101*, 532–40.
- Kay, N. E., Shanafelt, T. D., Strege, A. K., Lee, Y. K., Bone, N. D. and Raza, A. (2007). Bone biopsy derived marrow stromal elements rescue chronic lymphocytic leukemia B-cells from spontaneous and drug induced cell death and facilitates an "angiogenic switch". *Leukemia Research* *31*, 899–906.
- Kipps, T. J., Stevenson, F. K., Wu, C. J., Croce, C. M., Packham, G., Wierda, W. G., O'Brien, S., Gribben, J. and Rai, K. (2017). Chronic lymphocytic leukaemia. *Nature Reviews Disease Primers* *3*, 16096.
- Klein, U., Lia, M., Crespo, M., Siegel, R., Shen, Q., Mo, T., Ambesi-Impiombato, A., Califano, A., Migliazza, A., Bhagat, G. and Dalla-Favera, R. (2010). The DLEU2/miR-15a/16-1 cluster controls B cell proliferation and its deletion leads to chronic lymphocytic leukemia. *Cancer Cell* *17*, 28–40.
- Klein, U., Tu, Y., Stolovitzky, G. A., Mattioli, M., Cattoretti, G., Husson, H., Freedman, A., Inghirami, G., Cro, L., Baldini, L., Neri, A., Califano, A. and Dalla-Favera, R. (2001). Gene

- expression profiling of B cell chronic lymphocytic leukemia reveals a homogeneous phenotype related to memory B cells. *The Journal of Experimental Medicine* *194*, 1625–38.
- Koboldt, D. C., Zhang, Q., Larson, D. E., Shen, D., McLellan, M. D., Lin, L., Miller, C. A., Mardis, E. R., Ding, L. and Wilson, R. K. (2012). VarScan 2: somatic mutation and copy number alteration discovery in cancer by exome sequencing. *Genome Research* *22*, 568–76.
- Kolde, R. (2019). pheatmap: Pretty Heatmaps. R package version 1.0.12.
- Kraus, M., Alimzhanov, M. B., Rajewsky, N. and Rajewsky, K. (2004). Survival of resting mature B lymphocytes depends on BCR signaling via the Igalphabeta heterodimer. *Cell* *117*, 787–800.
- Krijthe, J. H. (2015). Rtsne: T-Distributed Stochastic Neighbor Embedding using Barnes-Hut Implementation. R package version 0.15.
- Kurtova, A. V., Balakrishnan, K., Chen, R., Ding, W., Schnabl, S., Quiroga, M. P., Sivina, M., Wierda, W. G., Estrov, Z., Keating, M. J., Shehata, M., Jäger, U., Gandhi, V., Kay, N. E., Plunkett, W. and Burger, J. A. (2009). Diverse marrow stromal cells protect CLL cells from spontaneous and drug-induced apoptosis: Development of a reliable and reproducible system to assess stromal cell adhesion-mediated drug resistance. *Blood* *114*, 4441–4450.
- Lagneaux, L., Delforge, A., Bron, D., De Bruyn, C. and Stryckmans, P. (1998). Chronic lymphocytic leukemic B cells but not normal B cells are rescued from apoptosis by contact with normal bone marrow stromal cells. *Blood* *91*, 2387–96.
- Lakens, D. (2017). Equivalence Tests: A Practical Primer for t Tests, Correlations, and Meta-Analyses. *Social Psychological and Personality Science* *8*, 355–362.
- Lam, K.-P., Kühn, R. and Rajewsky, K. (1997). In Vivo Ablation of Surface Immunoglobulin on Mature B Cells by Inducible Gene Targeting Results in Rapid Cell Death. *Cell* *90*, 1073–1083.
- Landau, D. A., Tausch, E., Taylor-Weiner, A. N., Stewart, C., Reiter, J. G., Bahlo, J., Kluth, S., Bozic, I., Lawrence, M., Böttcher, S., Carter, S. L., Cibulskis, K., Mertens, D., Sougnez, C. L., Rosenberg, M., Hess, J. M., Edelman, J., Kless, S., Kneba, M., Ritgen, M., Fink, A., Fischer, K., Gabriel, S., Lander, E. S., Nowak, M. A., Döhner, H., Hallek, M., Neuberg, D., Getz, G., Stilgenbauer, S. and Wu, C. J. (2015). Mutations driving CLL and their evolution in progression and relapse. *Nature* *526*, 525–30.
- Landrum, M. J., Lee, J. M., Benson, M., Brown, G. R., Chao, C., Chitipiralla, S., Gu, B., Hart, J., Hoffman, D., Jang, W., Karapetyan, K., Katz, K., Liu, C., Maddipatla, Z., Malheiro, A., McDaniel, K., Ovetsky, M., Riley, G., Zhou, G., Holmes, J. B., Kattman, B. L. and Maglott, D. R. (2018). ClinVar: improving access to variant interpretations and supporting evidence. *Nucleic Acids Research* *46*, D1062–D1067.
- Lanham, S., Hamblin, T., Oscier, D., Ibbotson, R., Stevenson, F. and Packham, G. (2003). Differential signaling via surface IgM is associated with VH gene mutational status and CD38 expression in chronic lymphocytic leukemia. *Blood* *101*, 1087–93.

- Letai, A. (2017). Functional precision cancer medicine-moving beyond pure genomics. *Nature Medicine* *23*, 1028–1035.
- Li, H. (2011). A statistical framework for SNP calling, mutation discovery, association mapping and population genetical parameter estimation from sequencing data. *Bioinformatics (Oxford, England)* *27*, 2987–93.
- Liberzon, A., Subramanian, A., Pinchback, R., Thorvaldsdóttir, H., Tamayo, P. and Mesirov, J. P. (2011). Molecular signatures database (MSigDB) 3.0. *Bioinformatics (Oxford, England)* *27*, 1739–40.
- Loayza, D. and De Lange, T. (2003). POT1 as a terminal transducer of TRF1 telomere length control. *Nature* *423*, 1013–8.
- Love, M. I., Huber, W. and Anders, S. (2014). Moderated estimation of fold change and dispersion for RNA-seq data with DESeq2. *Genome Biology* *15*, 550.
- Lovejoy, C. A., Lock, K., Yenamandra, A. and Cortez, D. (2006). DDB1 maintains genome integrity through regulation of Cdt1. *Molecular and Cellular Biology* *26*, 7977–90.
- Lukinavičius, G., Blaukopf, C., Pershagen, E., Schena, A., Reymond, L., Derivery, E., Gonzalez-Gaitan, M., D’Este, E., Hell, S. W., Wolfram Gerlich, D. and Johnsson, K. (2015). SiR-Hoechst is a far-red DNA stain for live-cell nanoscopy. *Nature Communications* *6*, 8497.
- Mattiazzi Usaj, M., Styles, E. B., Verster, A. J., Friesen, H., Boone, C. and Andrews, B. J. (2016). High-Content Screening for Quantitative Cell Biology. *Trends in Cell Biology* *26*, 598–611.
- Mayer, R. L., Schwarzmeier, J. D., Gerner, M. C., Bileck, A., Mader, J. C., Meier-Menches, S. M., Gerner, S. M., Schmetterer, K. G., Pukrop, T., Reichle, A., Slany, A. and Gerner, C. (2018). Proteomics and metabolomics identify molecular mechanisms of aging potentially predisposing for chronic lymphocytic leukemia. *Molecular & Cellular Proteomics : MCP* *17*, 290–303.
- Mertins, P., Mani, D. R., Ruggles, K. V., Gillette, M. A., Clauser, K. R., Wang, P., Wang, X., Qiao, J. W., Cao, S., Petralia, F., Kawaler, E., Mundt, F., Krug, K., Tu, Z., Lei, J. T., Gatza, M. L., Wilkerson, M., Perou, C. M., Yellapantula, V., Huang, K.-l., Lin, C., McLellan, M. D., Yan, P., Davies, S. R., Townsend, R. R., Skates, S. J., Wang, J., Zhang, B., Kinsinger, C. R., Mesri, M., Rodriguez, H., Ding, L., Paulovich, A. G., Fenyö, D., Ellis, M. J., Carr, S. A. and NCI CPTAC (2016). Proteogenomics connects somatic mutations to signalling in breast cancer. *Nature* *534*, 55–62.
- Moggridge, S., Sorensen, P. H., Morin, G. B. and Hughes, C. S. (2018). Extending the Compatibility of the SP3 Paramagnetic Bead Processing Approach for Proteomics. *Journal of Proteome Research* *17*, 1730–1740.
- Mootha, V. K., Lindgren, C. M., Eriksson, K.-F., Subramanian, A., Sihag, S., Lehar, J., Puigserver, P., Carlsson, E., Ridderstråle, M., Laurila, E., Houstis, N., Daly, M. J., Patterson,

- N., Mesirov, J. P., Golub, T. R., Tamayo, P., Spiegelman, B., Lander, E. S., Hirschhorn, J. N., Altshuler, D. and Groop, L. C. (2003). PGC-1 $\alpha$ -responsive genes involved in oxidative phosphorylation are coordinately downregulated in human diabetes. *Nature Genetics* *34*, 267–73.
- Mraz, M., Zent, C. S., Church, A. K., Jelinek, D. F., Wu, X., Pospisilova, S., Ansell, S. M., Novak, A. J., Kay, N. E., Witzig, T. E. and Nowakowski, G. S. (2011). Bone marrow stromal cells protect lymphoma B-cells from rituximab-induced apoptosis and targeting integrin  $\alpha$ -4- $\beta$ -1 (VLA-4) with natalizumab can overcome this resistance. *British Journal of Haematology* *155*, 53–64.
- Mun, D.-G., Bhin, J., Kim, S., Kim, H., Jung, J. H., Jung, Y., Jang, Y. E., Park, J. M., Kim, H., Jung, Y., Lee, H., Bae, J., Back, S., Kim, S.-J., Kim, J., Park, H., Li, H., Hwang, K.-B., Park, Y. S., Yook, J. H., Kim, B. S., Kwon, S. Y., Ryu, S. W., Park, D. Y., Jeon, T. Y., Kim, D. H., Lee, J.-H., Han, S.-U., Song, K. S., Park, D., Park, J. W., Rodriguez, H., Kim, J., Lee, H., Kim, K. P., Yang, E. G., Kim, H. K., Paek, E., Lee, S., Lee, S.-W. and Hwang, D. (2019). Proteogenomic Characterization of Human Early-Onset Gastric Cancer. *Cancer Cell* *35*, 111–124.e10.
- Murphy, K. (2012). *Janeway’s Immunobiology*. 8 edition, Garland Science.
- Murray, P. J. (2007). The JAK-STAT Signaling Pathway: Input and Output Integration. *The Journal of Immunology* *178*, 2623–2629.
- Navrkalova, V., Sebejova, L., Zemanova, J., Kminkova, J., Kubesova, B., Malcikova, J., Mraz, M., Smardova, J., Pavlova, S., Doubek, M., Brychtova, Y., Potesil, D., Nemethova, V., Mayer, J., Pospisilova, S. and Trbusek, M. (2013). ATM mutations uniformly lead to ATM dysfunction in chronic lymphocytic leukemia: application of functional test using doxorubicin. *Haematologica* *98*, 1124–31.
- Oren, M. and Rotter, V. (2010). Mutant p53 gain-of-function in cancer. *Cold Spring Harbor Perspectives in Biology* *2*, a001107.
- Orgueira, A. M., Rodríguez, B. A., Vence, N. A., López, Á. B., Arias, J. Á. D., Varela, N. D., Pérez, M. S. G., Encinas, M. M. P. and López, J. L. B. (2019). Time to treatment prediction in chronic lymphocytic leukemia based on new transcriptional patterns. *Frontiers in Oncology* *9*, 1–8.
- Panayiotidis, P., Jones, D., Ganeshaguru, K., Foroni, L. and Hoffbrand, A. V. (1996). Human bone marrow stromal cells prevent apoptosis and support the survival of chronic lymphocytic leukaemia cells in vitro. *British Journal of Haematology* *92*, 97–103.
- Pascutti, M. F., Jak, M., Tromp, J. M., Derks, I. A. M., Remmerswaal, E. B. M., Thijssen, R., van Attekum, M. H. A., van Bochove, G. G., Luijks, D. M., Pals, S. T., van Lier, R. A. W., Kater, A. P., van Oers, M. H. J. and Eldering, E. (2013). IL-21 and CD40L signals from autologous T cells can induce antigen-independent proliferation of CLL cells. *Blood* *122*, 3010–9.

- Pau, G., Fuchs, F., Sklyar, O., Boutros, M. and Huber, W. (2010). EBImage—an R package for image processing with applications to cellular phenotypes. *Bioinformatics* *26*, 979–981.
- Pemovska, T., Kontro, M., Yadav, B., Edgren, H., Eldfors, S., Szwajda, A., Almusa, H., Bepalov, M. M., Ellonen, P., Elonen, E., Gjertsen, B. T., Karjalainen, R., Kuleskiy, E., Lagström, S., Lehto, A., Lepistö, M., Lundán, T., Majumder, M. M., Marti, J. M. L., Mattila, P., Murumägi, A., Mustjoki, S., Palva, A., Parsons, A., Pirttinen, T., Rämetsä, M. E., Suvela, M., Turunen, L., Västriik, I., Wolf, M., Knowles, J., Aittokallio, T., Heckman, C. A., Porkka, K., Kallioniemi, O. and Wennerberg, K. (2013). Individualized systems medicine strategy to tailor treatments for patients with chemorefractory acute myeloid leukemia. *Cancer Discovery* *3*, 1416–29.
- Perrot, A., Pionneau, C., Nadaud, S., Davi, F., Leblond, V., Jacob, F., Merle-Béral, H., Herbrecht, R., Béné, M.-C., Gribben, J. G., Bahram, S. and Vallat, L. (2011). A unique proteomic profile on surface IgM ligation in unmutated chronic lymphocytic leukemia. *Blood* *118*, e1–15.
- Plander, M., Ugocsai, P., Seegers, S., Orsó, E., Reichle, A., Schmitz, G., Hofstädter, F. and Brockhoff, G. (2011). Chronic lymphocytic leukemia cells induce anti-apoptotic effects of bone marrow stroma. *Annals of Hematology* *90*, 1381–90.
- Podar, K., Shah, J., Chari, A., Richardson, P. G. and Jagannath, S. (2020). Selinexor for the treatment of multiple myeloma. *Expert Opinion on Pharmacotherapy* *21*, 399–408.
- Primo, D., Scarfò, L., Xochelli, A., Mattsson, M., Ranghetti, P., Espinosa, A. B., Robles, A., Gorrochategui, J., Martínez-López, J., de la Serna, J., González, M., Gil, A. C., Anguita, E., Iraheta, S., Munugalavadla, V., Quéva, C., Tannheimer, S., Rosenquist, R., Stamatopoulos, K., Ballesteros, J. and Ghia, P. (2018). A novel ex vivo high-throughput assay reveals anti-proliferative effects of idelalisib and ibrutinib in chronic lymphocytic leukemia. *Oncotarget* *9*, 26019–26031.
- Puła, B., Gołos, A., Górnjak, P. and Jamroziak, K. (2019). Overcoming Ibrutinib Resistance in Chronic Lymphocytic Leukemia. *Cancers* *11*, 1834.
- R Core Team (2018). R: A Language and Environment for Statistical Computing. R Foundation for Statistical Computing Vienna, Austria.
- Ramos, M., Schiffer, L., Re, A., Azhar, R., Basunia, A., Cabrera, C. R., Chan, T., Chapman, P., Davis, S., Gomez-Cabrero, D., Culhane, A. C., Haibe-Kains, B., Hansen, K., Kodali, H., Louis, M. S., Mer, A. S., Reister, M., Morgan, M., Carey, V. and Waldron, L. (2017). Software For The Integration Of Multi-Omics Experiments In Bioconductor. *Cancer Research* *77(21)*; e39-42.
- Ritchie, M. E., Phipson, B., Wu, D., Hu, Y., Law, C. W., Shi, W. and Smyth, G. K. (2015). limma powers differential expression analyses for RNA-sequencing and microarray studies. *Nucleic Acids Research* *43*, e47.
- Roberts, A. W., Davids, M. S., Pagel, J. M., Kahl, B. S., Puvvada, S. D., Gerecitano, J. F., Kipps, T. J., Anderson, M. A., Brown, J. R., Gressick, L., Wong, S., Dunbar, M., Zhu, M.,

- Desai, M. B., Cerri, E., Heitner Enschede, S., Humerickhouse, R. A., Wierda, W. G. and Seymour, J. F. (2016). Targeting BCL2 with Venetoclax in Relapsed Chronic Lymphocytic Leukemia. *The New England Journal of Medicine* *374*, 311–22.
- Roecklein, B. A. and Torok-Storb, B. (1995). Functionally distinct human marrow stromal cell lines immortalized by transduction with the human papilloma virus E6/E7 genes. *Blood* *85*, 997–1005.
- Roider, T., Seufert, J., Uvarovskii, A., Frauhammer, F., Bordas, M., Abedpour, N., Stolarczyk, M., Mallm, J.-P., Herbst, S. A., Bruch, P.-M., Balke-Want, H., Hundemer, M., Rippe, K., Goepfert, B., Seiffert, M., Brors, B., Mechtersheimer, G., Zenz, T., Peifer, M., Chapuy, B., Schlesner, M., Müller-Tidow, C., Fröhling, S., Huber, W., Anders, S. and Dietrich, S. (2020). Dissecting intratumour heterogeneity of nodal B-cell lymphomas at the transcriptional, genetic and drug-response levels. *Nature Cell Biology* *22*, 896–906.
- Roy, A., Krzykwa, E., Lemieux, R. and Néron, S. (2001). Increased efficiency of gamma-irradiated versus mitomycin C-treated feeder cells for the expansion of normal human cells in long-term cultures. *Journal of Hematotherapy & Stem Cell Research* *10*, 873–80.
- RStudio Team (2016). RStudio: Integrated Development Environment for R. RStudio, Inc. Boston, MA.
- Scheffold, A. and Stilgenbauer, S. (2020). Revolution of Chronic Lymphocytic Leukemia Therapy: the Chemo-Free Treatment Paradigm. *Current Oncology Reports* *22*, 16.
- Severin, F., Frezzato, F., Visentin, A., Martini, V., Trimarco, V., Carraro, S., Tibaldi, E., Brunati, A. M., Piazza, F., Semenzato, G., Facco, M. and Trentin, L. (2019). In Chronic Lymphocytic Leukemia the JAK2/STAT3 Pathway Is Constitutively Activated and Its Inhibition Leads to CLL Cell Death Unaffected by the Protective Bone Marrow Microenvironment. *Cancers* *11*, 1–16.
- Seymour, J. F., Kipps, T. J., Eichhorst, B., Hillmen, P., D’Rozario, J., Assouline, S., Owen, C., Gerecitano, J., Robak, T., De la Serna, J., Jaeger, U., Cartron, G., Montillo, M., Humerickhouse, R., Punnoose, E. A., Li, Y., Boyer, M., Humphrey, K., Mobasher, M. and Kater, A. P. (2018). Venetoclax-Rituximab in Relapsed or Refractory Chronic Lymphocytic Leukemia. *The New England Journal of Medicine* *378*, 1107–1120.
- Shaffer, A. L. and Schlissel, M. S. (1997). A truncated heavy chain protein relieves the requirement for surrogate light chains in early B cell development. *Journal of Immunology (Baltimore, Md. : 1950)* *159*, 1265–75.
- Sinha, A., Huang, V., Livingstone, J., Wang, J., Fox, N. S., Kurganovs, N., Ignatchenko, V., Fritsch, K., Donmez, N., Heisler, L. E., Shiah, Y.-J., Yao, C. Q., Alfaro, J. A., Volik, S., Lapuk, A., Fraser, M., Kron, K., Murison, A., Lupien, M., Sahinalp, C., Collins, C. C., Tetu, B., Masoomian, M., Berman, D. M., van der Kwast, T., Bristow, R. G., Kislinger, T. and Boutros, P. C. (2019). The Proteogenomic Landscape of Curable Prostate Cancer. *Cancer Cell* *35*, 414–427.e6.

- Snijder, B., Vladimer, G. I., Krall, N., Miura, K., Schmolke, A.-S., Kornauth, C., Lopez de la Fuente, O., Choi, H.-S., van der Kouwe, E., Gültekin, S., Kazianka, L., Bigenzahn, J. W., Hoermann, G., Prutsch, N., Merkel, O., Ringler, A., Sabler, M., Jeryczynski, G., Mayerhoefer, M. E., Simonitsch-Klupp, I., Ocko, K., Felberbauer, F., Müllauer, L., Prager, G. W., Korkmaz, B., Kenner, L., Sperr, W. R., Kralovics, R., Gisslinger, H., Valent, P., Kubicek, S., Jäger, U., Staber, P. B. and Superti-Furga, G. (2017). Image-based ex-vivo drug screening for patients with aggressive haematological malignancies: interim results from a single-arm, open-label, pilot study. *The Lancet Haematology* 4, e595–e606.
- Spaner, D. E., McCaw, L., Wang, G., Tsui, H. and Shi, Y. (2019). Persistent janus kinase-signaling in chronic lymphocytic leukemia patients on ibrutinib: Results of a phase I trial. *Cancer Medicine* 8, 1540–1550.
- Spaner, D. E., Wang, G., McCaw, L., Li, Y., Disperati, P., Cussen, M.-A. and Shi, Y. (2016). Activity of the Janus kinase inhibitor ruxolitinib in chronic lymphocytic leukemia: results of a phase II trial. *Haematologica* 101, e192–5.
- Srinivasan, L., Sasaki, Y., Calado, D. P., Zhang, B., Paik, J. H., DePinho, R. A., Kutok, J. L., Kearney, J. F., Otipoby, K. L. and Rajewsky, K. (2009). PI3 kinase signals BCR-dependent mature B cell survival. *Cell* 139, 573–86.
- Sterne-Weiler, T., Weatheritt, R. J., Best, A. J., Ha, K. C. H. and Blencowe, B. J. (2018). Efficient and Accurate Quantitative Profiling of Alternative Splicing Patterns of Any Complexity on a Laptop. *Molecular Cell* 72, 187–200.e6.
- Subramanian, A., Tamayo, P., Mootha, V. K., Mukherjee, S., Ebert, B. L., Gillette, M. A., Paulovich, A., Pomeroy, S. L., Golub, T. R., Lander, E. S. and Mesirov, J. P. (2005). Gene set enrichment analysis: a knowledge-based approach for interpreting genome-wide expression profiles. *Proceedings of the National Academy of Sciences of the United States of America* 102, 15545–50.
- Szankasi, P. and Bahler, D. W. (2010). Clinical laboratory analysis of immunoglobulin heavy chain variable region genes for chronic lymphocytic leukemia prognosis. *The Journal of Molecular Diagnostics : JMD* 12, 244–9.
- Tate, J. G., Bamford, S., Jubb, H. C., Sondka, Z., Beare, D. M., Bindal, N., Boutselakis, H., Cole, C. G., Creatore, C., Dawson, E., Fish, P., Harsha, B., Hathaway, C., Jupe, S. C., Kok, C. Y., Noble, K., Ponting, L., Ramshaw, C. C., Rye, C. E., Speedy, H. E., Stefancsik, R., Thompson, S. L., Wang, S., Ward, S., Campbell, P. J. and Forbes, S. A. (2019). COSMIC: the Catalogue Of Somatic Mutations In Cancer. *Nucleic Acids Research* 47, D941–D947.
- Ten Hacken, E. and Burger, J. A. (2016). Microenvironment interactions and B-cell receptor signaling in Chronic Lymphocytic Leukemia: Implications for disease pathogenesis and treatment. *Biochimica et Biophysica Acta* 1863, 401–13.
- Therneau, T. M. (2020). A Package for Survival Analysis in R. R package version 3.1-11.

- Tyner, J. W., Yang, W. F., Bankhead, A., Fan, G., Fletcher, L. B., Bryant, J., Glover, J. M., Chang, B. H., Spurgeon, S. E., Fleming, W. H., Kovacsovics, T., Gotlib, J. R., Oh, S. T., Deininger, M. W., Zwaan, C. M., Den Boer, M. L., Van Den Heuvel-Eibrink, M. M., O'Hare, T., Druker, B. J. and Loriaux, M. M. (2013). Kinase pathway dependence in primary human leukemias determined by rapid inhibitor screening. *Cancer Research* *73*, 285–296.
- Vangapandu, H. V., Chen, H., Wierda, W. G., Keating, M. J., Korkut, A. and Gandhi, V. (2018). Proteomics profiling identifies induction of caveolin-1 in chronic lymphocytic leukemia cells by bone marrow stromal cells. *Leukemia & Lymphoma* *59*, 1427–1438.
- Vasaikar, S., Huang, C., Wang, X., Petyuk, V. A., Savage, S. R., Wen, B., Dou, Y., Zhang, Y., Shi, Z., Arshad, O. A., Gritsenko, M. A., Zimmerman, L. J., McDermott, J. E., Clauss, T. R., Moore, R. J., Zhao, R., Monroe, M. E., Wang, Y.-T., Chambers, M. C., Slebos, R. J. C., Lau, K. S., Mo, Q., Ding, L., Ellis, M., Thiagarajan, M., Kinsinger, C. R., Rodriguez, H., Smith, R. D., Rodland, K. D., Liebler, D. C., Liu, T., Zhang, B. and Clinical Proteomic Tumor Analysis Consortium (2019). Proteogenomic Analysis of Human Colon Cancer Reveals New Therapeutic Opportunities. *Cell* *177*, 1035–1049.e19.
- Vorobjev, I. A. and Barteneva, N. S. (2017). Multi-parametric imaging of cell heterogeneity in apoptosis analysis. *Methods* *112*, 105–123.
- Wakasugi, M., Shimizu, M., Morioka, H., Linn, S., Nikaido, O. and Matsunaga, T. (2001). Damaged DNA-binding protein DDB stimulates the excision of cyclobutane pyrimidine dimers in vitro in concert with XPA and replication protein A. *The Journal of Biological Chemistry* *276*, 15434–40.
- Wan, Y. and Wu, C. J. (2013). SF3B1 mutations in chronic lymphocytic leukemia. *Blood* *121*, 4627–4634.
- Wang, L., Brooks, A. N., Fan, J., Wan, Y., Gambe, R., Li, S., Hergert, S., Yin, S., Freeman, S. S., Levin, J. Z., Fan, L., Seiler, M., Buonamici, S., Smith, P. G., Chau, K. F., Cibulskis, C. L., Zhang, W., Rassenti, L. Z., Ghia, E. M., Kipps, T. J., Fernandes, S., Bloch, D. B., Kotliar, D., Landau, D. A., Shukla, S. A., Aster, J. C., Reed, R., DeLuca, D. S., Brown, J. R., Neuberg, D., Getz, G., Livak, K. J., Meyerson, M. M., Kharchenko, P. V. and Wu, C. J. (2016). Transcriptomic Characterization of SF3B1 Mutation Reveals Its Pleiotropic Effects in Chronic Lymphocytic Leukemia. *Cancer Cell* *30*, 750–763.
- Wang, L., Fan, J., Francis, J. M., Georghiou, G., Hergert, S., Li, S., Gambe, R., Zhou, C. W., Yang, C., Xiao, S., Cin, P. D., Bowden, M., Kotliar, D., Shukla, S. A., Brown, J. R., Neuberg, D., Alessi, D. R., Zhang, C.-Z., Kharchenko, P. V., Livak, K. J. and Wu, C. J. (2017). Integrated single-cell genetic and transcriptional analysis suggests novel drivers of chronic lymphocytic leukemia. *Genome Research* *27*, 1300–1311.
- Wickham, H., Averick, M., Bryan, J., Chang, W., McGowan, L. D., François, R., Grolemond, G., Hayes, A., Henry, L., Hester, J., Kuhn, M., Pedersen, T. L., Miller, E., Bache, S. M., Müller, K., Ooms, J., Robinson, D., Seidel, D. P., Spinu, V., Takahashi, K., Vaughan, D.,

- Wilke, C., Woo, K. and Yutani, H. (2019). Welcome to the tidyverse. *Journal of Open Source Software* *4*, 1686.
- Wilkerson, D., M., Hayes and Neil, D. (2010). ConsensusClusterPlus: a class discovery tool with confidence assessments and item tracking. *Bioinformatics* *26*, 1572–1573.
- Wood, K., Hannah, R. and Moravec, R. A. (2006). Method for detection of ATP. US Patent *US7083911B*.
- Woyach, J. A. and Johnson, A. J. (2015). Targeted therapies in CLL: Mechanisms of resistance and strategies for management. *Blood* *126*, 471–477.
- Yang, M., Vesterlund, M., Siavelis, I., Moura-Castro, L. H., Castor, A., Fioretos, T., Jafari, R., Lilljebjörn, H., Odom, D. T., Olsson, L., Ravi, N., Woodward, E. L., Harewood, L., Lehtiö, J. and Paulsson, K. (2019). Proteogenomics and Hi-C reveal transcriptional dysregulation in high hyperdiploid childhood acute lymphoblastic leukemia. *Nature Communications* *10*, 1519.
- Zenz, T., Eichhorst, B., Busch, R., Denzel, T., Häbe, S., Winkler, D., Bühler, A., Edelmann, J., Bergmann, M., Hopfinger, G., Hensel, M., Hallek, M., Döhner, H. and Stilgenbauer, S. (2010). TP53 Mutation and Survival in Chronic Lymphocytic Leukemia. *Journal of Clinical Oncology* *28*, 4473–4479.
- Zhang, B., Wang, J., Wang, X., Zhu, J., Liu, Q., Shi, Z., Chambers, M. C., Zimmerman, L. J., Shaddox, K. F., Kim, S., Davies, S. R., Wang, S., Wang, P., Kinsinger, C. R., Rivers, R. C., Rodriguez, H., Townsend, R. R., Ellis, M. J. C., Carr, S. A., Tabb, D. L., Coffey, R. J., Slebos, R. J. C., Liebler, D. C. and NCI CPTAC (2014). Proteogenomic characterization of human colon and rectal cancer. *Nature* *513*, 382–7.
- Zhang, H., Liu, T., Zhang, Z., Payne, S. H., Zhang, B., McDermott, J. E., Zhou, J.-Y., Petyuk, V. A., Chen, L., Ray, D., Sun, S., Yang, F., Chen, L., Wang, J., Shah, P., Cha, S. W., Aiyetan, P., Woo, S., Tian, Y., Gritsenko, M. A., Clauss, T. R., Choi, C., Monroe, M. E., Thomas, S., Nie, S., Wu, C., Moore, R. J., Yu, K.-H., Tabb, D. L., Fenyö, D., Bafna, V., Wang, Y., Rodriguez, H., Boja, E. S., Hiltke, T., Rivers, R. C., Sokoll, L., Zhu, H., Shih, I.-M., Cope, L., Pandey, A., Zhang, B., Snyder, M. P., Levine, D. A., Smith, R. D., Chan, D. W., Rodland, K. D. and CPTAC Investigators (2016). Integrated Proteogenomic Characterization of Human High-Grade Serous Ovarian Cancer. *Cell* *166*, 755–765.
- Zhang, W., Trachootham, D., Liu, J., Chen, G., Pelicano, H., Garcia-Prieto, C., Lu, W., Burger, J. A., Croce, C. M., Plunkett, W., Keating, M. J. and Huang, P. (2012). Stromal control of cystine metabolism promotes cancer cell survival in chronic lymphocytic leukaemia. *Nature Cell Biology* *14*, 276–286.
- Zhao, Z., Goldin, L., Liu, S., Wu, L., Zhou, W., Lou, H., Yu, Q., Tsang, S. X., Jiang, M., Li, F., McMaster, M., Li, Y., Lin, X., Wang, Z., Xu, L., Marti, G., Li, G., Wu, K., Yeager, M., Yang, H., Xu, X., Chanock, S. J., Li, B., Hou, Y., Caporaso, N. and Dean, M. (2016). Evolution

of multiple cell clones over a 29-year period of a CLL patient. *Nature Communications* 7, 13765.

Zhu, Y. (2019). DEqMS: a tool to perform statistical analysis of differential protein expression for quantitative proteomics data. R package version 1.0.1.

## Supplementary Figures

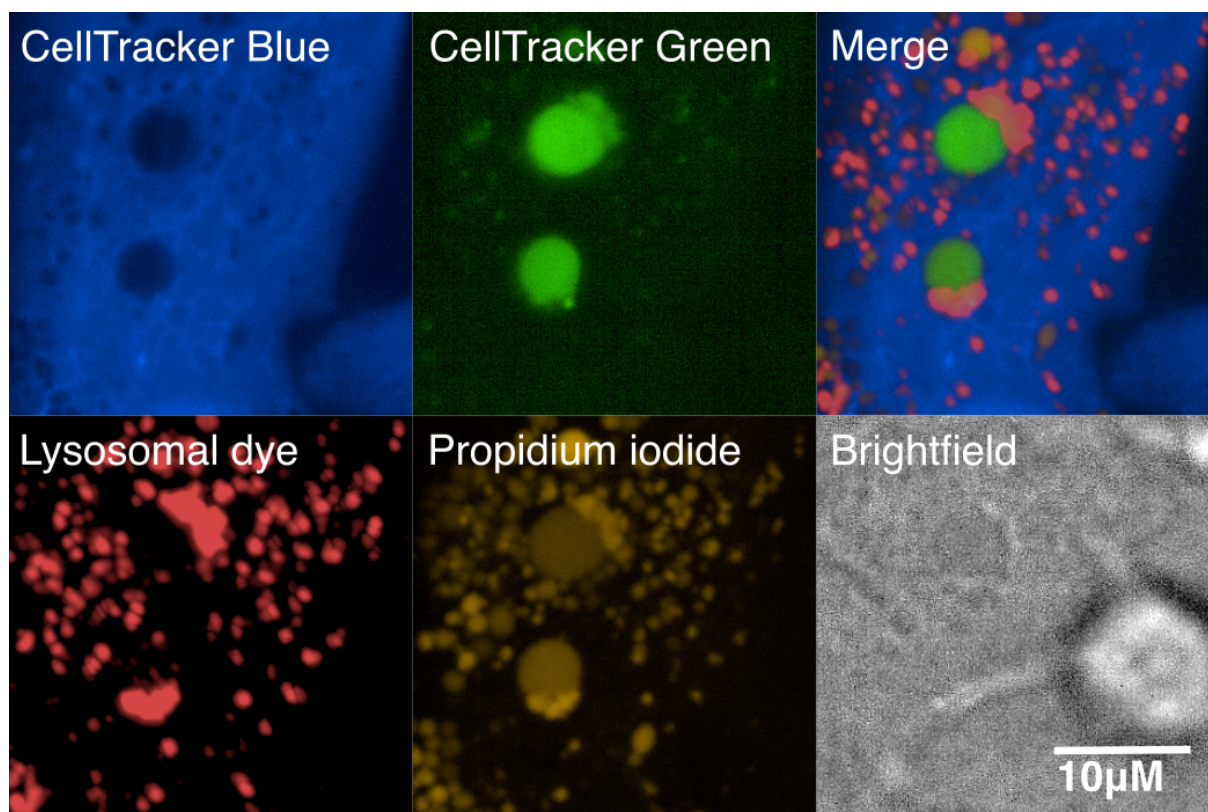


Figure S1: **Enlargement of two phagosomes.** Confocal microscopy images of co-cultures of CellTracker Blue labelled NKTert and CellTracker Green labelled CLL cells, previously treated with 63 nM venetoclax and stained with propidium iodide and lysosomal dye NIR. (Herbst et al., 2020b)

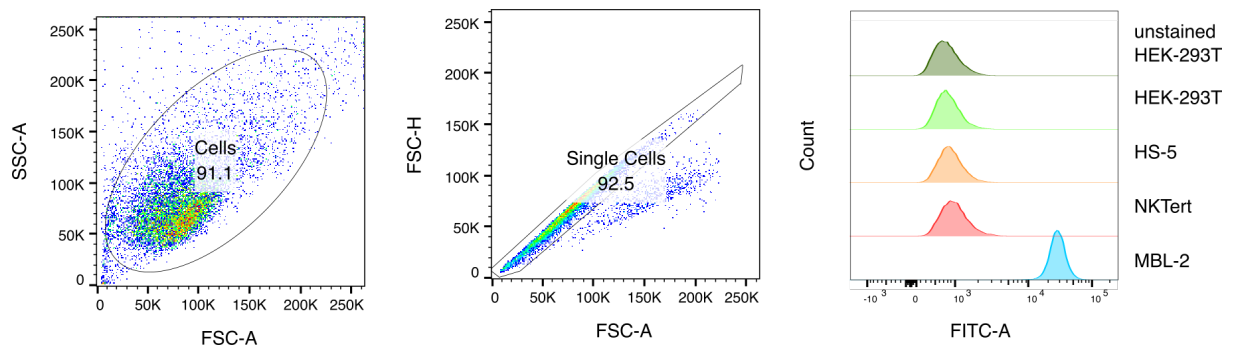


Figure S2: **CD45 flow cytometry of NK Tert, HS-5 and control cells.** Gating strategy and results of CD45 flow cytometry to assess whether stroma cell lines are of hematopoietic origin. HEK-293T cells were used as negative, MBL-2 cells as positive controls. (Herbst et al., 2020b)

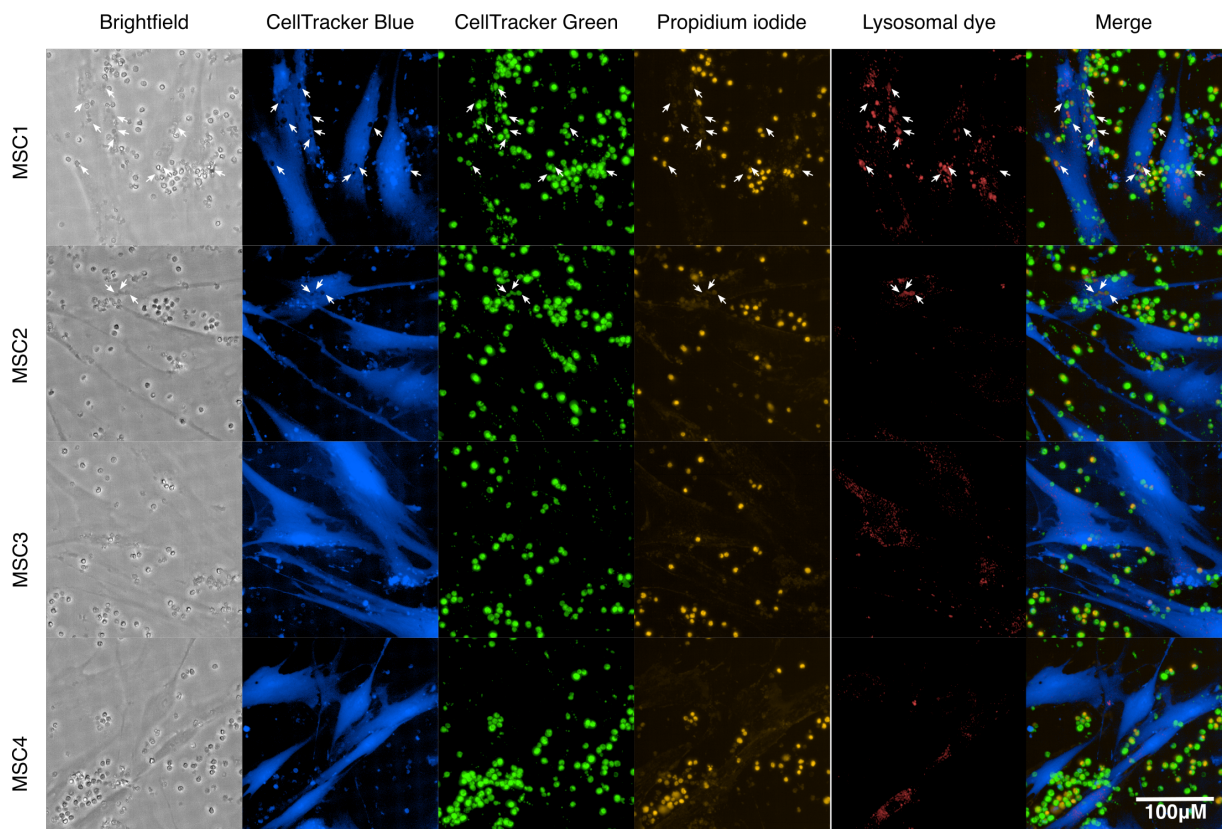


Figure S3: **Phagocytosis by different MSCs.** Representative confocal microscopy images of co-cultures of CellTracker Blue labelled MSCs from four different donors and CellTracker Green labelled CLL cells, previously treated with 63 nM venetoclax and stained with propidium iodide and lysosomal dye NIR. White arrows highlight all detected examples in which apoptotic CLL have been phagocytosed by MSC. (Herbst et al., 2020b)

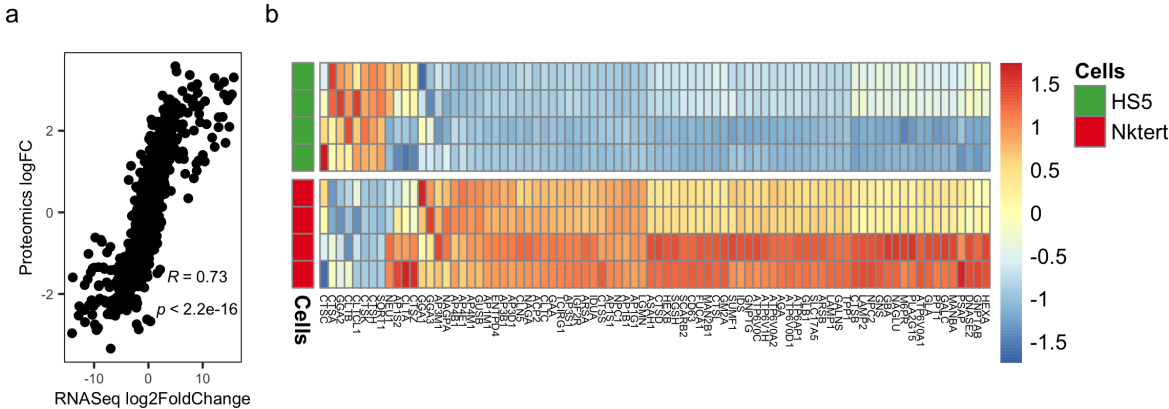


Figure S4: **Comparison of protein and gene expression patterns between NKTert and HS-5.** **a**, Spearman correlation and p-value between proteomics and RNA sequencing of the fold changes of NKTert versus HS-5 cells. **b**, Protein abundances of genes in the KEGG pathway 'Lysosome' in NKTert and HS-5. Most lysosomal genes were upregulated in NKTert. For each cell line quadruplicates were performed. (Herbst et al., 2020b)

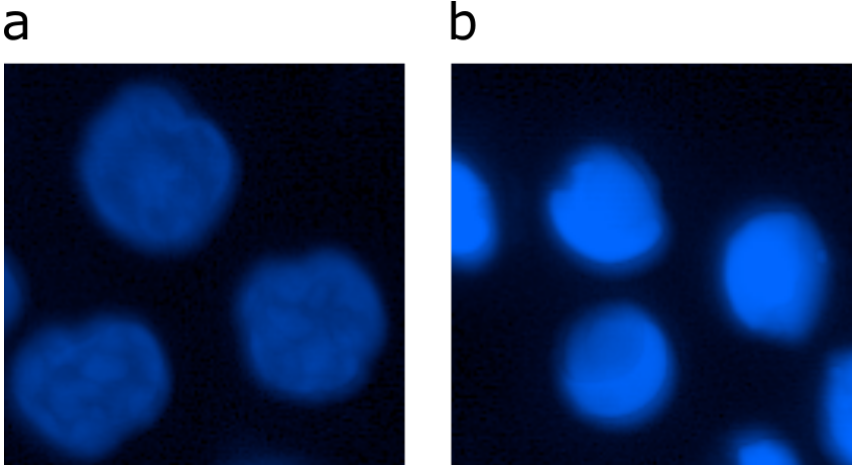


Figure S5: **Alive and dead CLL cells stained with Hoechst.** **a**, Alive CLL cells stained with Hoechst. **b**, Dead CLL cells stained with Hoechst.

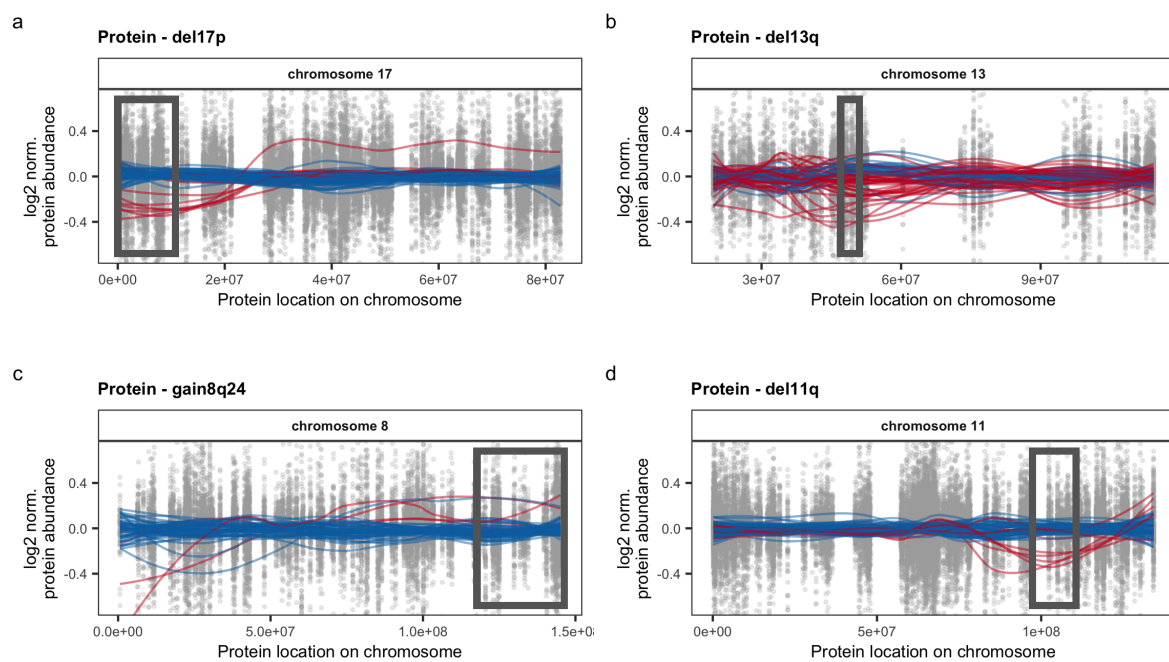


Figure S6: **Differential protein abundances in respect to chromosomal location.** Protein abundance levels for del17p13 (del17p) (a), del13q14 (del13q) (b), gain8q24 (c) and del11q (d) are shown. Points represent individual values for protein - patient pairs. Lines are locally weighted scatterplot smoothed values for individual patients with (red) or without (blue) the chromosomal aberration. The box is the region affected by the chromosomal aberration. (Herbst et al., 2020c)

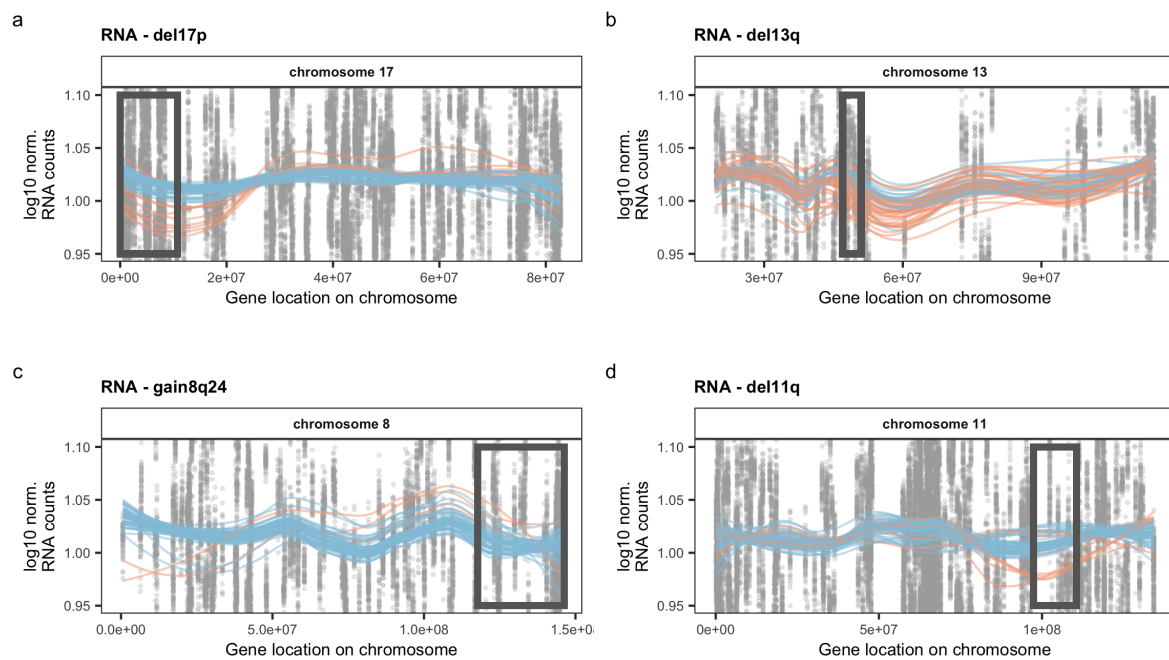


Figure S7: **Differential transcript abundances in respect to genetic alterations.** Gene expression levels for del17p13 (del17p) (a), del13q14 (del13q) (b), gain8q24 (c) and del11q (d) are shown. Points represent individual values for gene - patient pairs. Lines are locally weighted scatterplot smoothed values for individual patients with (red) or without (blue) the chromosomal aberration. The box is the region affected by the chromosomal aberration. (Herbst et al., 2020c)

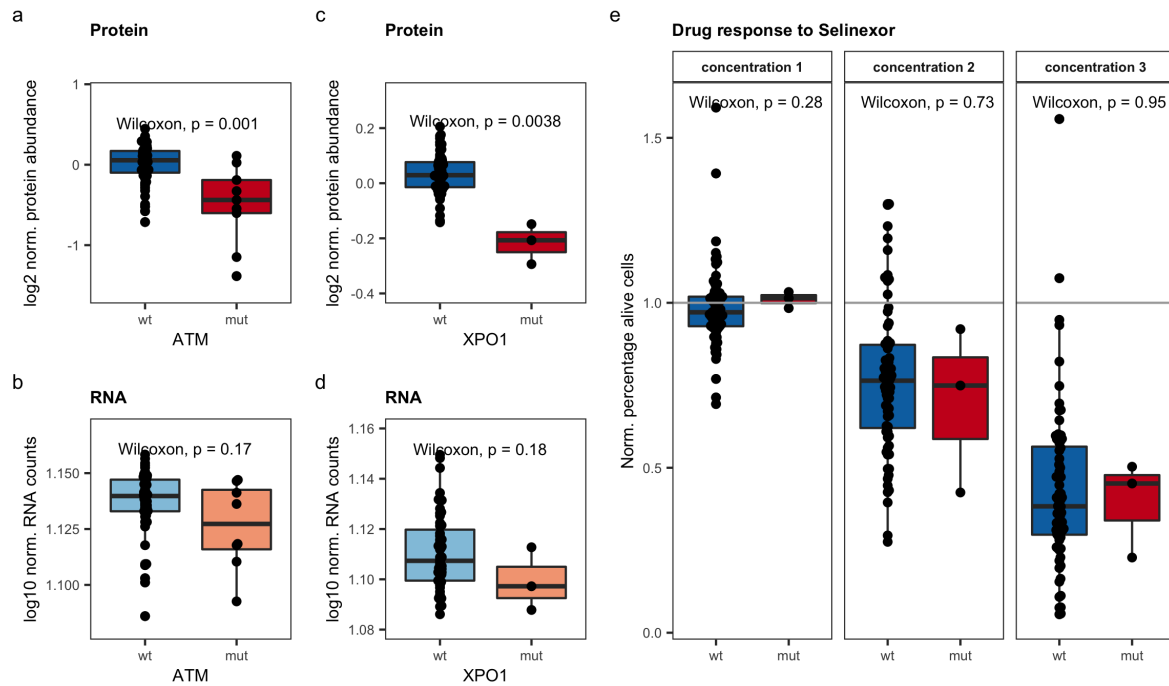


Figure S8: **Consequences of *ATM* and *XPO1* mutations.** **a**, *ATM* protein levels in *ATM* mutated (mut) and wild type (wt) CLL samples; Wilcoxon signed-rank test  $p = 0.001$ . **b**, *ATM* transcript levels in *ATM* mutated (mut) and wild type (wt) CLL samples; Wilcoxon signed-rank test  $p = 0.17$ . **c**, *XPO1* protein levels in *XPO1* mutated (mut) and wild type (wt) CLL samples; Wilcoxon signed-rank test  $p = 0.004$ . **d**, *XPO1* transcript levels in *XPO1* mutated (mut) and wild type (wt) CLL samples; Wilcoxon signed-rank test  $p = 0.18$ . **e**, Percentages, normalised to solvent control, of alive cells of *XPO1* mutated (mut) and wild type (wt) CLL samples treated *ex-vivo* with 40 nM (concentration 1), 0.6  $\mu$ M (concentration 2) or 9  $\mu$ M (concentration 3) selinexor for 3 days. (Herbst et al., 2020c)

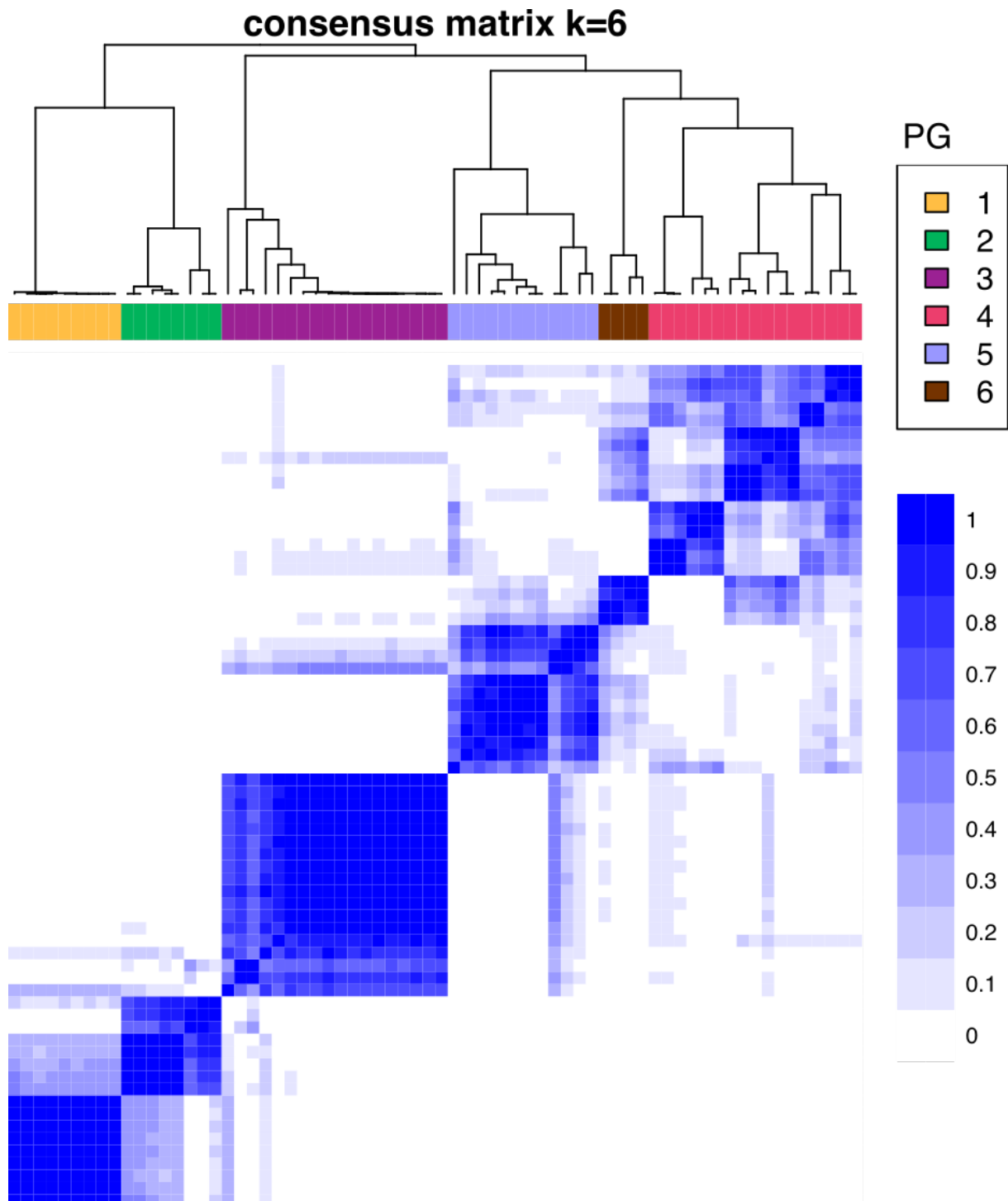


Figure S9: **Consensus cluster heatmap of proteomics data.** Consensus cluster plus identified six clusters within the proteomics data, which were named proteomics groups (PG). The blue scale visualises how often patient samples clustered together. (Herbst et al., 2020c)

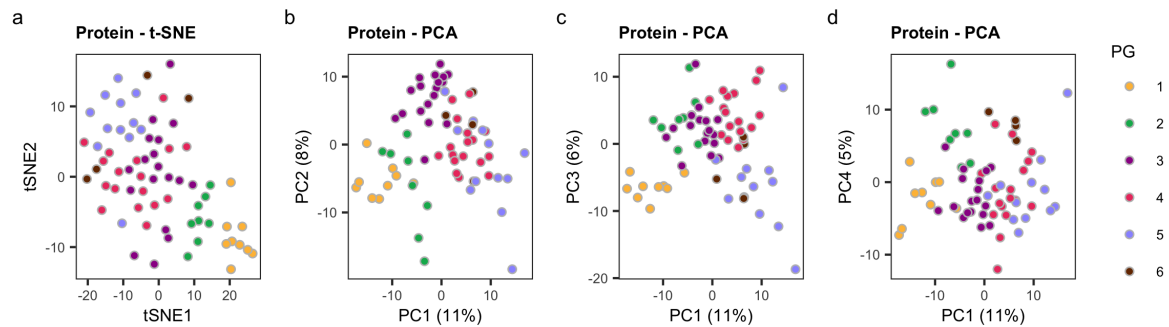


Figure S10: **T-distributed stochastic neighbour embedding (t-SNE) and principal component analysis (PCA) supported the partition into six subgroups.** **a**, t-SNE on proteomics data coloured by PG. **b-d**, Visualisation of the first four principle components (PC) of a PCA on the proteomics data coloured by PG. (Herbst et al., 2020c)

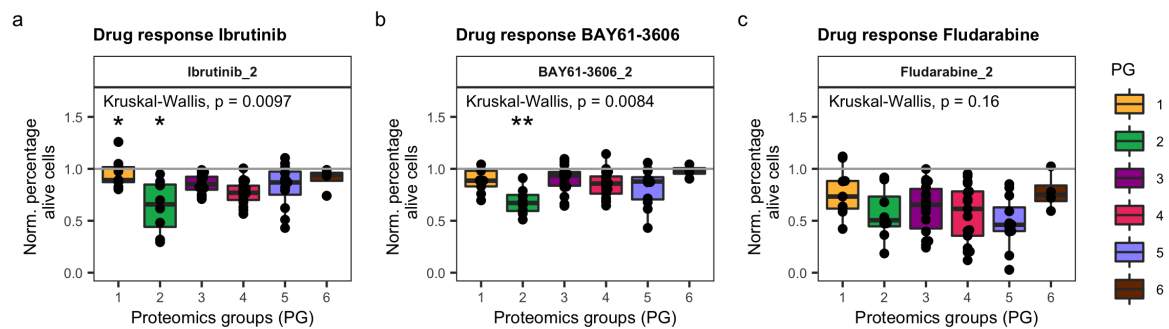


Figure S11: **Response of proteomics groups (PGs) to ibrutinib, BAY61-3606 and fludarabine.** Percentages of alive cells, normalised to solvent control, across PGs treated *ex-vivo* with **a**, 0.6  $\mu$ M ibrutinib (Ibrutinib\_2) or **b**, 0.6  $\mu$ M BAY61-3606 (BAY61-3606\_2) or **c**, 0.6  $\mu$ M fludarabine (Fludarabine\_2) for 3 days. (Herbst et al., 2020c)

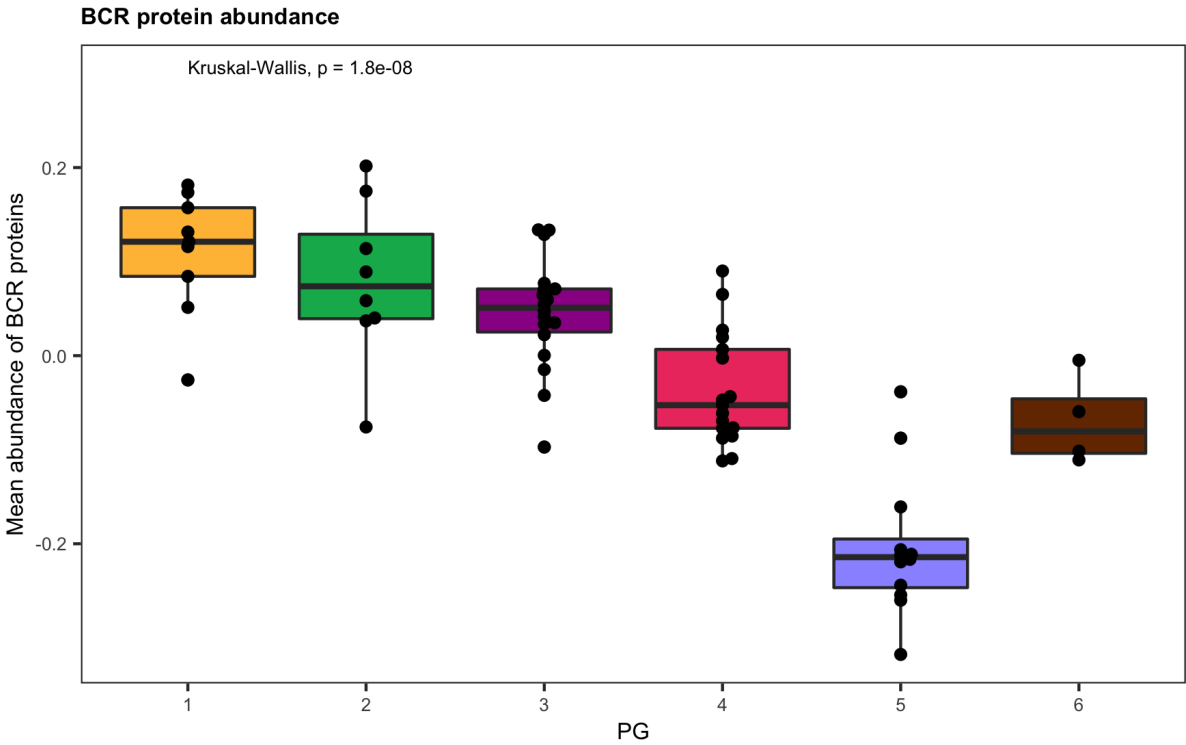


Figure S12: Mean protein abundances of B-cell receptor signalling proteins in the proteomics groups (PGs). Proteins abundances are shown as normalised, log transformed values. Kruskal-Wallis Test. (Herbst et al., 2020c)